

VIBRATION ANALYSIS OF
HEALTHY AND OSTEOARTHRITIC
KNEES

VIBRATION ANALYSIS OF HUMAN KNEE JOINT IN HEALTHY AND OSTEOARTHRITIC KNEES

by

(Siamak Salari Sharif)

A Thesis

Presented to the McMaster University

in Fulfillment of the

Thesis Requirement for the Degree of

(Master of Science)

in

(Chemical Engineering)

Hamilton, Ontario, Canada, 2007

©(Siamak Salari Sharif) 2007

Master of Science (2007)
(Chemical Engineering)

McMaster University
Hamilton, Ontario, Canada

TITLE: VIBRATION ANALYSIS OF HUMAN KNEE
JOINT IN HEALTHY AND OSTEOARTHRITIC
KNEES

AUTHOR: Siamak Salari Sharif, B.Sc. (Eng)

SUPERVISOR: Professor John F. MacGregor

NUMBER OF PAGES: xiv, 141

AUTHOR'S DECLARATION

I hereby declare that I am the sole author of this thesis. This is a true copy of the thesis, including any required final revisions, as accepted by my examiners.

I understand that my thesis may be made electronically available to the public.

Abstract

The goal of this thesis is to investigate the possibility of using vibration analysis to detect and assess a very common joint disease known as osteoarthritis (OA). For this purpose, patients with various levels of OA, healthy to severe OA, were recruited and MRI and vibration recordings were made on both knees. MRI images were analyzed by a radiologist and different symptoms related to osteoarthritis in the knee were scored for each observation. Vibration signals of the patients' knees were recorded using 5 accelerometers placed at different locations of the knee.

This thesis divides into two major sections; the first section deals with design of an apparatus (a function specific brace and the electronic hardware) for acquiring and recording vibration data from a patient's knee. The second section deals with the analysis of the recorded data using a combination of signal processing techniques (Fourier and wavelet transforms) and multivariate statistical methods (principal component (PCA) and partial least square (PLS)). The brace designed and built for the purpose of this research has several unique properties not found in commercial knee braces. It provides a robust and secure base for attachment of the sensors to the knee and shows very good adaptation to the dynamics of the knee during motion. In the analysis section we show that combining signal processing and multivariate statistical techniques (such as PCA and PLS) provides strong tools for analysis of the data.

The result of our analysis shows that there is a strong correlation between vibration analysis and some of the symptoms of osteoarthritis such as cartilage degeneration and

formation of osteophytes. We conclude that vibration signals of the knee joint (crepitus) during flexion/extension cycle of the knee, when it is under stress, can be a good indicator of the general severity of OA in patients.

Acknowledgements

I would like to thank Dr. John MacGregor for his expert supervision and support over the course of my studies. I would like to also thank Dr. Adachi for his help and support. I also like to thank Dr. Jim Reilly for his guidance throughout the project. I would like to thank Dr. Bobba and Dr. Karen Beattie for recruitment of patients and their help with the medical aspects of the research. I would especially like to thank Hao Wu my good friend for helping me through out the steps of the project and doing all the work related to MRI imaging and scoring. If it wasn't for him I would have not been able to finish this thesis. I would also like to thank all the graduate students in MACC and the staff of the chemical engineering department.

I would like to thank all the volunteers who patiently participated in my study and spent their precious time for the sake of this research

I would like to thank the department of chemical engineering (McMaster University), the McMaster Advanced Control Consortium (MACC).

And finally, many thanks to my family, and especially my mother, for their support and encouragement over the course of this research.

Table of Contents

AUTHOR'S DECLARATION.....	ii
Abstract	iii
Acknowledgements	v
Table of Contents	vi
List of Figures	viii
List of Tables.....	xiii
Chapter 1 Introduction	1
Chapter 2 Anatomy of human knee.....	7
2.1 Introduction	7
2.2 Knee Structure.....	8
2.2.1 Bones.....	9
2.2.2 The Joint.....	10
2.2.3 Cartilage and meniscus.....	12
2.2.4 Ligaments	14
2.2.5 Muscle and nerves	16
2.3 Kinematics of knee.....	17
2.3.1 Surface motion of tibiofemoral joint	20
2.3.2 Surface motion of patellofemoral joint	22
2.3.3 Skin-bone movement.....	23
2.4 Summary	24
Chapter 3 Knee diseases.....	25
3.1 Osteoarthritis	25
3.1.1 Symptoms and stages of OA	27
3.1.2 Symptoms of OA.....	30
3.1.3 Clinical diagnostic tools of OA.....	31
3.2 Meniscus and ACL damages.....	34
3.3 Discussion and summary.....	35
Chapter 4 Analysis of joint using vibration.....	36
4.1 Clinical Studies	36
4.2 Brace Design	43

4.2.1 Mechanical Hardware.....	43
4.2.2 Electronic hardware.....	49
4.3 Summary	53
Chapter 5 Analysis and results	54
5.1 PCA on Y Data.....	59
5.2 Analysis of Fourier transforms.....	61
5.2.1 FFT.....	61
5.2.2 PCA on FFT	72
5.2.3 PLS on FFT	79
5.2.4 Summary and conclusion	89
5.3 Analysis of wavelet transforms	90
5.3.1 Wavelet transforms	90
5.3.2 PCA on histograms of wavelet coefficients	100
5.3.3 PLS on the wavelets	108
5.3.4 Summary and conclusion	117
Chapter 6 Summary and Conclusion.....	119
6.1 Future work	122
Appendix A Product Data	124
Appendix B Detecting the FE axis of the knee	131

List of Figures

Figure 1: Major structure of the knee. Knee is made of two major joints, tibiofemoral joint and Patellofemoral joint. The surface of the bone in these joints are covered with articular cartilage.....	9
Figure 2: Knee joint from different views. Femoral condyles, fibula and patellar groove are shown clearly in the image.	10
Figure 3: location and structure of meniscus and articulating cartilage.....	13
Figure 4: pressure reduction effect of the meniscus, also known as the wedge effect.....	13
Figure 5: Tendon hierarchy, adapted from [50].....	16
Figure 6: (a) anterior and posterior views of ligaments. (b) ACL, PCL ligaments. (c) Lateral and medial collateral ligaments (adopted from www.eorthopod.com).....	16
Figure 7: A) frontal, sagittal and transverse planes in the human body. B) Depiction and nomenclature of the six degrees of freedom of knee motion. Adapted from [50].....	18
Figure 8: A) Range of motion of the tibiofemoral joint in the sagittal plane during level walking in one gait cycle. The shaded area indicates variation among 60 subjects (age range 20 to 65). B) Range of tibiofemoral joint motion in the sagittal plane during common activities (adopted from [50]).....	19
Figure 9: locating the instant center. B) Semicircular instant center pathway for tibiofemoral joint in a 19-year old man with normal knee (in sagittal plane) (adopted from [50]).....	21
Figure 10: A) Determining the instant center of patella in sagittal plane. B) The position of patella at different ranges of knee flexion motion (left). Contact areas during different degrees of flexion. Beyond 90° of flexion, the patella rotates slightly outwards. (adopted from [50]).....	23
Figure 11: A) schematics of healthy versus osteoarthritic joint. B) a closer look at the structure changes of the articular cartilage in OA (taken from [51]).....	28
Figure 12: T1-weighted 3D gradient echo images of a healthy knee joint (left) and a knee joint with severe damage to cartilage.....	29
Figure 13: x-ray images of OA knee. Left) angulation of the knee due to severe lateral compartment OA. Right) loss of joint space and appearance of osteophytes are present in the picture. Taken from [51].....	32

Figure 14: MRI images of the knee at different machine settings; fat suppressed t1 weighted 3D gradient echo (left), Proton density (middle) and t2 weighted (right) images	33
Figure 15: osteoarthritic (left) versus healthy knee (right). Damage to meniscus, cartilage surface and subchondral bone are clearly visible. Image has been colorized based on different T weights of MRI	34
Figure 16: Left) meniscus tear shown in MRI Image, Right) different types of meniscus tear.....	35
Figure 17: MRI score sheet used for this study.....	41
Figure 18: universal commercial brace donated by GII Orthotics Inc	44
Figure 19: final design of the brace with accelerometers attached to it	46
Figure 20: Left) Patella Sensor and the adjustable arm, Right) location of the sensors on the knee	47
Figure 21: Top view of the brace assembled to the knee	48
Figure 22: Side and rear views of the brace when mounted on the knee	48
Figure 23 diagram of Data Acquisition hardware	50
Figure 24: PCB 1000 mv/g accelerometers and their circuit diagram (right)	51
Figure 25: PCB miniature impact hammer and its frequency range diagram (right)	52
Figure 26: a) Model overview plot of the Y Data. b) Variable overview plot for the first component	59
Figure 27: P ₁ /P ₂ loading plot of the Y Data.	61
Figure 28: Left) Wavelet decomposition of the original signal, Right) thresholded wavelet coefficients and the reconstructed signal	66
Figure 29: Periodogram of the knee signal before and after thresholding.	67
Figure 30: Left: original signal. Right: signal after detrending.....	68
Figure 31: Positive and Negative half cycles of a signal.....	71
Figure 32: Frequency spectrums for positive and negative half cycles.....	72
Figure 33: model overview plot of the Standing Data (Power Spectrum)	73
Figure 34: Component contribution plot for the first component (PCA on Frequency)	74
Figure 35: Component Contribution plot for the second component (PCA on Frequency).....	74
Figure 36: Component contribution plot for the third component (PCA on Frequency).....	75

Figure 37: t1/t2 and t3/t2 Scatter plots of the PCA model for frequency data.....	76
Figure 38: component contribution plot (Comp 2) between healthy (0-1) and unhealthy (2-3) cartilage knees (X: Inverse of power spectra). (a: for all sensors, b: only patella sensor, positive half cycle	77
Figure 39: t2/t3 Scatter plot colored according to average severity of osteophyte formation in the knees.....	78
Figure 40: Variable Importance Plot (VIP), PLS model (Frequency Data).....	81
Figure 41: t ₁ /t ₂ scatter plot of the PLS components (Frequency Analysis Data), colored according to average severity of the cartilage damage.....	81
Figure 42: Left) Loading Plot before pruning the variables, Right) Loading Plot after pruning the variables (Y: Average Cartilage score (SumCart)). PLS analysis on the frequency data.	82
Figure 43: Observed VS predicted Y (Ave. Level of cartilage degeneration) for PLS model (X = Frequency Data, Y = Ave. Cart. Degeneration).....	83
Figure 44: t1/t2 scatter plot of the PLS model (Y= average osteophyte formation level). PLS on the frequency data	85
Figure 45: Observed VS Predicted average osteophyte formation level. PLS on the frequency data	85
Figure 46: Loading plots (p1/p2) for meniscus degeneration level after variable pruning. PLS on the frequency data	86
Figure 47: Short Time Fourier Transform (STFT).....	91
Figure 48: A mother wavelet and convolution with s(t).....	91
Figure 49: db2 wavelet (Ψ) at different scales (a).....	92
Figure 50: Decomposition of the signal “s” into its detail and approximate ($s = D_1 + A_1$)	94
Figure 51: DWT in two stages	95
Figure 52: DWT (Left) versus Packet Wavelet analysis (Right)	96
Figure 53: center frequency (F_c) of a wavelet (adopted from wavelet toolbox tutorial, mathworks inc).....	97
Figure 54: different wavelet shapes.....	98
Figure 55: distributions of wavelet coefficients at different levels for the coefficients of a stationary wavelet transform	100

Figure 56: model overview plot (PCA on wavelet histograms).....	102
Figure 57: Component Contribution plot for coefficient histograms at all details (only patella sensor variables shown); Comp. #1 (PCA on wavelet histograms), Level 110 = approximate at level 10 (the numbers on the abscissa show the approximate range of variables for each detail)	103
Figure 58: Component Contribution plot for coefficient histograms, at all details; Comp. #2 (PCA on wavelet histograms, only patella sensor variables shown), Level 110 = approximate at level 10 (the numbers on the abscissa show the approximate range of variables for each detail)	103
Figure 59: Component Contribution plot for coefficient histograms, at all details; Comp. #4 (PCA on wavelet histograms, only patella sensor variables shown), Level 110 = approximate at level 10 (the numbers on the abscissa show the approximate range of variables for each detail)	104
Figure 60: t1/t2 and t4/t2 score plots of the PCA model for wavelet dataset.....	105
Figure 61: Contribution plot between healthy (0-1) and unhealthy (2-3) cartilage knees (wavelet scales 2 to 10); a) for all sensors, b) only shown for the patella sensor.	106
Figure 62: Contribution plot for the difference of unhealthy from healthy knee; Left: low frequency (Det. 6), Right: High Frequency (Det. 2)	107
Figure 63: t2/t4 score plot of the PCA model for the wavelet dataset colored according to average osteophyte score.....	108
Figure 64: Model Overview Plot of the PLS model on the cartilage variables (after pruning extra variables).....	109
Figure 65: t1/t3 Score Scatter plot, colored according to average cartilage score.....	110
Figure 66: Y, Observed VS Predicted for cartilage score at a: Medial Femur (FMed), b: Lateral Femur (FLat).....	110
Figure 67: Y, Observed VS Predicted for cartilage scores at a: Medial Tibia (Tmed), b: Lateral Tibia (Tlat).....	111
Figure 68: Y, Observed VS Predicted for cartilage scores at a: Trochlea (FT), b: Patella.....	111
Figure 69: Model overview plot for PLS model on individual osteophyte scores (after Pruning).....	112

Figure 70: t_1/t_2 (left) and t_1/t_3 (right) score plots of the PLS model colored according to average osteophyte score.....	113
Figure 71: Model Overview Plot for average cartilage and osteophyte scores.....	114
Figure 72: X/Y Overview plot of the PLS model for average cartilage and osteophyte scores.....	114
Figure 73: Observed versus Predicted value for a: Average Cartilage Score, b: Average Osteophyte Score.....	115
Figure 74: 3A AND 3B. (A) Diagrammatic representation of axes in AP view with axis parallel to the plate. A is the angle the FE axis makes with the shaft of the femur; B is the angle between the FE and L.R axes in the AP plane. C is the angle between the LR axis and the tibial plateau. The distances D, W, and T_m are the distances between the FE axis and the joint surface, the AP width of the tibia, and the medial tibia and the LR axis respectively. (B) Diagrammatic representation of axes in axial lateral view with x-ray beam parallel to the FE axis. E is the angle between the LR axis and the tibial plateau in the axial lateral plane; X is the distance between the anterior femoral shaft and the posterior-medial femoral condyle. R is the distance between the FE axis and the posterior-medial femoral condyle. Y is the perpendicular distance between the two axes. Z is the AP dimension of the tibia and T_a is the distance of the L.R axis from the anterior tibia.	132

List of Tables

Table 1: X and Y variables obtained from MRI and vibration recordings of the knee	42
Table 2: “X matrix of the spectrum magnitudes for PCA and PLS analysis; Pat: Patella, FLat: Lateral Femur, FMed: Medial Femur, TLat: Lateral Tibia, TMed: Medial Tibia	73
Table 3: Quality of fit for different combination of sensors (PLS model, Y= Ave. Cartilage degeneration level, no variable pruning). PLS on Frequency data.	83
Table 4: quality of fit before and after data pruning for different combination of individual groups of Y variables (Cartilage and Osteophyte)	88
Table 5: Scale frequency for levels 1 to 10 of db1 wavelet	101
Table 6: Percentage of error due to Pure Error and the component of it due to round-off.....	117
Table 7: A) Location of axes of rotation, B) Location of the axes described as a percent of femoral and tibial dimensions. Tm/W, percentage ration locating tibia axis on AP view; Ta/Z percentage ratio locating tibial axis on axial lateral view; Y/W percentage ratio depicting interaxial distance relative to tibial plateau width; R/X percentage ratio locating femoral axis on axial lateral view.....	133

Chapter 1

Introduction

Kuettner Et al [1] defines Osteoarthritis (OA) as “a result of both mechanical and biologic events that destabilize the normal coupling of degradation and synthesis of articular cartilage chondrocytes¹ and extracellular matrix and subchondral bone. Although they may be initiated by multiple factors, including genetic, developmental, metabolic and traumatic, Osteoarthritis (OA) diseases involve all of the tissues of the diarthrodial² joint. Ultimately, OA diseases are manifested by morphologic, biochemical, molecular and biomechanical changes of both cells and matrix which lead to a softening, fibrillation, ulceration³, loss of articular cartilage, sclerosis⁴ and eburnation⁵ of subchondral bone, osteophytes and subchondral cysts. When clinically evident, OA diseases are characterized by joint pain, tenderness, limitation of movement, crepitus, occasional effusion, and variable degrees of inflammation without systemic effects⁶”. In other words OA refers to degenerative abnormalities in the joint area which in time would lead to pain and disability.

¹ Chondrocyte: A cartilage cell, Merriam Webster dictionary

² Diarthrodial: joints that are able to move in several directions, Encarta dictionary

³ Ulcer: defects

⁴ Sclerosis: Hardening and thickening of body tissue as a result of unwarranted growth, Encarta Dictionary

⁵ Eburnation; an abnormal hardening of the surfaces of bones in a joint that have lost their cartilage, Encarta Dictionary

⁶ Systemic effects are the disorders that will effect other parts of the body

Along with heart and chronic lung disease, knee OA is one of the major causes of disability [2]. It is anticipated that over 18% of US population alone would develop OA by 2020 [3]. Unfortunately OA is a persistent disease and there is no cure yet found for it. A majority of people over the age of 55 years will develop some symptoms of this joint disease. At least 10% of the population over the age of 60 suffers significant disability due to OA related symptoms [4]. Due to its importance in mobility and daily activity, knee OA is among the most noticeable types of OA. One of the main causes of OA development is aging. Like any other mechanical device, our joints have limited duration of healthy activity. Studies show [5, 6, 7] that the prevalence of knee OA in women increases from 1 to 4% in people between 24 to 45 years of age to more than 53% at the age of 80 years and over. There are also other factors that increase the risk of OA development. Among them the most related ones are physical injuries, nutrition, genetic factors and weight. More details and stats about these risk factors are given in chapter 3 of this thesis.

Since the articular cartilage of the knee does not have any sensory system, symptomatic signs of OA are not usually detected until the advance stages. Progression of the disease from cartilage surface to neighboring tissues (meniscus and bone) results in pain and inflammation of the joint. Overall, major symptomatic signs of OA include pain, inflammation, morning stiffness, bony enlargement and crepitus. The most common technological tools for detecting and studying OA are radiographic techniques and the most widely used is X-Ray imaging. Over time many protocols have been developed to

enhance the readings and diagnosis of OA [8, 9, and 10]. However the drawback of X-Ray imaging besides the harmful radiations is that it only shows the changes to bony tissue and the joint narrowing which are the signs of advance stages of OA and cannot visualize the changes to the soft tissue (starting at earlier stages). The other drawback of X-Ray imaging is its two dimensional nature which greatly reduces the ability to diagnose and localize OA related problems [11, 12]. Over the recent years there has been a shift towards magnetic resonance imaging (MRI). The ability of MR imaging in detecting soft tissue changes and the three dimensional visualization of the joint has made this technology extremely popular. Unfortunately high costs of MR Imaging still prevents it from wide spread use.

As mentioned earlier, crepitus or the grinding sound generated during the knee joint movement is one of the symptomatic signs of OA. O'Rourke Et Al's Study [13], found strong correlation between crepitus and OA. Crepitus is usually a palpable sensation; however in patients with severe OA it is even audible. Using auscultation dates back to 2000 years ago to Hippocrates [14]. In 17th century Robert Hookes used auscultation for detection and assessing the joint problems [14]. Invention of stethoscope opened a new era to this type of diagnostic method. Many scientists tried to use auscultation to identify joint diseases. In 1937, Steindler [15] used a combination of stethoscope and microphone to record knee joint sounds for analysis. With all the efforts using stethoscope and microphone combinations there was yet no robust method for detection or even recording of the joint vibrations. The low signal to noise ratio (SNR) in the recordings obtained by

these methods prevented the scientists from recording useful data. In 1980 and in two separate studies, Mang et al and Mollan et al used accelerometers instead of microphones. They both indicated strong evidence in the ability of the knee joint vibration signals to detect OA. McCoy et al [16] concluded in their paper (published in 1987) that using vibration arthrography it is possible to categorize signals related to many knee symptoms especially meniscus lesions and even in some cases the type of meniscus lesion. In 1988 Rangayyan et al used knee joint vibration analysis to investigate the correlation between knee vibrations and chondromalacia⁷ and meniscus lesions in 16 patients before arthroscopy. Their study showed such injuries have distinct frequency signature compared to the healthy knees [17]. In a more recent paper that they published in 2001, they used auditory display (sonification) of knee vibration signals to be used by orthopedic surgeons to detect OA in several healthy and unhealthy patients [18]. Rangayan and Krishman also published several other papers on automatic denoising and analysis of knee joint vibrations [19, 20, 21 and 22]. Despite all the efforts toward implementation of this technology, auscultation or vibration arthrography (VAG) has not yet become a useful technique in diagnosis of joint problems. There are several reasons for this misfortune; probably the main reason has been the lack of a robust method for analysis of VAG signals. The second reason might be due to the absence of technological instruments for recording and analysis of large quantities of data.

⁷ Chondromalacia: Abnormal softness of cartilage, Merriam Webster dictionary

The aim of this project is to design and develop an apparatus to simultaneously record knee vibration signals from several locations on the knee and to analyze the signals to assess any correlation between VAG signals and OA related joint abnormalities detected by magnetic resonance imaging (MRI). According to the reviewed literature above, our hypothesis is that there is evidence of correlation between knee joint disease known as osteoarthritis and VAG signals.

Throughout the upcoming chapters we will discuss and cover following topics and issues:

Chapter two; anatomy of human knee: Having an understanding of the structure and functions of human knee is essential for understanding the rest of the topics in this project. Since many of the readers of the thesis belong to the engineering field and may not be familiar with the field of medicine, the concepts have been simplified to convey the essence of the topic.

Chapter three; Osteoarthritis: in this chapter a brief overview of osteoarthritis, its risk factors and available diagnosis tools will be given.

Chapter four; Analysis of joint vibration signals: this chapter divides into 3 sections:

- Section one; clinical studies, describes the methodology and procedure of the tests and signal recording.
- Section two; brace design, covers the process of designing the mechanical apparatus for securely attaching the sensors to the knee. It also discusses the problems faced and the solutions found in the design process.

- Section three talks about the hardware setup and software developed for data acquisition in a Matlab environment.

Chapter five; Results and discussion; this chapter divides into three major sections:

- Section one discusses the analysis of the Fourier transforms of the data
- Section two discusses the analysis of the Wavelet transforms
- Section three contains the summary and conclusion

Chapter 2

Anatomy of human knee

2.1 Introduction⁸

In order to better understand the function and properties of the knee joint, we need to understand its structure and components. The knee is the largest joint in the human body and bears the weight of the body as well as enables us to move and run. Unlike the general believe this joint has a complex set of motion. In addition to flexion/extension (varus/valgus⁹) in the sagittal plane it also has rotational and rotational motion in the other two planes. As we will discuss later, this joint has an axis of rotation that is not exactly perpendicular to the sagittal plane, and with the femoral condyles' conical shape, each flexion/extension (FE) cycle is a combination of rotation and flexion in and out of the sagittal plane.

The articulating surface of the bones in the knee is covered with hyaline cartilage. This slippery glossy cartilage has very low coefficient of friction that enables it to smoothly articulate on the other surface. In some people as a result of aging or injury this smooth surface may start to degenerate, which will eventually lead to a very common disease known as Osteoarthritis (O.A).

⁸ Most of the contents of this chapter has been adapted from following books referenced by numbers [23] and [50] in the bibliography

⁹ Varus/valgus: flexion/extension of the joint

In this chapter we will discuss some of the major components of the knee joint and their properties and functions. Further we will briefly discuss the kinetics of the knee. The content of this chapter will later be used in the design of the brace used to support the sensors for vibration measurements. Knowing the kinematics of the knee allows us to design the brace with proper flexibility and secure fit.

2.2 Knee Structure

The knee is made up of two joints; tibiofemoral and patellofemoral joints. On the lateral¹⁰ side of the knee we also have the tibiofibular¹¹ joint. However since this joint does not come in contact with the knee itself, it is not considered part of the knee joint. The knee is a synovial joint. Synovial joints are enclosed by a ligament capsule and contain a fluid called synovium that lubricates the joints. As mentioned before, the articulating surfaces of the bone are covered with cartilage. In addition to that, another layer of cartilage known as meniscus lies in between the tibiofemoral joint space. Following figure (Figure 1) shows the structure of the knee and its components. In the following subsections we will discuss each component more closely and in more detail.

¹⁰ Lateral: outer side, Medial: inner side

¹¹ Relating to the tibia and fibula, the bones of the lower leg, Encarta dictionary

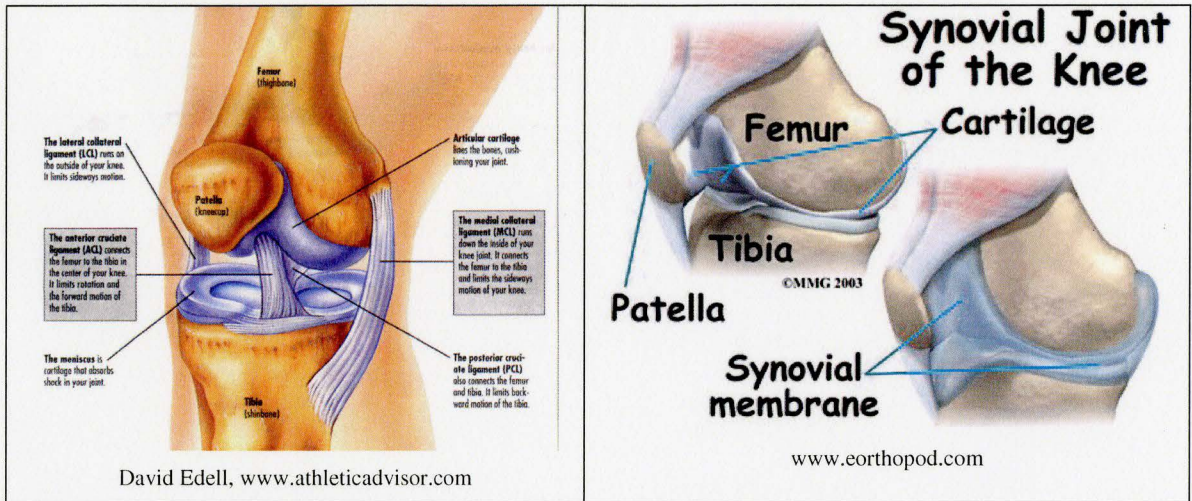


Figure 1: Major structure of the knee. Knee is made of two major joints, tibiofemoral joint and Patellofemoral joint. The surface of the bone in these joints are covered with cartilage.

2.2.1 Bones

The knee joint consists of 3 bones; femur, patella and tibia. The femur or thigh bone is the only bone in the thigh. It is the heaviest and strongest bone in the body. The head of femur articulates with the acetabulum¹² of the hip bone in a deep secure socket [23]. Despite being the strongest bone in the body the neck of femur is a common fracture site especially in old age. The femur slants medially and it runs downward to join the leg bones; this brings the knee inline with the body's centre of gravity. The medial course of the femur is more noticeable in females because of the wider female pelvis. Distally¹³ on the femur are the lateral and medial condyles. These round knobs sit on the surface of tibia plateau. The patella glides inside the groove between the two femoral

¹² Acetabulum: the cup-shaped socket in the hip bone, Merriam Webster dictionary.

condyles [24]. Ligaments and tendons attach these bones to each other. The patella is almost part of the patellar tendon. It acts as an extending lever of the quadriceps muscles and increases the momentum applied by these muscles during extension motion. Figure 2 shows the bony structure of the knee from different views.

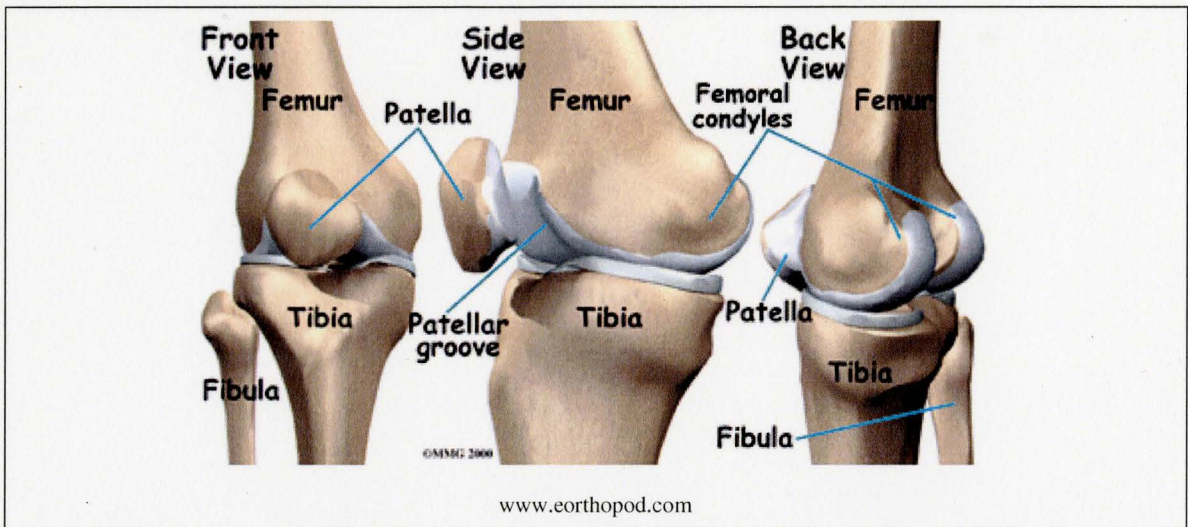


Figure 2: Knee joint from different views. Femoral condyles, fibula and patellar groove are shown clearly in the image.

2.2.2 The Joint

Except for the hyoid bone¹⁴ of the neck every bone in the body forms a joint with at least one other bone. Joints, also called articulations, have two functions; they hold the bones together securely but also give the rigid skeleton mobility [23]. Joints are classified in

¹³ Distal: Anatomy used to describe a body part situated away from a point of origin, Encarta dictionary

¹⁴ Hyoid bone: a U-shaped bone positioned at the base of the tongue that supports the tongue and its muscles, Encarta Dictionary

two ways, functionally or structurally. Functional classification focuses on the amount of movement allowed by the joint. In functional basis the joints are divided into three groups; immovable, slightly movable and freely movable joints. Knee joints and the majority of the joints in lower limb belong to the latter class. Structurally there are fibrous, cartilaginous and synovial joints. This classification is based on whether fibrous tissue, cartilage or a joint cavity separates the bony regions at the joints. As a general rule fibrous joints are immovable and synovial joints are freely movable. Since the knee joint is a synovial joint we will discuss this type of joint in more detail.

Synovial Joints

Synovial joints are those in which articulating bone ends are separated by a joint cavity containing synovial fluid. They account for all joints in the limbs. All synovial joints have four distinguishing features:

- **Articular cartilage:** Articular (hyaline) cartilage covers the ends of the bones forming the joints.
- **Fibrous articular capsule:** the joint surface is enclosed by a sleeve or capsule of fibrous connective tissue and the capsule is lined by a smooth synovial membrane (the reason these joints are called synovial).
- **Joint cavity:** the articular capsule encloses a cavity called the “Joint cavity”, which contains lubricating synovial fluid.
- **Reinforcing ligaments:** the fibrous capsule is usually reinforced with ligaments.

2.2.3 Cartilage and meniscus

Articular cartilage covering the knee bones is in fact hyaline cartilage. It can be distinguished by its bluish glossy surface. This type of cartilage is very smooth and has very low friction coefficient. The reason this cartilage has very low friction is the fact that it is mostly composed of water. It contains 68 to 85% water, 10 to 20% collagen (type II) and 5 to 10 % proteoglycan¹⁵. Under load, water is expelled from the surface of cartilage and the two surfaces actually articulate on a molecular layer of fluid.

Meniscus, which is another type of cartilage (fibro-cartilage), lies in the tibiofemoral joint space. This type of cartilage is composed of 60 to 70% water, 15 to 20% collagen (type I) and 1 to 2 % proteoglycan. Although meniscus has a similar chemical composition as articular cartilage, its different collagen structure gives it different mechanical properties. The meniscus acts as a shock absorber and fills the curvature space between the two joints therefore providing more surface area and thus less pressure on the articulating surfaces. This effect is known as the wedge effect (Figure 4). Meniscus also provides stability for the leg. Patients with their meniscus removed feel less stability and control over the functions of the knee. Figure 3 shows the location and structure of the meniscus and articular cartilage of the knee.

¹⁵ Proteoglycan: any of a class of glycoproteins of high molecular weight that are found in the extracellular matrix of connective tissue, are made up mostly of carbohydrate consisting of various polysaccharide side

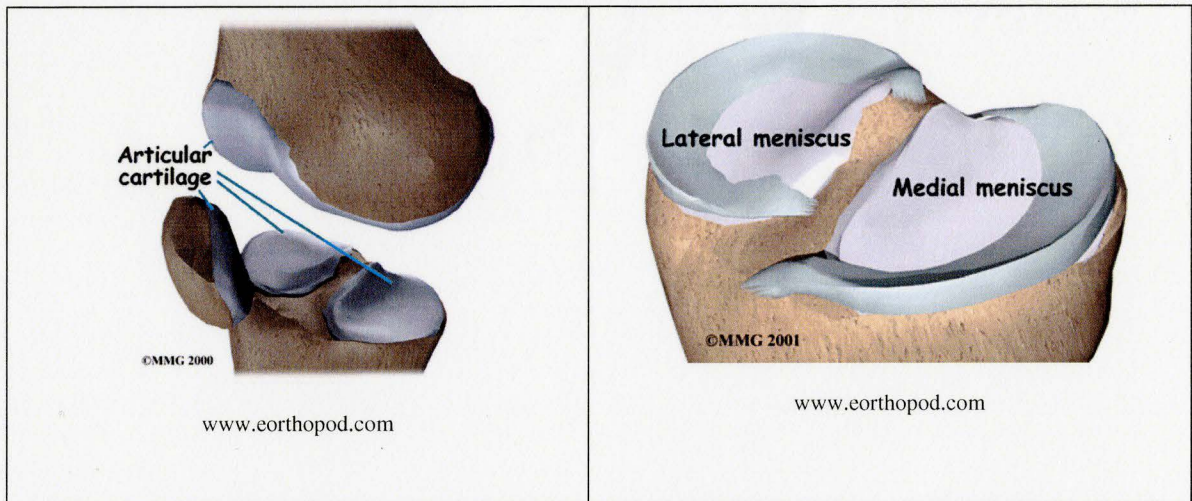


Figure 3: location and structure of meniscus and articulating cartilage

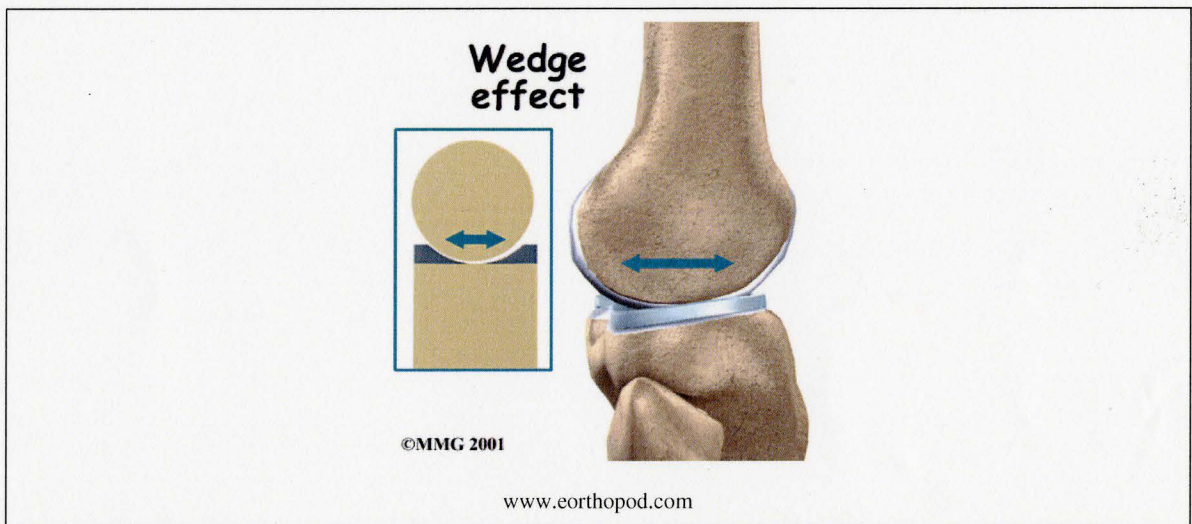


Figure 4: pressure reduction effect of the meniscus, also known as the wedge effect

chains linked to a protein, and resemble polysaccharides rather than proteins in their properties, Merriam Webster Dictionary

Like any mechanical surface, the meniscus and articular cartilage are subject to wear and tear. As people grow older, the cartilage starts to degenerate. Degeneration can also happen as a result of damage to the knee due to injury. Athletes who have torn their anterior cruciate ligaments (ACL) or meniscus are also in danger of developing osteoarthritis. We will discuss osteoarthritis in the upcoming chapters in more details.

In medical literature the meniscus is divided into four regions; Medial Anterior¹⁶ Horn (MAH), Lateral Anterior Horn (LAH), Medial Posterior¹⁷ Horn (MPH) and Lateral Posterior Horn (LPH). In this document we also divide the cartilage area of the knee joint into six areas; cartilage covering the medial femur, lateral femur, medial tibia, lateral tibia, trochlea¹⁸ and patella.

2.2.4 Ligaments

There are essentially four separate ligaments that stabilize the knee joint. On the sides of the joint, the Lateral Collateral Ligament (LCL) and the Medial Collateral Ligament (MCL) connect the “lower limb”¹⁹ to the tibia and fibula. These two ligaments stabilize the side to side movements of the knee. MCL is a broader ligament and is actually made up of two ligaments. LCL has a distinct cord like structure. At the front part of the centre of the joint is the anterior cruciate ligament (ACL). This ligament is a very important

¹⁶ Anterior: at or near the front of something (Encarta dictionary), front of the knee

¹⁷ Posterior: situated at the rear or behind of something (Encarta dictionary), behind the knee

¹⁸ Trochlea: an anatomical structure resembling a pulley: as the articular surface on the medial condyle of the humerus that articulates with the ulna. Merriam Webster Dictionary

¹⁹ Lower limb: lower part of the leg, shin and foot

stabilizer of the femur on the tibia and prevents the tibia from rotating and sliding forward during agility²⁰, jumping and decelerating activities. Directly behind the ACL is its opposite, the posterior cruciate ligament (PCL). The PCL prevents tibia from sliding backwards [25]. Figure 6 shows the structure and location of the ligaments on the knee joint. Figure 5 shows the tendon hierarchy.

Ligaments and tendons are composed of parallel fibred collagenous tissues. They have low cellularity (fibroblast < 20% of volume) and high water content (almost 70% of the wet weight matrix and 30% weight of solid matrix) [26]. Figure 5 shows the inter structure of the ligament. Structurally, tendons are similar to ligaments except that they connect muscle to bones where as ligaments connect bones to bones. The patellar ligament, located in the anterior²¹ of the knee, connects the tibia bone to the patella. It covers the patella and then connects it to the quadriceps muscles. At this point it is called the quadriceps tendon.

²⁰ Agility: a combination of physical speed, suppleness and skill, Encarta dictionary

²¹ Anterior: relating to or situated near or toward the head or toward the part in headless animals most nearly corresponding to the head

2 : situated toward the front of the body : **VENTRAL** -- used in human anatomy because of the upright posture of humans, Merriam Webster Dictionary

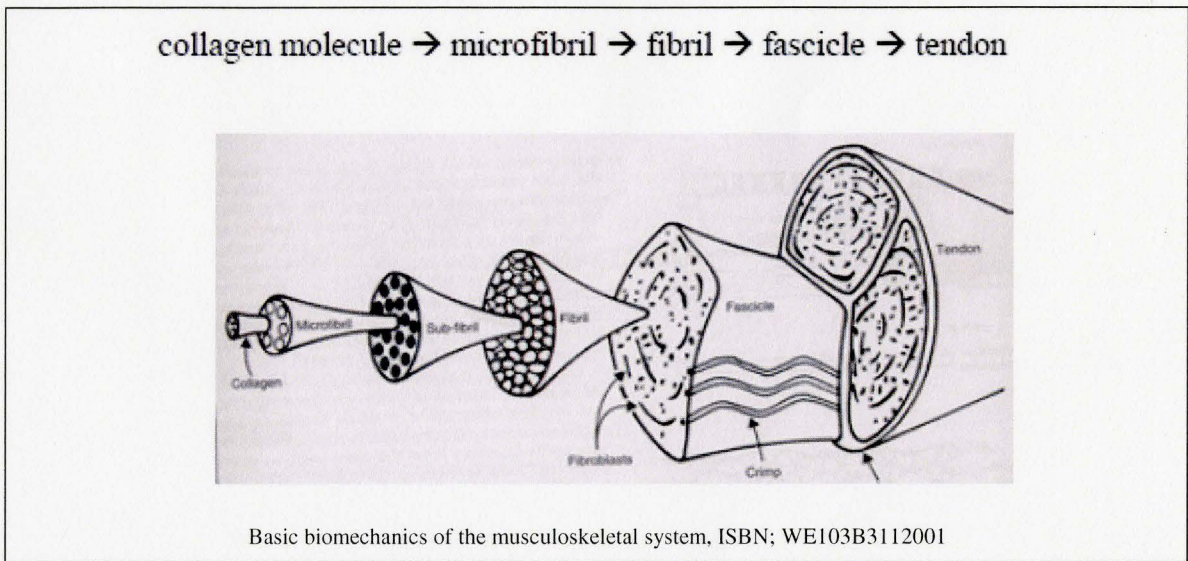


Figure 5: Tendon hierarchy, adapted from [50]

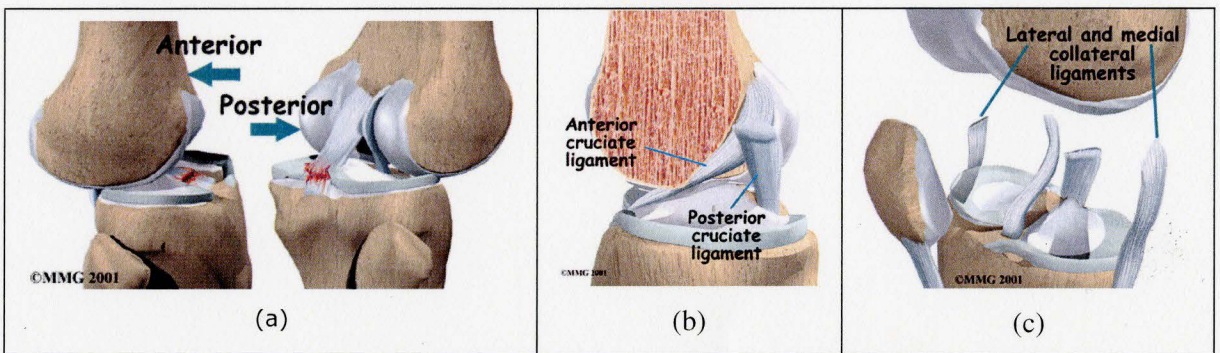


Figure 6: (a) anterior and posterior views of ligaments. (b) ACL, PCL ligaments. (c) Lateral and medial collateral ligaments (adopted from www.eorthopod.com)

2.2.5 Muscle and nerves

The quadriceps muscles extend the knee. They are connected to the tibia through the quadriceps tendon. The patella acts as an extending lever arm and therefore reduces the momentum needed for extension of the knee. People whose kneecap (patella) is removed

due to injury have less ability to extend the knee. Hamstring muscles on the back of the knee provide the flexion force. During the flexion/extension (FE) motion, the patella slides inside the patellar groove. During activities that require the knee to bend more than average, for example climbing up the stair forces, almost up to 3 to 4 times body weight are applied by the quadriceps muscles to lift the body.

Muscle control is provided by the “popliteal nerve” that runs through the back of the knee. This large nerve also provides sensation to the knee. “The tibial nerve travels on the back of the leg and ‘peroneal nerve’ travels around the outside of the knee and down the front of the leg to the foot. Both of these nerves can be damaged by injuries around the knee” [24].

2.3 Kinematics of knee

In this section we will discuss the range and surface motion of the knee. In the medical literature, motion is defined in three planes; the frontal (coronal), sagittal and transverse (horizontal) planes (Figure 7). The knee consists of two joints; patellofemoral and tibiofemoral joints. The range of motion in the tibiofemoral joint is maximal in the sagittal plane but also takes place in the two other planes. The sagittal motion of the knee from full extension to full flexion ranges from 0 to 140 degrees. The range of motion in the two other planes depends on the position (angle) of the knee in the sagittal plane. Because of the interlocking mechanism of the knee (also known as screw-home mechanism), the joint motion becomes very limited in the fully extended position. This interlocking mechanism occurs mainly because of the different radius of medial and

lateral condyles. This mechanism helps the knee to stabilize when the leg is fully stretched and reduces dependency of the knee on muscles to maintain stability. Off-sagittal motion increases as the knee flexes from 0 to 90°. At 90° the range of rotation is from 45° internally to 30°externally. The range of tibiofemoral joint motion required for performing various activities is given in the following table. These tables are determined by conducting kinematics analysis on patients. Nordin and Frankel [26] indicate that the range of motion from 0 to 117° in tibiofemoral joint, in sagittal plane is required for a person to perform various daily activities (Figure 8).

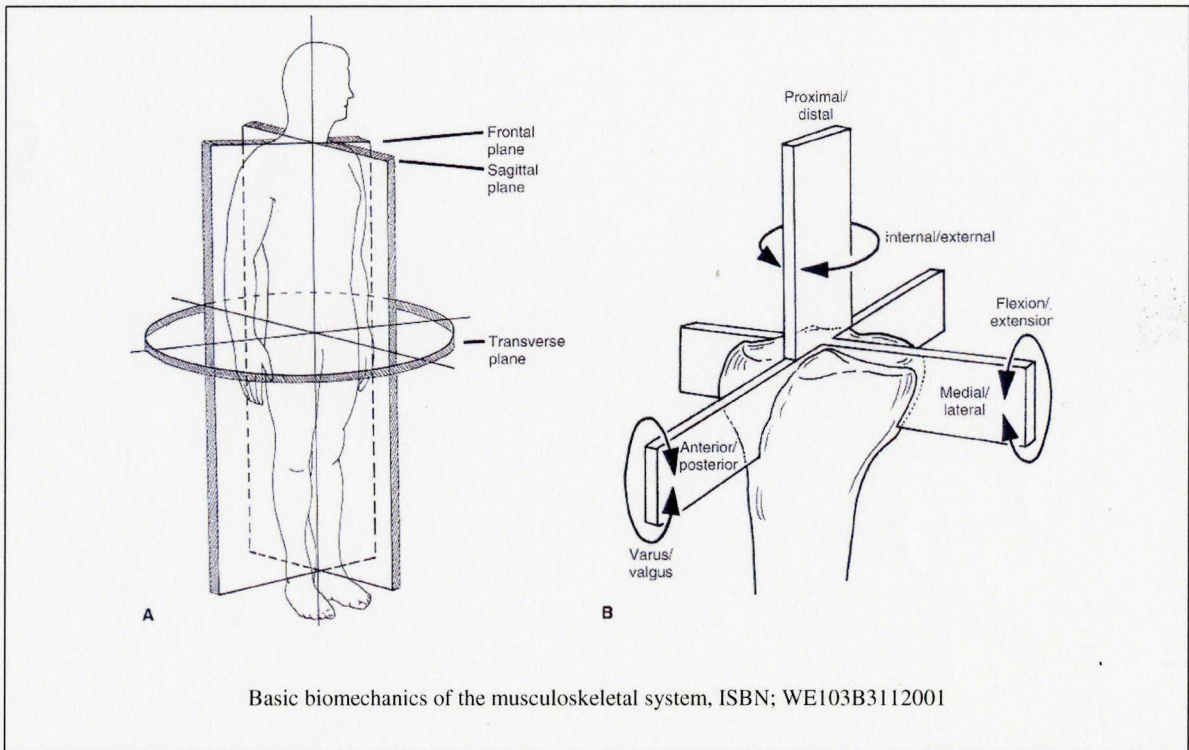


Figure 7: A) frontal, sagittal and transverse planes in the human body. B) Depiction and nomenclature of the six degrees of freedom of knee motion. Adapted from [50]

Let us assume tibia and femur are in the same plane when the tibia is flexed at 90°. As the knee starts to extend, tibia will depart from this plane and starts to move outwards. It also rotates externally during extension. In order to design an effective brace that would follow the knee movement from full flexion to full extension, we need to consider this outward rotation and departing. The brace should have enough flexibility to allow the knee to follow its natural path. Otherwise undesired forces will be applied to the knee and the sensors.

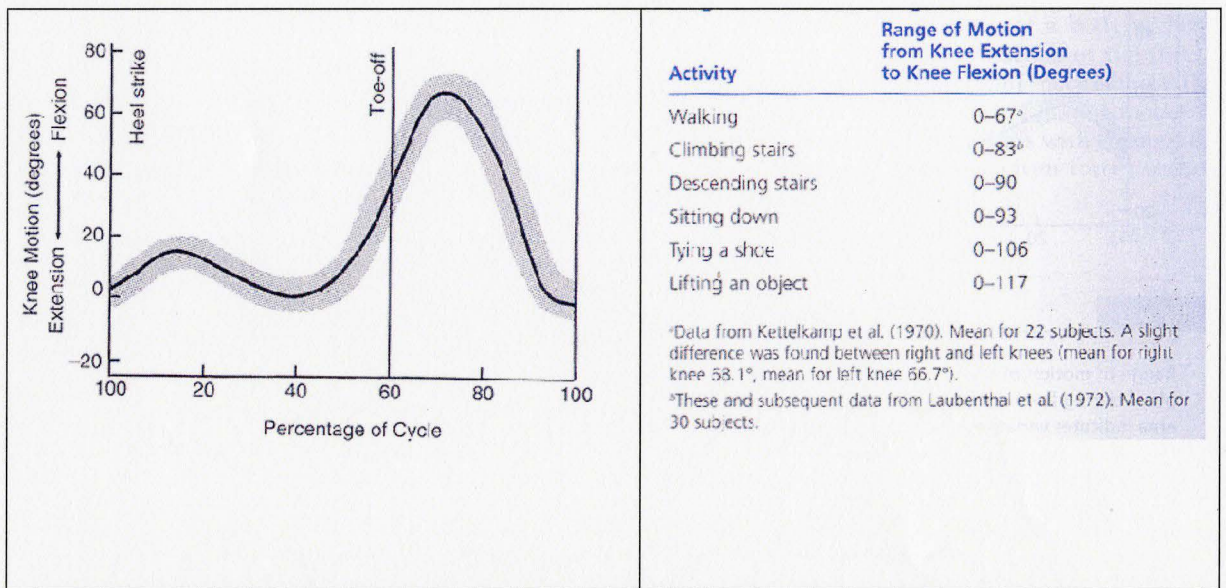


Figure 8: A) Range of motion of the tibiofemoral joint in the sagittal plane during level walking in one gait cycle. The shaded area indicates variation among 60 subjects (age range 20 to 65). B) Range of tibiofemoral joint motion in the sagittal plane during common activities (adopted from [50])

2.3.1 Surface motion of tibiofemoral joint

Surface motion between articulating surfaces in a joint can be measured using stereophotogrammetric methods [27]. However due to the complexity of this technique an older yet simpler method developed by Reulaux (1878) is still being used. This method is called instant centre of motion and tends to find the centre of relative motion between two joints in the uniplanar space. In this method, the centre of motion is found in the sagittal or in the frontal plane. A centre of motion at each instance is a point in the space on the link (bone) that has zero velocity with respect to other link.

Finding centre of motion for tibiofemoral joint:

In order to find the centre of motion for tibiofemoral joint, after fixing one link (one of the bones, usually tibia) two fixed points are selected and marked on the moving link. XRAY images are taken from the knee at different positions (angles) and these points are marked on each image. After flexing the knee in several steps and marking the location of the two points on images, the pictures are overlapped and for each marker, adjacent points (identified after moving the knee several steps) are connected to each other with lines. For each angle (step) the bisector of these connecting links for each marker will give the instant centre of motion of the joint (Figure 9). This method however has a drawback; the centre of motion identified this way is a projection of the actual knee motion into the image (usually sagittal) plane. But the fact is that knee is rotating in the three dimensional space. Recording the centre of motion this way implies that knee

motion is a combination of sliding and gliding moves and does not have a fix axis of rotation.

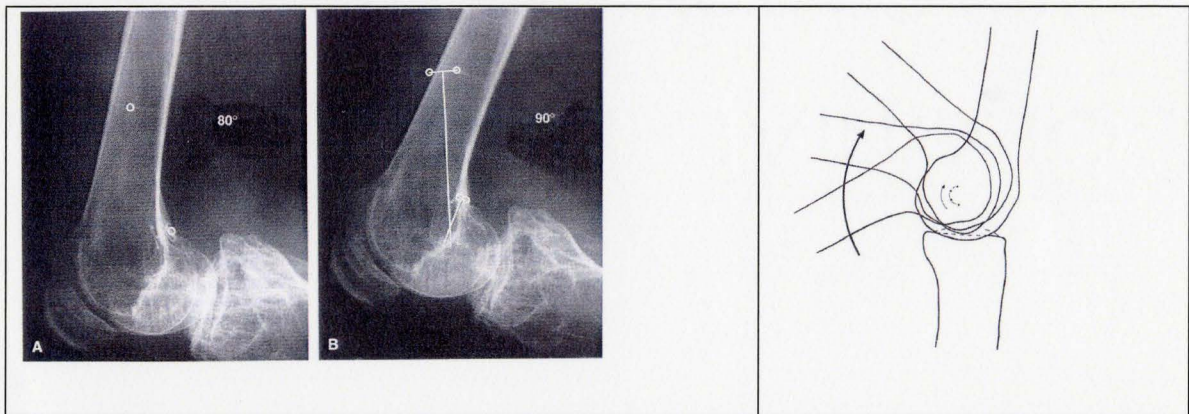


Figure 9: locating the instant center. B) Semicircular instant center pathway for tibiofemoral joint in a 19-year old man with normal knee (in sagittal plane) (adopted from [50])

Hollister et al [28] revealed that knee joint, in fact does have a fixed axis of rotation. Using mechanical axis finder they managed to find the axis of rotation for 7 fresh specimens. According to their paper, the flexion/extension (FE) axis runs through the collateral ligament origins and superior to the intersection of the cruciate ligaments. They also managed to confirm the results using MRI scanning. They conclude that motion of human knee occur about two fixed, non-orthogonal axes. The study claims that knee motion is pure rotation about these axes the FE axis is not in the coronal plane, nor is LR in the sagittal plain. Most of motion takes place in sagittal plane but there is still rotation and motion outside of this plane. For more details on this study refer to Appendix B.

2.3.2 Surface motion of patellofemoral joint

The skin surface of patella is the most exposed surface of the knee. Therefore it is a very suitable spot for placing vibration sensors. However since the patella slides a significant distance under the skin it is important to be able to track its movement by the brace. It is also important to maintain a fixed amount of force on the sensors to avoid change of signal magnitude. Understanding the patellar motion and knowing its approximate centre of motion enables us to track its movement and maintain constant pressure on the sensor as well as minimize unwanted skin movement underneath the sensors.

According to Nordin and Frankel, during FE motion, the patella articulates to both facets of the femoral condyle. The average articulation distance is about 7 cm. At full extension the patella sinks into the inter-condylar groove (Good fellow et al). Beyond 90° flexion, patella rotates externally and only the medial side of the condyles articulates with the patella (see Figure 10b). The centre of motion for the patellofemoral articulation can also be found using the technique described in the last subsection (Figure 10a).

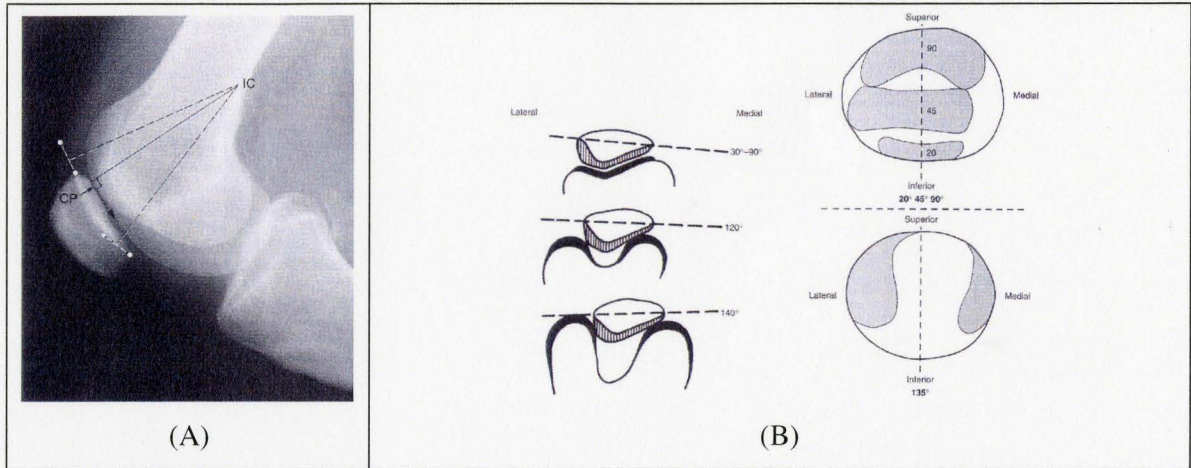


Figure 10: A) Determining the instant center of patella in sagittal plane. B) The position of patella at different ranges of knee flexion motion (left). Contact areas during different degrees of flexion. Beyond 90° of flexion, the patella rotates slightly outwards.

(adopted from [50])

2.3.3 Skin-bone movement

Sati et al [29] in 1995 conducted a set of experiments to measure and mathematically estimate the skin movement at various locations on the knee joint. They found that skin bone movement varies significantly over medial and lateral condyles (2 to 17 mm). This problem adds to the fact that patella moves a great distance under the skin. In other words it is not practical to maintain a constant fix position for the sensors as the knee is doing the FE cycle. We are required to maintain the position on the knee by tracking the movement of the bone underneath. The method for performing such task is discussed in the coming chapters.

2.4 Summary

This anatomy and kinematics literature review indicates that FE cycle of the knee is not just a simple two dimensional, uniplanar motion. Because of the offset of the FE axis from sagittal plane and the conical shape of the femoral condyles, a combination of sagittal, varus/valgus and rotational motion is observed. As it will be discussed in the coming chapters, one of the problems of using rigid knee braces for securing sensing devices to the knee is that they only allow movement in sagittal plane with little flexibility in other directions. This is in addition to the fact that different people have different knee sizes and therefore different sizes of brace must be prepared for different people.

Another issue that was raised here is the surface motion of the patellofemoral joint. As mentioned before the patella on average, moves a distance of 7 cm on in the condylar groove under the skin. If a sensor was placed directly on the patella in the flexed position, after extension it will not maintain its position with respect to the patella. This is because the skin does not move as much as patella does. Another problem is maintaining constant forces being applied to the sensors through out the FE cycle or at least keeping them within a specific range to have proper contact between the sensors and the bone. This problem can be solved by finding the approximate centre of motion for the patellofemoral joint. As we will see later, by placing the rotation axis of the force within a close proximity of joint's rotation axis we can reduce the variation of the force and keep its direction perpendicular to the surface.

Chapter 3

Knee diseases

3.1 Osteoarthritis²²

Osteoarthritis (OA) is referred to abnormalities; biological events and physical deformities that would lead to degeneration of articular cartilage matrix or the surrounding bone structures in synovial joints. This degeneration will restrict normal functions of the joint and will eventually lead to pain and disability. OA can be a result of both natural and imposed causes. Depending on the initiating source, OA is divided into two groups, primary and secondary; primary is the group of OA that has been initiated by natural causes such as genetic disorders or diseases that would lead to changes in the biomaterial or biochemical structure of the joints and thus their weakness. These changes will eventually lead to OA. Primary type of OA in general occurs in both knees simultaneously. The secondary type of OA usually happens in one knee rather than both. This type is usually caused by factors such as joint injury. There are several factors that affect development and progression rate of OA:

Weight

One of the major factors that accelerate development of OA is excessive body weight. Studies show that a higher body mass index (BMI) increases the risk of bilateral knee OA

²² Most of the content of this chapter have been adapted from [51] please refer to the book for more information

[30]. Other studies show that development of OA due to higher BMI will involve both patellofemoral and tibiofemoral joints [31, 32].

Age

As people grow older, many of the biological functions of the body including the reparability of the articular surfaces slow down. The composition of the articular cartilage changes and the muscles become weaker. These factors increase the risk of developing osteoarthritis. A longitudinal study on women between the ages of 50 to 70 done by Hart et al. [33] shows that knee osteophyte development increases 4% every year.

Gender

Women have more risk of developing OA than men [5, 7]. The reason for this increased risk could be due to various factors such as hormonal changes in the body, weaker muscle strength and higher BMI in women. The volume of cartilage in general is greater in men than women. However if the cartilage volume is adjusted for differences in height, weight, and bone size this difference greatly reduces [34]. In general the difference in cartilage volume between men and women is only because men have larger joint surface area and not because of thicker cartilage [35].

Activity and Sports

Although the articular cartilage in synovial joints requires regular loading and exercise, extreme activities: that is prolonged and/or excessive loading of the joint can also increase the damage risk. Jobs that require regular knee bending such as carpentry and

floor laying can increase the risk of OA [7]. Kujala et al [36] studied development of OA among female athletes in different fields of sports. They realized that soccer players have higher risk of developing tibiofemoral OA and in the case of patellofemoral OA; weight lifters have the highest prevalence. Again sports that require prolong hours of kneeling and knee bending or lifting contribute to development of patellofemoral OA

Injury

Knee injury can directly or indirectly lead to development of OA. Direct damage to the cartilage surface or weakening of the meniscus or ligaments can be cause of primary or secondary types of OA. Patients who have torn meniscus or have their meniscus removed, almost double the rate of cartilage degeneration (14% total volume lost versus 6% in patients with healthy meniscus, over a two year period study) [37].

3.1.1 Symptoms and stages of OA

The factors mentioned above each can contribute in a different way to OA but overall, inability of the body to repair damaged cartilage at the same rate as degeneration leads to development of this disease. As mentioned previously, excessive loading, aging and some joint diseases can change the structure of cartilage and prevent it from performing as required. Also long term immobilization of the knee and not loading it regularly can make cartilage tissue vulnerable. There is no vasculature inside the articulating surface and it receives nutrients from circulation of synovium in the porous surface of the cartilage. Synovium circulates inside the cartilage tissue under regular loadings of the knee. Therefore when the knee is not loaded regularly and is immobilized for long term,

nutrients can not reach the articular surface which in turn will lead to degeneration or death of the cartilage cells [38, 39]. Cartilage is a porous permeable surface reinforced by collagen fibers. This porous surface is filled with water (Figure 11b). The surface of the cartilage is lubricated by synovium. Presence of cosminglycan molecules and special chemicals inside the articular cartilage, which increase the negative charge inside the cartilage surface, greatly influences its mechanical and osmosis properties. Formation of a film of water between the articulating surfaces is the result of this property and is the main reason for very low friction coefficient between articulating surfaces. Water acts as a bearing and therefore articulating surfaces hardly have any contact at all. And in case of any contact, the synovium fluid acts as a lubricant which further more reduces any possible damage to cartilage.

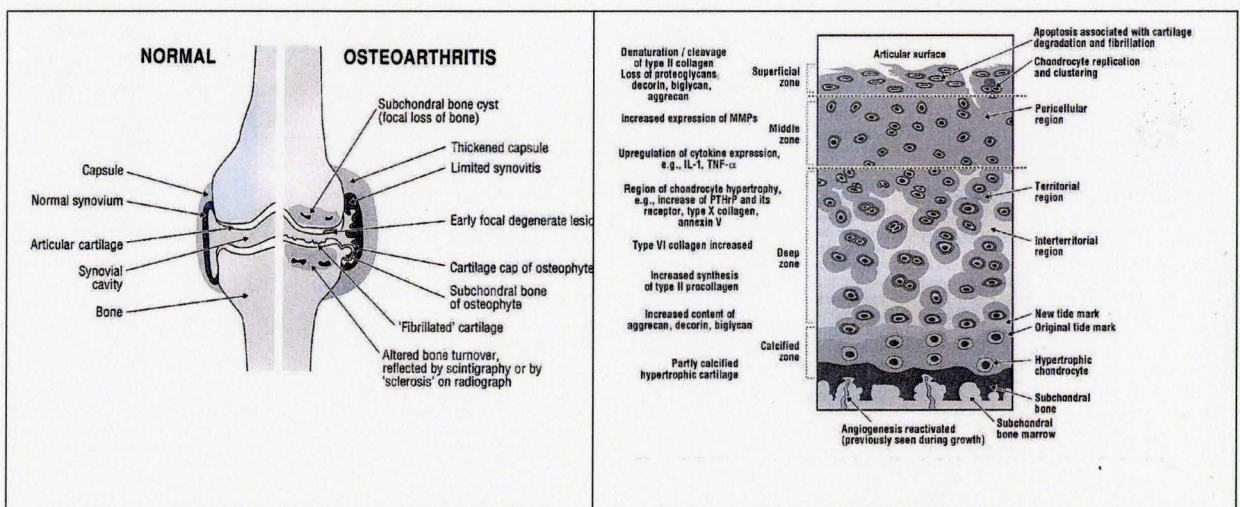


Figure 11: A) schematics of healthy versus osteoarthritic joint. B) a closer look at the structure changes of the articular cartilage in OA (taken from [51])

The chemical and biomechanical properties of cartilage change as people age. Reduced level of osmosis leads to increased friction coefficient. The tensile strength of the

cartilage fibers also decreases, which in turn increases the risk of damage to articulating surfaces. Continuous damage to the cartilage and its inability to repair with the same speed eventually leads to destruction of the cartilage layer and exposure of the bone (Figure 11a). Partially, some of the lost cartilage is replaced by “repair cartilage” but this cartilage has different characteristics; less proteoglycan in the matrix, which is of major importance in maintaining osmosis properties, decreases the ability to withstand loadings as well as the hyaline cartilage. Osteoarthritis starts by fibrillation of the articulating surface. These loose fibers eventually penetrate the cartilage surface and cause further damage. Chondromalacia or softening of articular cartilage and cartilage fibrillation are early signs of osteoarthritis. The following figure shows the MRI images of a healthy and a knee joint surface with severe damage to the cartilage. In the healthy joint the cartilage has a clear margin whereas the damaged joint the cartilage is lost in various locations and the signal is not clear.

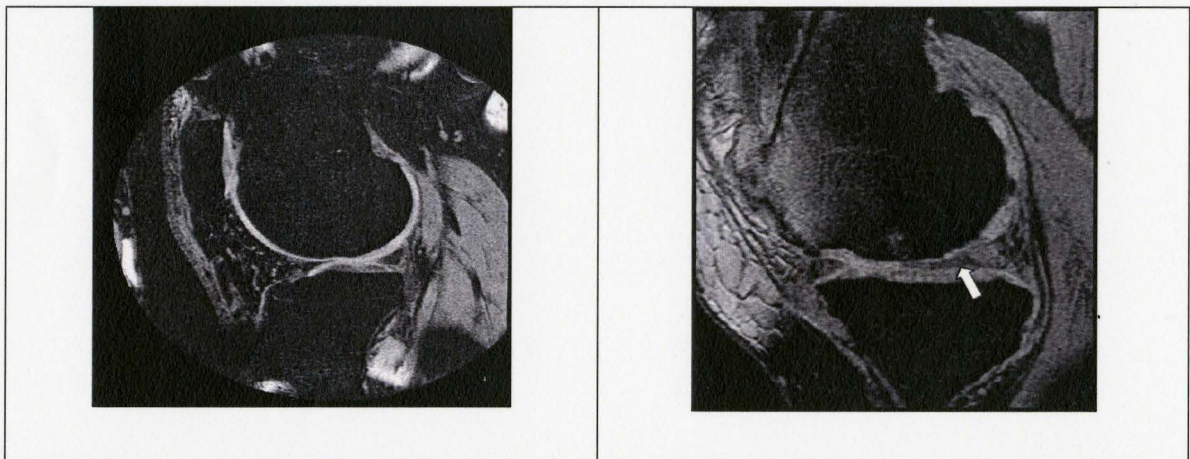


Figure 12: T1-weighted 3D gradient echo images of a healthy knee joint (left) and a knee joint with severe damage to cartilage

An osteophyte is a formation of bone and cartilage at areas peripheral to articulating surfaces. In addition to osteophyte, subchondral bone; the underlying bony surface of cartilage also becomes affected by damage to articulating surfaces. Deformation of subchondral bone on the margins of bone constitutes osteophytes. It is not clear why osteophytes form but studies show that they may help stabilize osteoarthritic joints [40].

3.1.2 Symptoms of OA

In osteoarthritis the symptoms vary from person to person but overall, pain, stiffness, limited motion and crepitus are common among patients.

Pain

Pain is the first and most dominant symptom of OA. However studies show that there is no direct correlation between pain and loss of cartilage. Study done by Felson et al shows bone marrow swelling or edema strongly correlates with pain in patients [41]. Another study done by Kijowsky et al [42] indicates that in addition to bone marrow edema (BME) there is a strong correlation between pain location and meniscus tear location. They point out that other factors than BME must be responsible for knee pain. In the early stages of OA the occurrence of pain is limited to extreme loading conditions and usually dissipates by resting and unloading the knee but at later stages of OA more frequent occurrence is reported. At the end stages the pain becomes chronic and persistent [43].

Stiffness and limited joint function

Stiffness of knee refers to slowness and tightness of the knee in the mornings and usually does not last for more than 30 minutes. OA may limit the joint function. Limited range of motion is associated with muscle weakness and increased cartilage friction, which makes moving the knee harder. It is sometimes accompanied by pain [44].

Crepitus

“Crepitus is an audible or palpable sensation of roughness, crinkling or crackling over a joint during active or passive movement [26]. In a study done by O'Rourke et al on OA patients, they compared the crepitus felt at different compartments of knee joint with arthroscopic observations. They found very strong correlation between cartilage damage and crepitus when knee motion was assisted by stressing maneuvers [13]

In addition to, the above factors, there are other signs such as musculature changes, joint malalignment and joint enlargement that would show up in OA patients.

3.1.3 Clinical diagnostic tools of OA

There are several tools and techniques that aid physicians in the diagnosis of osteoarthritis; one of which is radiography. Although routine radiography can detect changes such as bone deformation, presence of osteophytes and cyst and narrowing of joint space, it can not detect signs of early stages of OA such as fibrillation or meniscus damage. Figure 13 shows angulation and formation of osteophyte in two knees with severe osteoarthritis.

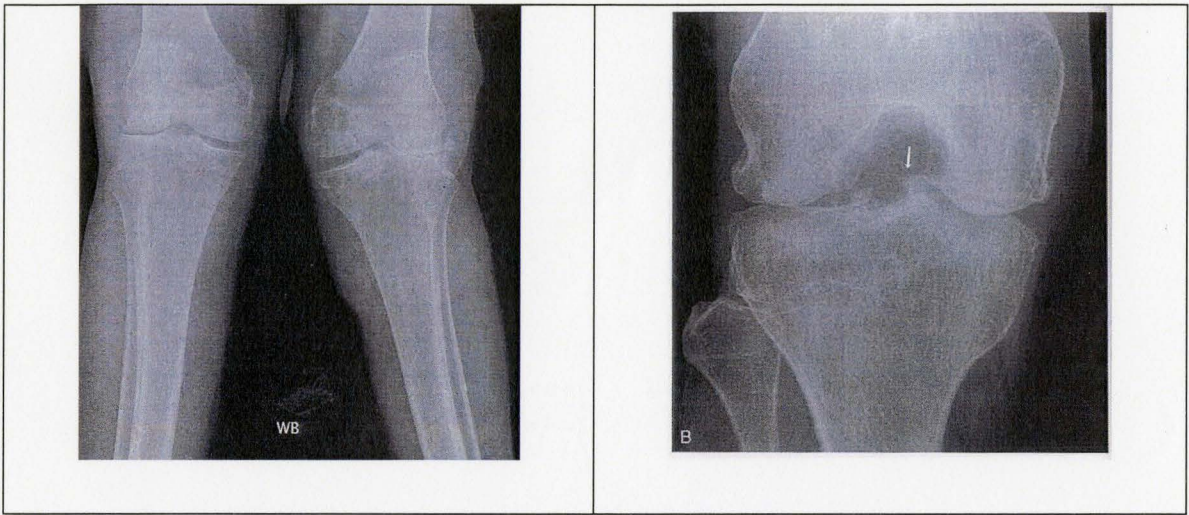


Figure 13: x-ray images of OA knee. Left) angulation of the knee due to severe lateral compartment OA. Right) loss of joint space and appearance of osteophytes are present in the picture. Taken from [51]

Magnetic resonance imaging (MRI) is the state of the art in medical imaging. MRI is based on the response of paramagnetic atoms such as hydrogen to RF disturbances in the presence of strong magnetic fields. Based on the frequency and timing of the RF pulses, it is possible to create 3D images of different sections of the body. By changing the settings on the MRI machine it is possible to take images at different contrasts for different types of tissue (see Figure 14). There has been much attention to the application of MRI in diagnosing osteoarthritis. Compared to radiography imaging, MRI can provide images from various depths of the body, and has the ability to visualize soft tissue clearly. Ability to visualize soft tissue enables physicians to detect changes to cartilage surface which are the earlier signs of osteoarthritis compared to X-Ray imaging signs (see for example Figure 15). Despite these facts even MRI imaging is not sensitive enough to detect

preclinical symptoms of OA such as cartilage softening and fibrillation [45]. MRI does not radiate any harmful radiation, which makes it one of the safest body imaging techniques that has been developed. On the other hand MRI is very expensive and is not as accessible as radiography machines.

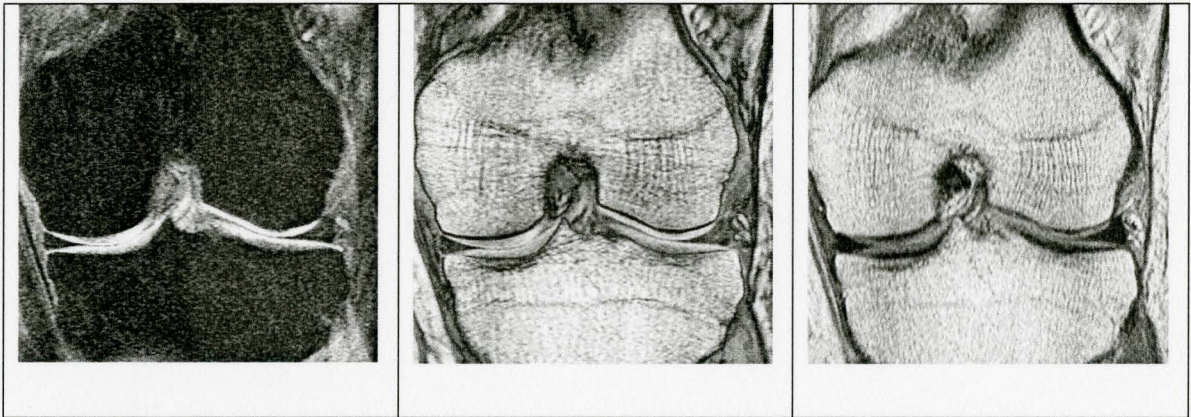


Figure 14: MRI images of the knee at different machine settings; fat suppressed t1 weighted 3D gradient echo (left), Proton density (middle) and t2 weighted (right) images

In addition to x-ray and MRI there are also other technologies, such as Cat-Scan and Ultrasound that have been used for diagnostic of OA but overall the most widely used technique still remains x-ray imaging. Since X-ray imaging can not detect OA at early stages, and MRI imaging still remaining a costly, not readily available procedure, there is need for other technologies and tools that would help physicians detect joint degeneration at early stages.

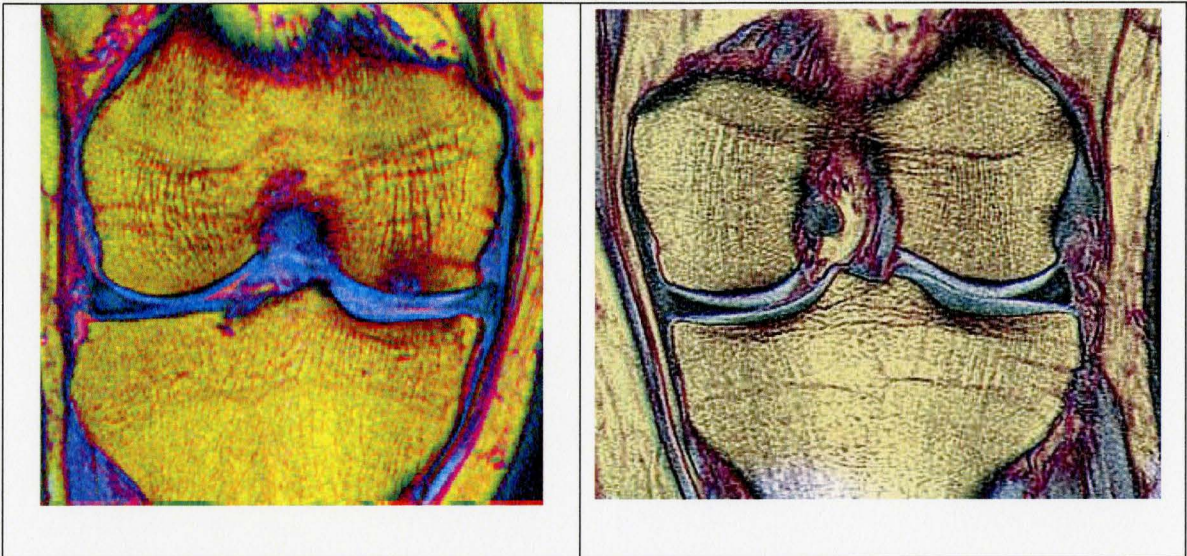


Figure 15: osteoarthritic (left) versus healthy knee (right). Damage to meniscus, cartilage surface and subchondral bone are clearly visible. Image has been colorized based on different T weights of MRI

3.2 Meniscus and ACL damages

Meniscus and ACL tears are usually results of extreme loading or actions in sports activities. Damage to either one can, in the long term, lead to degeneration of articular surfaces. Meniscus degeneration is very common in patients with osteoarthritis. Common symptoms of meniscus tear are knee pain, swelling of the knee, tenderness, popping and limited motion of the knee. Radiography is used to diagnose meniscus tear, however it can only show the after effects of meniscus tear such as degenerative or arthritic changes of the knee joint. MRI can visualize the soft tissues (cartilage and meniscus) but is expensive.

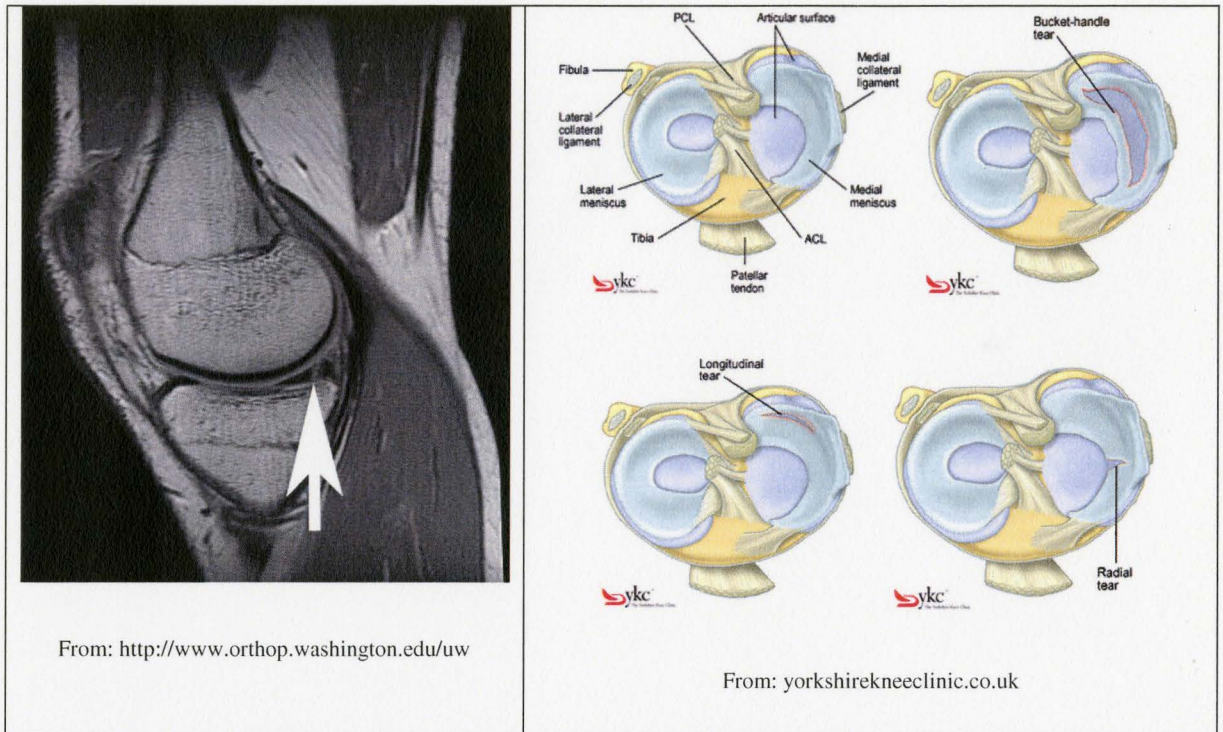


Figure 16: Left) meniscus tear shown in MRI Image, Right) different types of meniscus tear

3.3 Discussion and summary

In this chapter we briefly discussed one of the major joint diseases; osteoarthritis, its progression and the factors that initiate and accelerate it. We also discussed the signs and symptoms that usually occur during development of OA. In the last section some of the tools and technologies that help physicians detect OA were discussed and it was concluded that there is still need for cheaper and more convenient tools and technologies for detection and diagnostic of OA, particularly in the early stages.

Chapter 4

Analysis of joint using vibration

4.1 Clinical Studies

This chapter builds upon previous research done by Yacoub [14], who showed that there is a strong relationship between recorded knee vibrations and severity of osteoarthritis. The goal of this work was to further investigate this correlation with more advanced equipment and apparatus and to find correlation between knee vibrations and MRI scores. In Yacoub's work vibration from three different locations of the knee were recorded by hand holding the accelerometers on the skin. Holding the accelerometers on the skin is a subjective and tedious process and for each location on the knee it requires the patients to repeat the test. It was decided to improve this method by designing and building a brace that would firmly hold 5 sensors on the skin simultaneously. Sensors should be located on the patella, lateral and medial femur and lateral and medial tibia. More details about the brace are available in the next subsection. After the brace was successfully tested and ready for tests and ethics approval obtained for continuation of the research, we recruited 50 volunteers for the study. Both knees of each patient were imaged by a radiologist (Hao Wu) using the one Tesla MRI machine (Ortho-One) available in St. Joseph Hospital's rheumatology clinic. After the MRI, their knee vibrations were recorded during a series of activities; swinging the knee, squatting and impact. Patients were recruited from a wide range of age groups (20 to 78) with different grades of osteoarthritis (healthy to

severe OA). Out of 50 patients 20 were men and 30 were women. In general, there is more occurrence of osteoarthritis in women than men [30].

For each knee, 4 sets of MRI images were captured:

- Sagittal, fat-suppressed, T1 weighted, 3D gradient echo
- T1 weighted, Fast Spin Echo in coronal plane
- Sagittal inversion recovery FSE sequence
- T2 weighted fat-suppressed FSE in axial plane

These images were later analyzed by a radiologist (Hao Wu) to complete a score sheet that identified different problems and its level of severity at different compartments of each knee. Knee vibrations from both knees of each patient were recorded. In the first step of the vibration test, after putting the brace on the patient's knee, they were asked to sit on a bench and swing the knee from 0 (fully flexed) to approximately 90 degrees several times at an approximate rate of 0.5 cycle per second, continuously for 20 seconds. The accelerometers continuously recorded the vibrations and the instantaneous knee angle (angle between thigh and shin) of the knee. In order to have a measure of repeatability of the test, each test was repeated three times, and before each repeat, the sensors or the brace were displaced a little to make sure the results are repeatable and not corrupted because of improper skin-sensor contact. Due to the short time available for each test, it was not possible to dismount and remount the brace again. So we had to

restrict ourselves by just displacing the sensors. In the second part of the test, patients were asked to stand up with their weight evenly distributed on both legs. Then they were asked to squat for 20 seconds in a range of 0 (fully extended) to 45 degrees. Again like the previous part, this test was repeated 3 times with sensors or the brace displaced before each sequence. In the last part of the test, patients were asked to stand still with the knee bent (5 to 10 degrees from fully extended). Then they were gently tapped on the shin several times with an impact hammer. Both the impact hammers input signal and the response signals by the accelerometers were recorded during the test. Again like previous parts we displaced the sensors couple of times during the test to have a measure of repeatability of the test.

Each set of MRI images were analyzed by a radiologist. The surface of the knee was divided into 5 compartments; lateral and medial femur, lateral and medial tibia and the patella. For each compartment, the following observations were graded based on the level of their severity:

- **Cartilage grading;** the level of damage to articular cartilage, with a zero to four grade: Grade 0: healthy with clear bright cartilage surface and completely visible edges, Grade 1: one adjacent images area of low signal intensity (SI) extending to normal cartilage surface, Grade 2: mild cartilage surface irregularity, with focal defect less than $\frac{1}{2}$ the thickness of the cartilage, Grade 3: sever surface irregularity or defect with more then half of the thickness of the cartilage but not exposed to bone, Grade 4: Cartilage defect exposing bone

MRI Scoring Sheet

Patient ID: _____ Date of MRI: _____
 Date of Scoring: _____ Scoring Physician: _____

Artifacts: a) Motion Artifact: 0 1 2 3 b) Susceptibility Artifact: 0 1 2 3 c) Image Noise: 0 1 2 3 d) Fat Saturation: 0 1 2 3	Image Contrast: a) Cartilage and bone: 0 1 2 3 b) Cartilage and fluid: 0 1 2 3 c) Cartilage and fat: 0 1 2 3 d) Cartilage and meniscus: 0 1 2 3 e) Bone and fluid: 0 1 2 3
--	--

	Medial Femur	Lateral Femur	Medial Tibia	Lateral Tibia	Trochlea	Patella
Car Grad. (0–4)						
Sub Cyst (0–3)						
BME (0–3)						
Osteophyte (0-2)						

Cartilage Grading:
 Grade 0: normal
 Grade 1: one adjacent images area of low SI extending to normal cartilage surface
 Grade 2: mild cartilage surface irregularity, focal defect < 1/2 thickness
 Grade 3: severe surface irregularity or defect > 1/2 < full thickness
 Grade 4: Cartilage defect exposing bone

Bone Marrow Edema (BME): 0= none 1:mild (<1 cm) 2= moderate (1-2 cm) 3=severe (>2 cm)
Subchondral Cyst : 0 = none, 1 = mild (<1cm) , 2 = moderate (1-2 cm) 3= severe (>2cm)
Osteophyte 0 = none, 1 = present (<0.5 cm in length), 2 = Present (>0.5 in length)

Meniscus:
 [0= normal, 1= degeneration (inter substance high SI); 2= tear (high SI extending to articular surface)]

Medial AH	Medial PH	Lateral AH	Lateral PH
0 1 2	0 1 2	0 1 2	0 1 2

Ligaments:
 [0 = no tear, 0.5 = partial tear 1 = tear]

ACL	PCL	Patellar Tendon
0 0.5 1	0 0.5 1	0 0.5 1

Loose Body: Absent Present
Popliteal Cyst : Absent Present
Joint Effusion none mild moderate severe

Figure 17: MRI score sheet used for this study

Following table summarizes the X and Y variables used in this study:

of severity, meaning that if 80 percent of cartilage is healthy but 20% has grade 3 degeneration, then grade three is assigned, as the score, to that cartilage region²⁵. Figure 17 shows a sample of MRI score sheet used for the study.

²⁵ Since this method is not a strong indicator, it was corrected later for the future analysis. the analysis done in this thesis are based on the method mentioned in the text

MRI Scoring Sheet

Patient ID: _____ Date of MRI: _____
 Date of Scoring: _____ Scoring Physician: _____

Artifacts: a) Motion Artifact: 0 1 2 3 b) Susceptibility Artifact: 0 1 2 3 c) Image Noise: 0 1 2 3 d) Fat Saturation: 0 1 2 3	Image Contrast: a) Cartilage and bone: 0 1 2 3 b) Cartilage and fluid: 0 1 2 3 c) Cartilage and fat: 0 1 2 3 d) Cartilage and meniscus: 0 1 2 3 e) Bone and fluid: 0 1 2 3
--	--

	Medial Femur	Lateral Femur	Medial Tibia	Lateral Tibia	Trochlea	Patella
Car Grad. (0-4)						
Sub Cyst (0-3)						
BME (0-3)						
Osteophyte (0-2)						

Cartilage Grading:
 Grade 0: normal
 Grade 1: one adjacent images area of low SI extending to normal cartilage surface
 Grade 2: mild cartilage surface irregularity, focal defect < ½ thickness
 Grade 3: severe surface irregularity or defect > ½ < full thickness
 Grade 4: Cartilage defect exposing bone

Bone Marrow Edema (BME): 0: none 1:mild (<1 cm) 2= moderate (1-2 cm) 3:severe (>2 cm)
Subchondral Cyst : 0 = none, 1 = mild (<1cm), 2 = moderate (1-2 cm) 3= severe (>2cm)
Osteophyte 0 = none, 1 = present (<0.5 cm in length), 2 = Present (>0.5 in length)

Meniscus:
 [0= normal, 1= degeneration (inter substance high SI); 2= tear (high SI extending to articular surface)]

Medial AH	Medial PH	Lateral AH	Lateral PH
0 1 2	0 1 2	0 1 2	0 1 2

Ligaments:
 [0 = no tear, 0.5 = partial tear 1 = tear]

ACL	PCL	Patellar Tendon
0 0.5 1	0 0.5 1	0 0.5 1

Loose Body: Absent Present
Popliteal Cyst : Absent Present
Joint Effusion none mild moderate severe

Figure 17: MRI score sheet used for this study

Following table summarizes the X and Y variables used in this study:

X variables		Y variables	
Sitting position:	Vibration from: Patella Medial side of tibia Lateral side of tibia Medial side of femur Lateral side of femur Angle of the knee during cycle	Medial femur:	Cartilage grading; (0 – 4) Osteophytes; (0 – 3) BME; (0 – 3) Subchondral cyst; (0 – 2)
		Lateral femur:	Cartilage grading; (0 – 4) Osteophytes; (0 – 3) BME; (0 – 3) Subchondral cyst; (0 – 2)
Standing Position:	Vibration from: Patella Medial side of tibia Lateral side of tibia Medial side of femur Lateral side of femur Angle of the knee during cycle	Medial Tibia	Cartilage grading; (0 – 4) Osteophytes; (0 – 3) BME; (0 – 3) Subchondral cyst; (0 – 2)
		Lateral Tibia	Cartilage grading; (0 – 4) Osteophytes; (0 – 3) BME; (0 – 3) Subchondral cyst; (0 – 2)
		Patella	Cartilage grading; (0 – 4) Osteophytes; (0 – 3) BME; (0 – 3) Subchondral cyst; (0 – 2)
Impact test:	Impulse response recorded at: Patella Medial side of tibia Lateral side of tibia Medial side of femur Lateral side of femur Input impulse transmitted by the hammer	Meniscus health: (0 – 2)	Lateral posterior horn Medial posterior horn Lateral anterior horn Medial posterior horn
		ACL health, PCL health, Patellar tendon health (0 – 1) Presence of loose body (0 – 1), Popliteal cyst: (0 – 1), Joint effusion level (0 – 3)	
Patient’s height, weight and age			

Table 1: X and Y variables obtained from MRI and vibration recordings of the knee

4.2 Brace Design

4.2.1 Mechanical Hardware

The accelerometers used for this research project require a firm grip to the skin to record signals properly. These types of sensors are very sensitive to vibration (1000 mv/g) and even the slightest vibration transmitted through external equipment will be picked up by them. On the other hand the brace must be adjustable to different knee sizes and must adapt to the motion of the knee without restricting its natural movement. It must also be comfortable enough for patients to be put on for several minutes without causing pain.

In the first attempt, a commercial brace was employed and the sensors were mounted on it. After carefully examining the brace on the knee, we noted several problems that required us to change the overall design. First problem was the noise generated by the rigid hinges of the brace. The noise could easily be picked up by the sensors and therefore corrupt the vibration signal from the knee. Another problem was the time and experience that was needed to put on and to adjust the brace on the knee. If the brace was not put on properly it would start moving on the knee and relocate the sensors. Because of its relatively heavy weight, the brace needed to be rapped around the thigh or otherwise it would slide down. During the flexion/extension (FE) cycles, the quadriceps muscles generate a lot of vibration due to expansion and contraction. Because of the rigid design of the brace, these vibrations are transmitted through the brace arms to the sensors.



Figure 18: universal commercial brace donated by GII Orthotics Inc

Because of the problems mentioned above, we realized it would be best if we designed our own brace from scratch and consider these essential characteristics into it. Overall the brace should have the following properties:

- 1- provide a secure tight fit for the sensors on the knee
- 2- be adjustable to different knee sizes
- 3- should be comfortable for the patient
- 4- produce minimum amount of mechanical noise and vibration
- 5- be able to track the patellar movement under the skin
- 6- adapt to the off-sagittal motion of the knee
- 7- prevent/minimize displacement of the sensors on the skin

The very first and most important feature that must be embedded in the brace design is the ability to hold the sensors on the knee at proper locations and to provide a firm grip

on the skin. The second important issue to the design is the adjustability of the brace for different knee sizes. We realized that the best solution to these problems would be to use stretchable rubber bands to hold the sensors around the knee. Using rubber bands also eliminates the mechanical noise generated by the solid hinges in the previous brace design. It also makes the brace very lightweight and eliminates the need for wrapping it around the thigh for more stability. It was also important that the brace adapt to the off plane motions of the knee. In the previous brace design, because of the solid rotational hinges used on the brace, the brace would have only allowed movement in the sagittal plane. Because of this inability to move off sagittal, stretching the knee could cause all the sensors to displace on the skin. In the new brace design, we solved this problem by separating the lower part of the brace from upper part. Lower part of the brace is supported by being wrapped around the shinbone using two rows of stretchable Velcro bands. Support for upper part of the brace is provided by a roller support on the back of the knee. The roller support also acts as a non-stationary hinge for the side arms; the ones that hold the accelerometers on the femur. During FE cycle, the only stationary point on the skin will be the sensors themselves and this prevents the sensors from sliding on the skin. Figure 19 to Figure 22 show the brace and its components and how it is mounted on the knee.

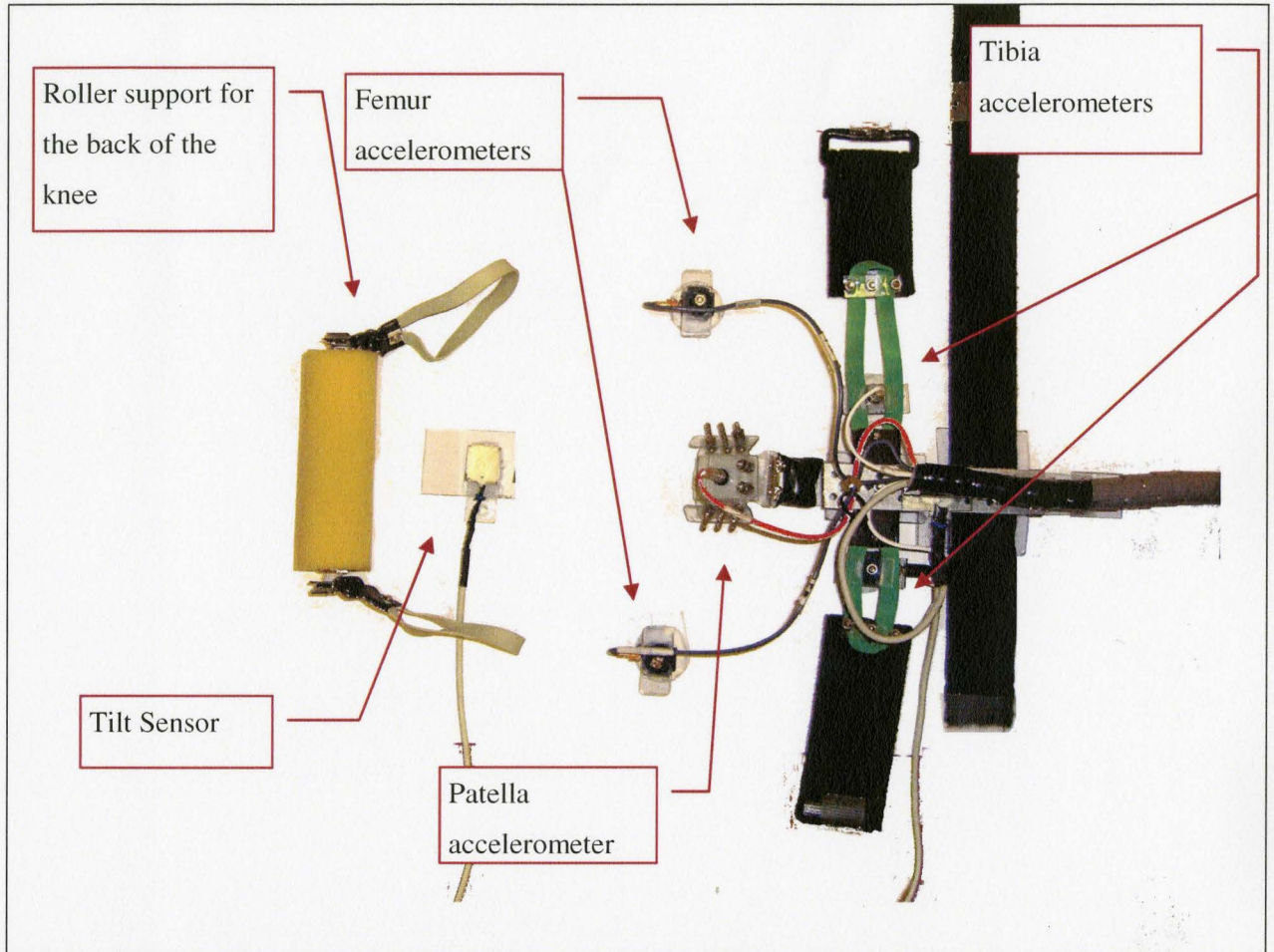


Figure 19: final design of the brace with accelerometers attached to it

As mentioned in previous section, the patella moves fairly a long distance on the femur and under the skin. If the patella sensor is only attached to the skin and not guided by external means, it would fail to track the patellar movement during the FE cycle. We discussed in the anatomy chapter that the patella is attached to the tibia by a ligament. During the FE cycle, the distance between patella and the attachment point on tibia always remains the same. With this knowledge we can solve the patella-tracking problem by extending an arm from patella sensor to the shinbone and securing it to the skin at the

attachment point of the patellar ligament and tibia. This extending arm is made of semi flexible plastic and can adapt to the bends and rotations of the patella but always keeps the same distance between the patella sensor and the tibia. This allows the patella sensors to always stay on top of the patella during the cycle. The length of the arm is adjustable through its lower end. This allows it to be adjusted for different patients.

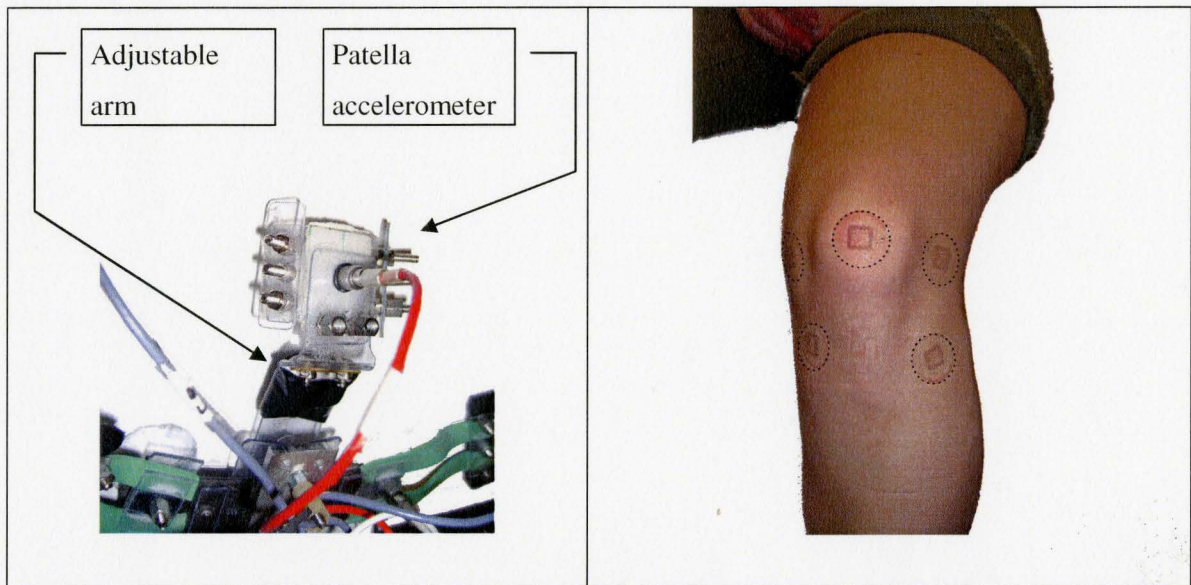


Figure 20: Left) Patella Sensor and the adjustable arm, Right) location of the sensors on the knee

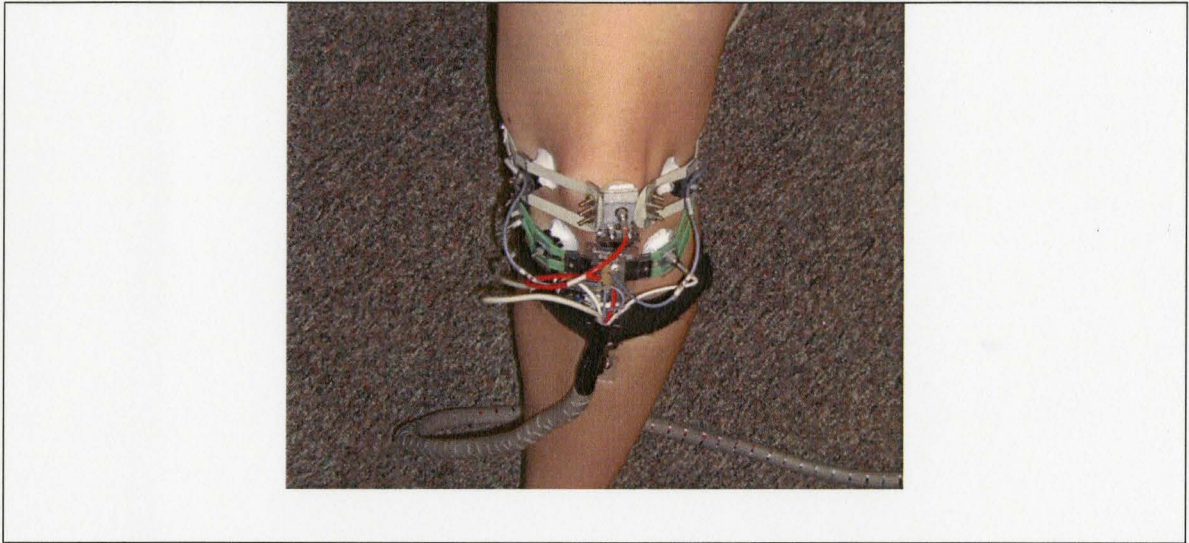


Figure 21: Top view of the brace assembled to the knee

The lower part of the brace supports the tibia sensors. Again elastic rubber bands provide tight adjustable and noise free grip for the sensors. Two rows of elastic bands with Velcro on the ends makes mounting of the brace very fast and easy.

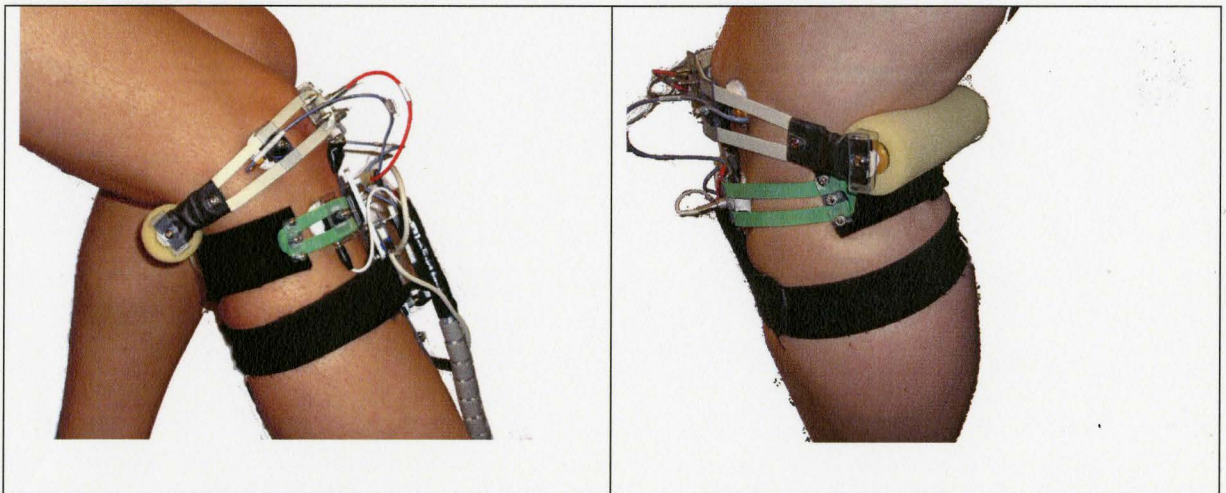


Figure 22: Side and rear views of the brace when mounted on the knee

Providing momentum and stability for the sensors:

The rubber bands holding the sensor in place, in addition to providing the vertical force on the accelerometer also provides horizontal force components in opposite directions that cancel each other. Since this source of horizontal force is at a distance away from the base of the sensor, any imbalance during the FE cycle can create a momentum that can cause the sensors to flip over. By increasing the base cross section of the sensors we were able to prevent the sensors from flipping over as a cause of these horizontal forces. Increasing the base cross section of the sensors also makes it more comfortable for the patient to wear.

4.2.2 Electronic hardware

The data acquisition hardware consists of 5 1000 mv/g ceramic shear ICP ® accelerometers (by PCB and Kjaer), two national instruments (NI) USB data acquisition boards, one miniature impact hammer and one electronic goniometer. Appendix A contains the details on electronic hardware used for this project. Figure 23 shows combination of these parts together:

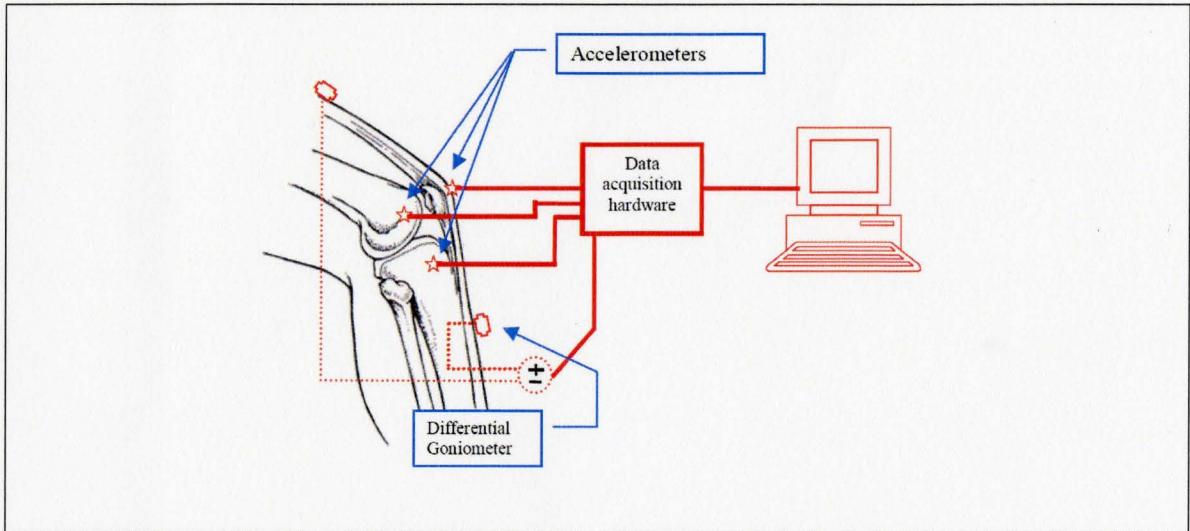


Figure 23 diagram of Data Acquisition hardware

Accelerometers:

5, 1000 mv/g accelerometers (Figure 24) are used to record the vibration from the surface of the skin. Inside each accelerometer there is a piezoelectric component that translates mechanical vibration into electronic voltage. These accelerometers are powered by a constant current power source. Using this type of accelerometer with external current source has several advantages:

- Fixed voltage sensitivity makes the output independent of the voltage or cable length
- Low impedance output signal greatly reduces the loss of signal quality
- Low wired operation using low cost coaxial data cables.
- Low noise voltage-output signal output makes them compatible with many data acquisition or signal processing equipment

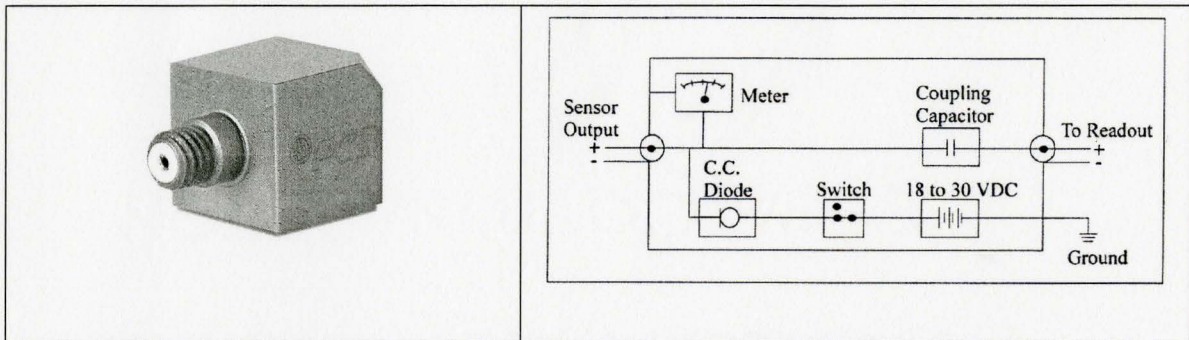


Figure 24: PCB 1000 mv/g accelerometers and their circuit diagram (right)

These accelerometers have high sensitivity and low susceptibility to external noise. The range of frequency related to knee joint problem has been reported to be in range of 0 to 1000 KHz [46]. However in order to prevent aliasing effects we need to record signals at much higher frequency rates. The recommended sampling rate is 10 times the maximum frequency. For this project we chose a sampling rate of 6250 Hz.

Impact Hammer:

Frequency response analysis is a method in which an input signal is introduced to a medium and the response traveling through the medium is recorded in another location. Analyzing the input/output relationship between the frequencies is called frequency response analysis. By analyzing the response of a system to an input signal it is possible to obtain information about its physical characteristics. For the purpose of this project we acquired a miniature, modally tuned impact hammer made by PCB® electronics (Figure 25). This type of hammer transmits an impulse signal to the medium upon impact. The small force sensor inside the hammer measures the amount of force being applied as a

function of time and converts it into voltage. This voltage is sent to the data acquisition device where it is converted into digital data and saved in to the computer's memory. These impact hammers are modally tuned and when they hit a hard surface, they transmit a near impulse force signal into the surface. Impulse input contains a wide range of frequencies. The range of frequency depends on the type of hammer tip and the surface hardness. As the signal travels through the system, depending on its physical characteristics some of the frequency components attenuate. By recording the output signal and comparing the output (accelerometer) frequency magnitudes to the input signal's frequency magnitude it is possible to calculate the impulse response of the system.

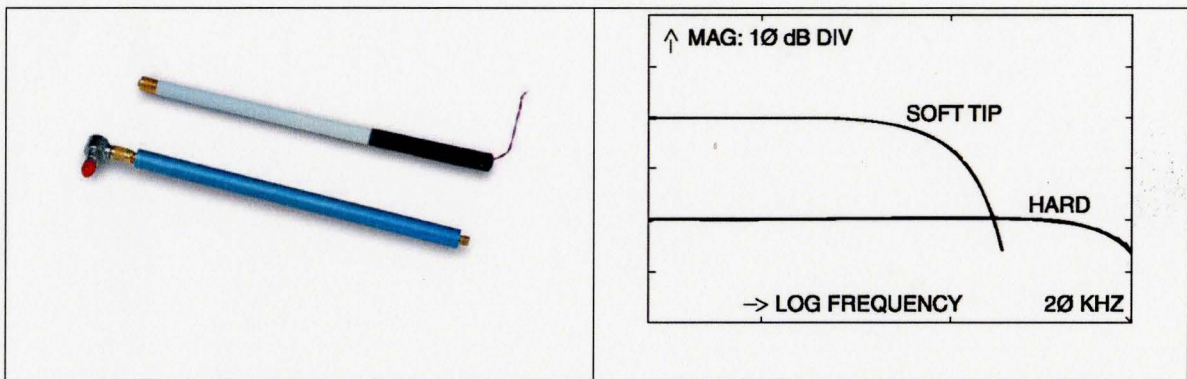


Figure 25: PCB miniature impact hammer and its frequency range diagram (right)

As a part of the tests, the patient is asked to stand still with knees slightly bent. The examiner then hits the patient carefully on the shin with the hammer. The response to this impulse is collected by the accelerometers and is saved into the computer's memory for later analysis. The aim is to see if the impulse response analysis can reveal any

information about the structure and quality of the knee joint such as cartilage thickness and meniscus health.

Electronic Goniometer

An electronic goniometer attached to the leg measures the relative angle between the thigh and the shinbone (Figure 23). The goniometer is composed of two tilt sensors, one placed on the shin and the other taped to the thigh. They are coupled in a series circuit and each accelerometer (tilt sensor) transmits a voltage proportional to its angle with the horizon. The difference between the two voltages from each tilt sensor will be proportional to the relative angle between the shin and thigh.

4.3 Summary

In the clinical studies section the procedures of the tests and the variables collected for each patient were described and discussed. In the next two sections of the chapter we talked about the hardware design for the project. Our experiments showed that commercial braces available in the market were not suitable for our purpose, therefore based on the previous findings in chapter 2; a brace was designed to securely mount the recording sensors to the knee. The newly designed brace was capable to mount the sensors securely to the knee, be flexible enough to follow movements of the knee without restricting it and was designed in such a way that could be mounted easily to the knee in a short time. In addition to the brace design we also talked about the electronic hardware employed for the study.

Chapter 5

Analysis and results

Analysis of data consists of two parts, preprocessing and feature extraction. In the preprocessing or preparation part, time domain data is converted into frequency or pseudo-frequency domain (using Wavelets) and then using PCA and PLS features related to responses (Y) and the “X” space are extracted from the ill conditioned data matrix.

Principal Component Analysis

In principal component analysis (PCA), principal directions that contain maximum amount of variance of the data matrix are found and used to reconstruct the data set or to regress against feature space variables. Mathematically speaking, finding principal components is equivalent to finding eigenvectors associated with largest eigenvalues of a matrix. Any matrix (X) regardless of its shape and condition number can be decomposed into:

$$X = U\Sigma V^T \quad (5.1)$$

Where U is an orthogonal matrix associated with eigenvectors of XX^T ; V is an orthogonal matrix associated with eigenvectors of $X^T X$ and Σ is a diagonal matrix with eigenvalues of X along its diagonal. Here, superscript T represents the transpose operator.

$$X = U\Sigma V^T \equiv U \begin{bmatrix} \sigma_1 & 0 & \cdots & 0 \\ 0 & \sigma_2 & \cdots & 0 \\ \vdots & \vdots & \ddots & \\ 0 & 0 & & 0 \end{bmatrix} V^T \quad (5.2)$$

Equation (5.2) can be written as the sum of outer products of U, Σ and V as:

$$X = \sigma_1 u_1 v_1 + \sigma_2 u_2 v_2 + \cdots + \sigma_n u_n v_n \quad (5.3)$$

Assuming $t_i = \sigma_i u_i$ and $p_i = v_i$, above equations will translate into standard notations for PCA. With the new notation X can be rewritten as:

$$X = t_1 p_1 + t_2 p_2 + \cdots + t_n p_n \quad (5.4)$$

Or

$$X = TP^T \rightarrow XP = T \quad (5.5)$$

Small t vectors are the principal component scores of matrix (X) and the p vectors are called the loading vectors. Several methods are available for calculating principal components of matrices and, depending on the size and application, they can be chosen. These methods include singular value decomposition, NIPALS algorithm and kernel methods. When the matrix is large and it is not required to extract all the eigenvalues and eigenvectors, or when there are missing data in the matrix, then recursive methods such as NIPALS are the method of choice. Principal component analysis is used to extract the common cause of variation in a data set. When several variables in a dataset matrix are highly correlated, it is probably due to a common source of variation. Loading vectors and principal components can be interpreted as the common cause of these variations. Once the principal components of the data matrix are found, there are several graphs and tables that can be used to provide useful information about the nature of data. Some of these graphs and plots will be briefly discussed here:

Model overview plots: present the cumulative contribution of each component to overall fit in the model.

X/Y overview plots: present cumulative fit of variables (columns of the data matrix) by component. In other words shows that what percentage of variance of each variable has cumulatively been captured by the components.

Component contribution plots: show what percent of each variable is explained and predicted by each component

Component scatter plots: Scatter plots with respect to 2 or 3 components (3d) of a data matrix can show how the observations in that matrix are related to each other with respect to these components. For example observations with similar properties usually show up being close to each other in clusters in the score space (T)

Loading Plots: 2 or 3 dimensional loading scatter plots that correspond to the component scatter plots among variables (columns of data matrix) that explain the variation seen in the component scatter plot. Variables with loadings lying close to one another are highly correlated.

In addition to above plots, we will briefly talk about some of the definitions used in principal component analysis:

R^2_x : is the percentage of fit by the first A principal components of the X matrix:

$$R^2_x = \frac{SS_x \text{ calculated from principal components}}{SS_x} \quad (5.6)$$

Q_x^2 : is the same as R_x^2 but the data used for prediction is not used for building the model.

$$Q_x^2 = \frac{SS_x \text{ predicted}}{SS_x} \quad (5.7)$$

DmodX: or distance to the model is the distance of each observation to the n dimensional plane described by the A first principal components of the model. If this distance is large, that means the model cannot explain that observation using the first A set of components

$$D \text{ mod } X = \left(\frac{\sum_k e_{ik}^2}{K - A - 1} \right)^{1/2} \quad (5.8)$$

The e_{ik} 's are the elements of the residual matrix $E = X - TP^T$. "A" is the number of components and k is the number of observations. Partial least squares or PLS is similar to PCA in nature. In PCA the goal is to find vectors v_i that maximize (5.9). The solution to (5.9) turns out to be the eigenvectors associated with largest eigenvalues of $X^T X$ (variation matrix of X)

$$\begin{aligned} \max_{v_i} (v_i X^T X v_i) \\ \text{S.T. } v_i^T v_i = 1 \end{aligned} \quad (5.9)$$

In PLS we try to maximize:

$$\begin{aligned} \max_{w_i} (w_i X^T Y Y^T X w_i) \\ \text{S.T. } w_i^T w_i = 1 \end{aligned} \quad (5.10)$$

Where Y is the response matrix. Again the solution again turns to be largest eigenvectors associated with the $X^T Y Y^T X$ matrix (covariance matrix of X and Y). Plots and graphs used for principal component analysis can also be used for PLS analysis. In PLS analysis, there are some additional terms and plots that will be briefly discussed here:

R^2_y and Q^2_y show the amount of variance in the Y space explained and predicted by the model using the first n principal components.

t_n/u_n scatter plots: show the linearity of correlation between X and Y space. If t_n/u_n plot is not linearly scattered then it means the correlation between X and Y is non-linear and therefore a non-linear PLS should be used to fit the data.

Coefficient plots: describe the coefficients “ β ” of the prediction equation $\hat{Y} = X\beta$. The larger the coefficient, the stronger the influence of that variable is on the prediction.

Variable Importance Plots (VIP): Rearranging the variables based on the weighted root mean square of the loadings [SIMCA Tutorial by Umetrics Inc] gives the VIP plot. VIP plot is useful for determining most influential variables in the overall model, for the entire Y matrix.

Contribution plots: show why an observation or a group of observations is different from another observation or group of observations in the score (t_1, t_2, \dots) space or in the residual (SPE) space. In other words these plots show which X variables contribute most to the changes in the score space, with changes from between two observations or

between the mean of two groups of observations in the score space or the residual (SPE) space.

5.1 PCA on Y Data

Principal component analysis (PCA) on the observed response data (Y in Table 1) gives a model with 1 component explaining 31% of the variation in Y space (Figure 26a).

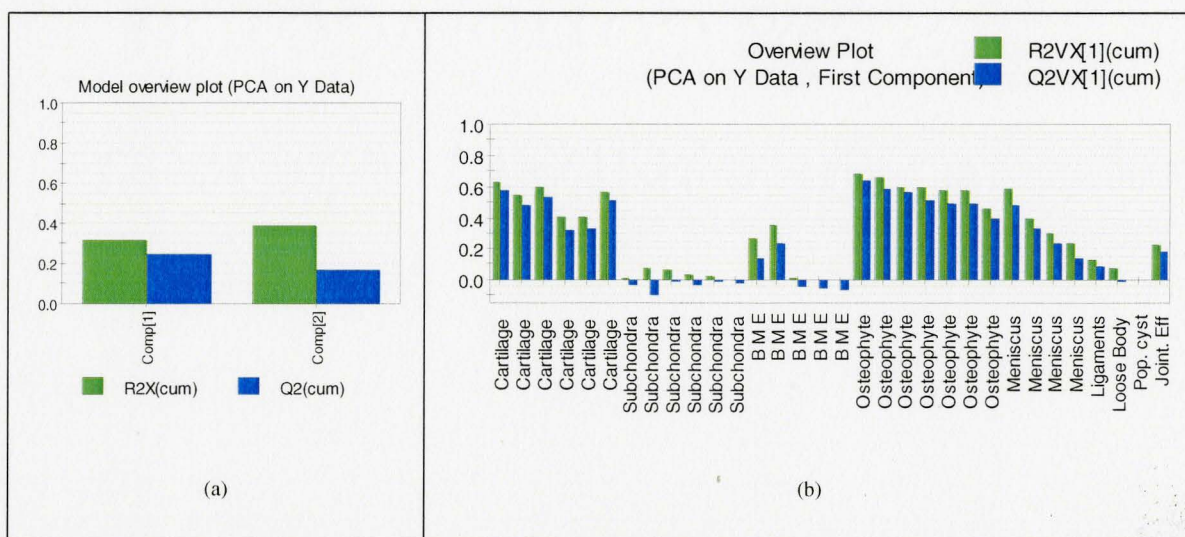


Figure 26: a) Model overview plot of the Y Data. b) Variable overview plot for the first component

Although the second component does not increase the prediction (Q^2) of the model, it still improves the visualization of the plots and therefore is included. The X/Y overview plot shows that the first component is mainly capturing the variations caused by cartilage degeneration and osteophyte formation (Figure 26b). This plot also shows that the correlated behavior among cartilage and osteophyte scores explains the major variation in dataset. The P_1/P_2 loading plot (Figure 27) shows that there is a strong positive correlation between osteophyte formation and cartilage degeneration, especially in the

medial compartment of the knee. It appears that meniscus degeneration in the medial anterior horn (M-AH) is also strongly correlated with cartilage degeneration and osteophyte formation. It also seems that Bone Marrow Edema (BME) in the medial compartment is related or correlated to osteophyte formation and cartilage degeneration. However BME in the lateral compartment of the knee does not appear to be correlated to osteophyte and cartilage problems. There is also some clustering towards the direction of the second loading axis but due to the small number of non-zero variables in this direction it is not really possible to assess the results. Perhaps increasing the number of patients in the study would improve interpretation of variations in this direction as well.

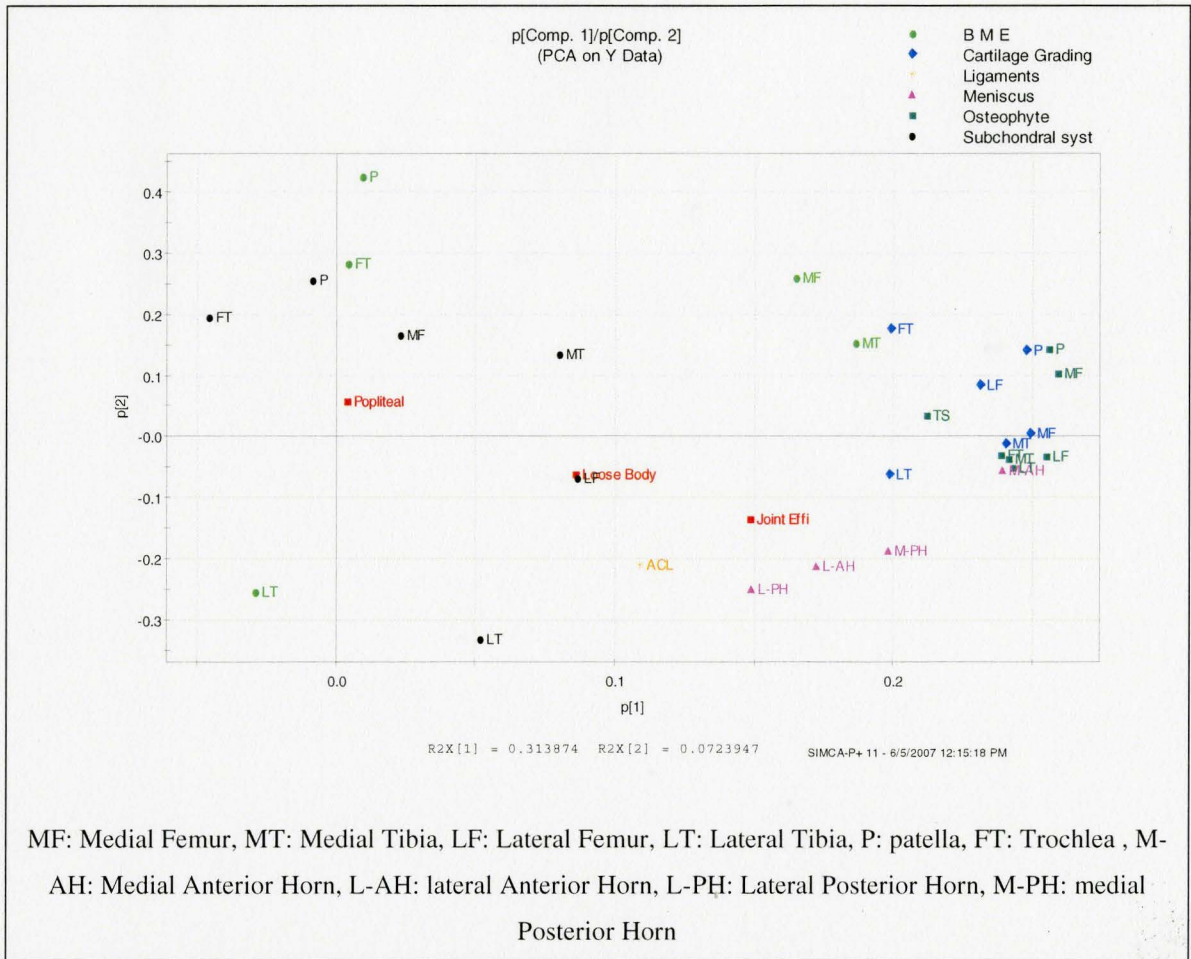


Figure 27: P₁/P₂ loading plot of the Y Data.

5.2 Analysis of Fourier transforms

5.2.1 FFT

A signal can be expressed in different domains. While time domain is appropriate for presenting local and spatial changes in a signal, the frequency domain will present the periodic reoccurrence of a phenomenon in the signal. For a continuous analog signal, Fourier transformation from time domain to frequency is defined by:

$$X(f) = FT(x(t)) = \int_{-\infty}^{+\infty} x(t)e^{-j2\pi ft} dt \quad (5.11)$$

Where f is the frequency, j is $\sqrt{-1}$ and t is time. $X(f)$ can be written as:

$$X(f) = |X(f)|e^{j\angle X(f)} \quad (5.12)$$

where $|X(f)|$ is called magnitude of the signal and $\angle X(f)$ is called phase. The inverse of a continuous Fourier transform is written as:

$$x(t) = IFT(X(f)) = \int_{-\infty}^{+\infty} X(f)e^{j2\pi ft} df \quad (5.13)$$

Definition: Impulse Function

Impulse function; $\delta(t-t_0)$ is a function with the following properties:

$$\int_{-\infty}^{+\infty} \delta(t-t_0) dt = 1 \quad (5.14)$$

$$\int_{-\infty}^{+\infty} \delta(t-t_0)g(t) dt = g(t_0) \quad (5.15)$$

Fourier transform of an impulse function is:

$$FT(\delta(t)) = \int_{-\infty}^{+\infty} \delta(t)e^{-j2\pi ft} dt = e^{-j2\pi f(0)} = 1 \quad (5.16)$$

This means that the frequency spectrum of an ideal impulse function is flat [47] pp20-21] and contains all frequencies. As it will be described in the upcoming sections, this property of the impulse function affects the overall shape of the frequency spectrum of the knee motion because of the impulse shaped clicks of the knee.

In the real world, all signals are continuous. In order to work with these signals we need to transform them into digital signals sampled from original continuous signals. Nyquist or Shannon theory indicates that for a signal with maximum bandwidth of f_c , the minimum sampling rate that is needed to fully reconstruct the original signal is $f_s \geq 2f_c$. If the signal is sampled at $f_s = 2f_c$ but it contains frequencies above f_c then these frequencies above f_c will be super imposed on the frequencies within the frequency range ($0 < f \leq f_s$). Therefore it is necessary to pre-filter the signal using analog filters and remove these high frequencies before digitally converting it and processing it using Fourier analysis. If there is no previous knowledge of the shape of the signal it is best to look at the power spectrum of the signal and if the power spectrum decays towards zero then it is unlikely that the signal contains any higher frequency components (Press et al 1992) [48]. Assuming N points have been sampled at a sampling rate of f_s then the N point discrete Fourier transform of the signal for frequencies: $f_n = \frac{n}{N} f_s$ from $\frac{-f_s}{2}$ to $\frac{+f_s}{2}$ can be obtained as:

$$X(f_n) = \int_{-\infty}^{+\infty} x(t) e^{-j2\pi f_n t} dt \rightarrow X(f_n) = \sum_{k=0}^{N-1} x_k e^{-j2\pi f_n t_k \frac{1}{f_s}} \quad (5.17)$$

For f_n from $\frac{-f_s}{2}$ to $\frac{+f_s}{2}$. Equation (5.17) can alternatively be written as:

$$X_n = \sum_{k=0}^{N-1} x_k e^{-j2\pi \frac{kn}{N}} \quad \text{for } n = \frac{-N}{2} \text{ to } \frac{+N}{2} \quad (5.18)$$

If $x(t)$ is real then the magnitude of frequency is symmetric about $f = 0$ and only 1 half of the spectrum (for example from 0 to $f_s/2$) is needed for analysis. Inverse of discrete Fourier transform is:

$$x_k = \frac{1}{N} \sum_{n=0}^{N-1} X_n e^{j2\pi \frac{kn}{N}} \quad (5.19)$$

Throughout the rest of this section we will use Fast Fourier Transform (FFT), which is a fast algorithm for calculating discrete Fourier transform of signals.

In many people, during the FE cycle, the knee generates clicking sounds. These sounds are generated during the movement of the patella on the femur. This clicking sound is not associated with arthritis and is very common in physically active people. From signal processing point of view, these clicks resemble impulse signals and contain a wide range of frequency components and in a knee that clicks frequently, they can easily alter the frequency spectrum. According to equation (5.20) when two signals are summed, their Fourier transforms are also added:

$$F(\alpha x_1 + \beta x_2) = \alpha F(x_1) + \beta F(x_2) \quad (5.20)$$

Before analyzing the knee vibration signals, these clicks must be removed using thresholding techniques. As it will be discussed in the next subsection, wavelet transform

is a good candidate for this purpose. In wavelet thresholding, first, each signal is decomposed into its wavelet coefficients. After calculating the standard deviation of the coefficients at each level, any coefficient that has an absolute value larger than 3 standard deviations is trimmed to 3 standard deviations. Once all the coefficients have been thresholded, the original signal is reconstructed from the new coefficients. The following figure shows the process:

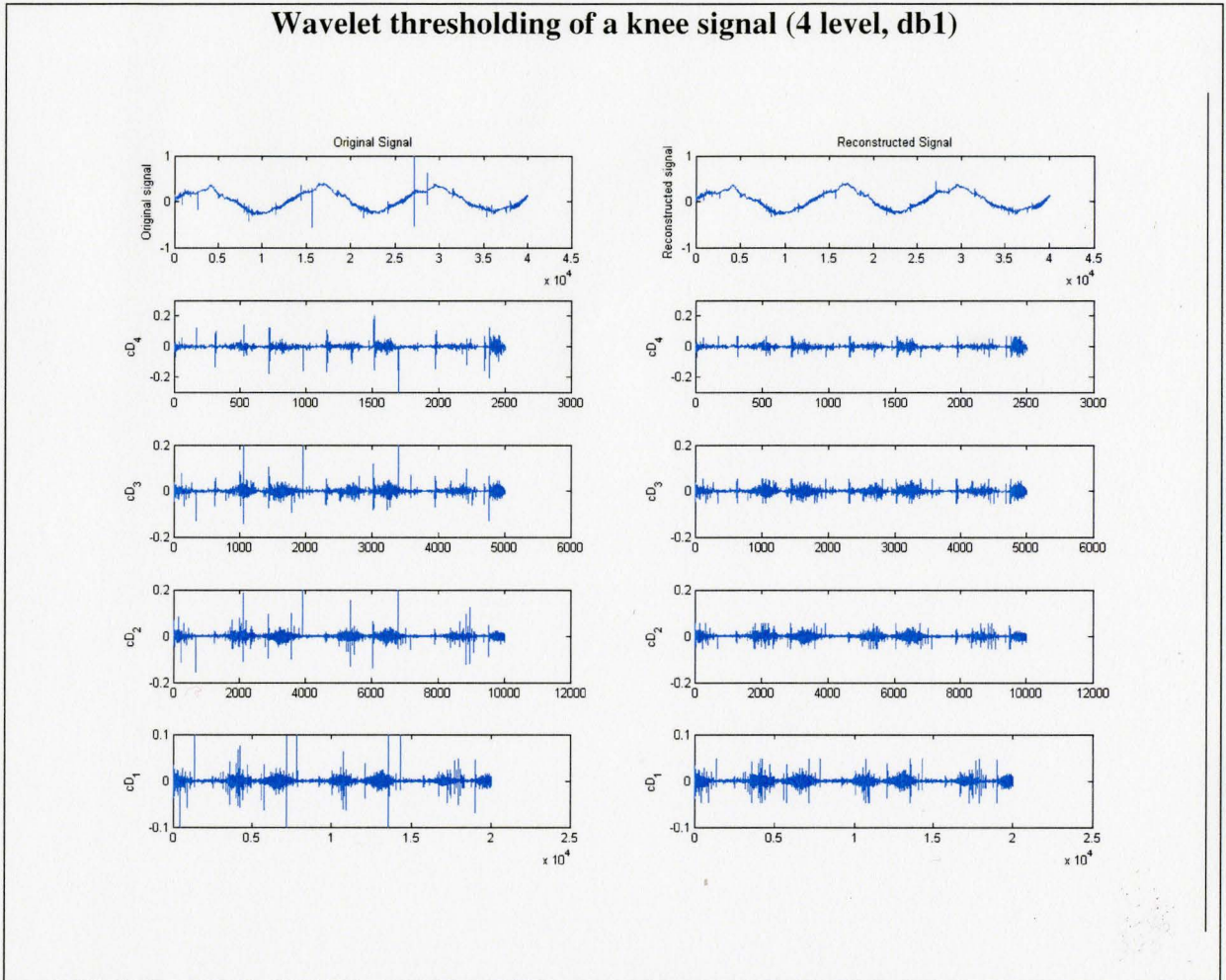


Figure 28: Left) Wavelet decomposition of the original signal, Right) thresholded wavelet coefficients and the reconstructed signal

The top graphs in Figure 28 are the original and the reconstructed signals after thresholding. We can see that the clicks in the reconstructed image have been removed.

The following figure shows the change to the power spectrum of the above signal, before and after removing the spikes (clicks):

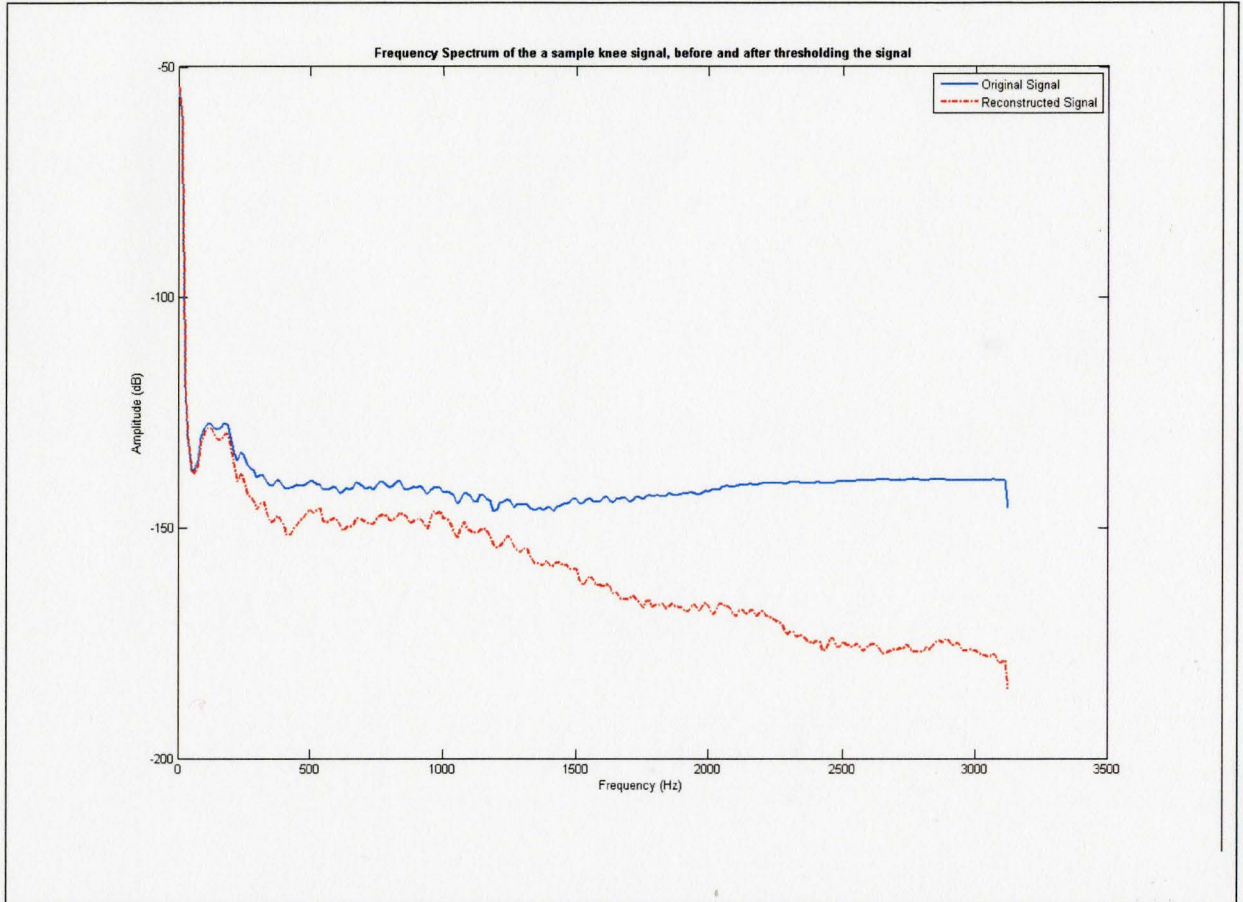


Figure 29: Periodogram of the knee signal before and after thresholding.

The next step in preprocessing is de-trending or removing the linear trend of the signal. The reason is that some of the patients do not perform the FE cycles in the same angular range (as shown in Figure 30). Analysis showed that removing the linear trend from the signal provides better results. Detrending can be done by fitting a straight line into the signal and subtracting it from the signal.

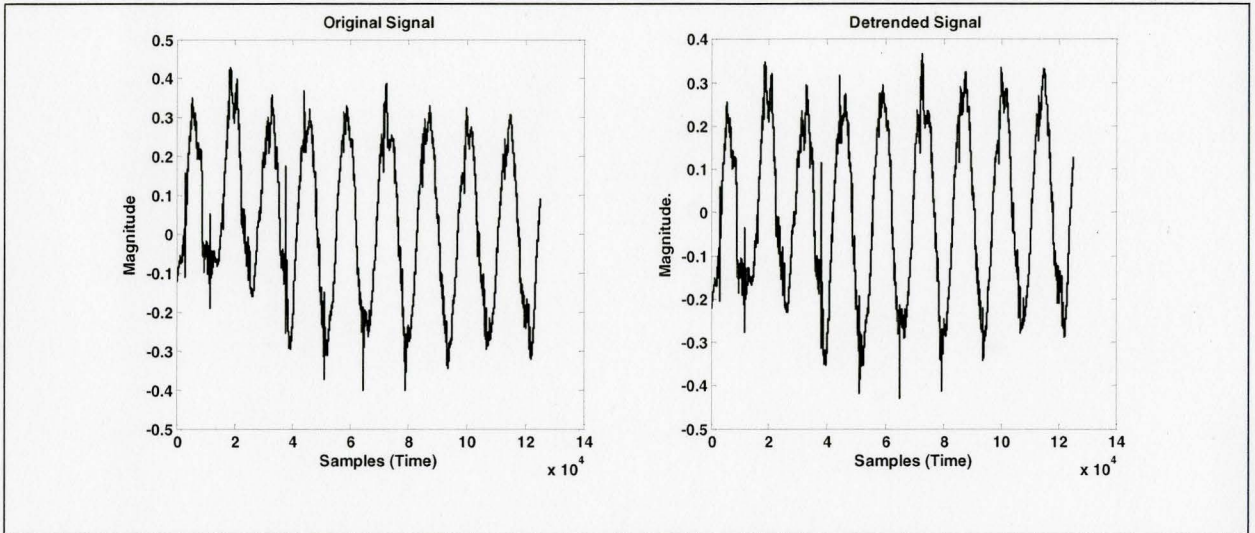


Figure 30: Left: original signal. Right: signal after detrending

Once the signal is corrected for the clicks it can be analyzed by a combination of spectral and principal component analysis.

Power Spectral Density (PSD) of a signal is defined as:

$$\phi(\omega) = \lim_{N \rightarrow \infty} E \left\{ \frac{1}{N} \left| \sum_{k=1}^N x(k) e^{-i\omega k} \right|^2 \right\} \quad (5.21)$$

Where E is the expected value of the equation in the bracket, N is the number of samples, $x(k)$ is the measured signal at time k and ω is the angular frequency in radians.

ω is a periodic function ($\omega = 2\pi f$) with period of 2π , $\omega \in [-\pi, \pi]$, frequency of the equation can be defined as $f = \omega/2\pi$. This implies that the interval of F is between $[-F_s/2, F_s/2]$. In real life the number of samples measured is always limited and therefore

equation (5.21) cannot be used directly. A Periodogram is a simplified form of PSD and is defined as:

$$\phi(\omega) = \frac{1}{N} \left| \sum_{k=1}^N x(k) e^{-i\omega k} \right|^2 \quad (5.22)$$

The problem with this method is that the magnitude of discrete Fourier transform is not a consistent estimate of the true power spectrum; i.e. its variance does not decrease with more data (increasing N). Increasing N rather provides estimates at more frequency points and not more accurate ones. However as N gets smaller the power spectrum estimates get biased²⁶. There are other methods of non-parametric PSD estimation that tend to minimize the variation and bias. The most common method is the Welch method. Simply put, in Welch method, the signal is split into S overlapping segments. Each segment is defined by:

$$\begin{aligned} x_j(t) &= x((j-1)K + t) \\ t &= 1, \dots, M \\ j &= 1, \dots, S \end{aligned} \quad (5.23)$$

where M is the size of the window or the segment. If $K = M$ then the segments wouldn't overlap. Each segment of data is then multiplied by a smoothing window $v(t)$ with the

²⁶ For more information on spectral analysis and PSD see "Introduction to Spectral Analysis" by Petre Stoica, ISBN: 0-13258419-0

same size of the segment and then periodograms of all segments are averaged. The windowed periodogram is computed as:

$$\hat{\phi}_j(\omega) = \frac{1}{MP} \left| \sum_{t=1}^M v(t) x_j(t) e^{-i\omega t} \right|^2 \quad (5.24)$$

Here, P is calculated as:

$$P = \frac{1}{M} \sum_{t=1}^M |v(t)| \quad (5.25)$$

$v(t)$ is the smoothing window and S is the average of all periodograms for each segment:

$$\hat{\phi}_w(\omega) = \frac{1}{S} \sum_{j=1}^S \hat{\phi}_j(\omega) \quad (5.26)$$

Through out the rest of this chapter, the spectral analysis is done on the Welch power spectral estimations of the signals. Changing the size of the smoothing window, overlap of the segments and number of frequency points being selected can change bias and variance of the signal.

Once the signals are preprocessed, the periodogram of each segment, $\hat{\phi}_j(\omega)$, is calculated and averaged over the “half-cycles” of the knee. A half-cycle is part of a FE cycle that is confounded by two zeros (roots) of the signal. Roots of the signal are the approximate points where the signal value equals the overall average of the signal (Figure 31). In case of a mean centered signal this value is zero. Therefore equation (5.26) changes to:

$$\begin{cases} \hat{\phi}_{Wp}(\omega) = \frac{1}{S_+} \sum_{j=1}^{S_+} \hat{\phi}_j(\omega) & j \in \text{positive cycles} \\ \hat{\phi}_{Wn}(\omega) = \frac{1}{S_-} \sum_{j=1}^{S_-} \hat{\phi}_j(\omega) & j \in \text{negative cycles} \end{cases} \quad (5.27)$$

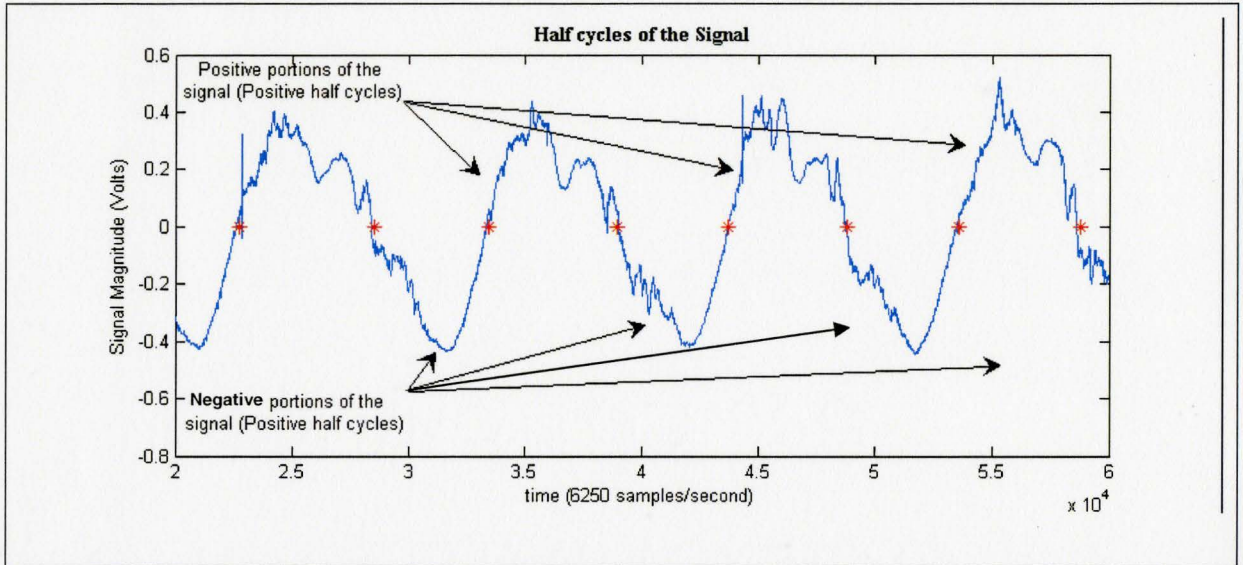


Figure 31: Positive and Negative half cycles of a signal

The reason for dividing the signal into two main portions (positive and negative half cycles) is to maintain some of the spatial information of the signal that might further help to localize symptoms such as meniscus tears. Since there is more information in the low frequency region of the spectrum than the high frequency region, frequencies are chosen in a Log-wise manner over a range of 0 to 3125 Hz (1/2 sampling range) at 150 points. Figure 32 shows the positive and negative spectrums for a sample signal.

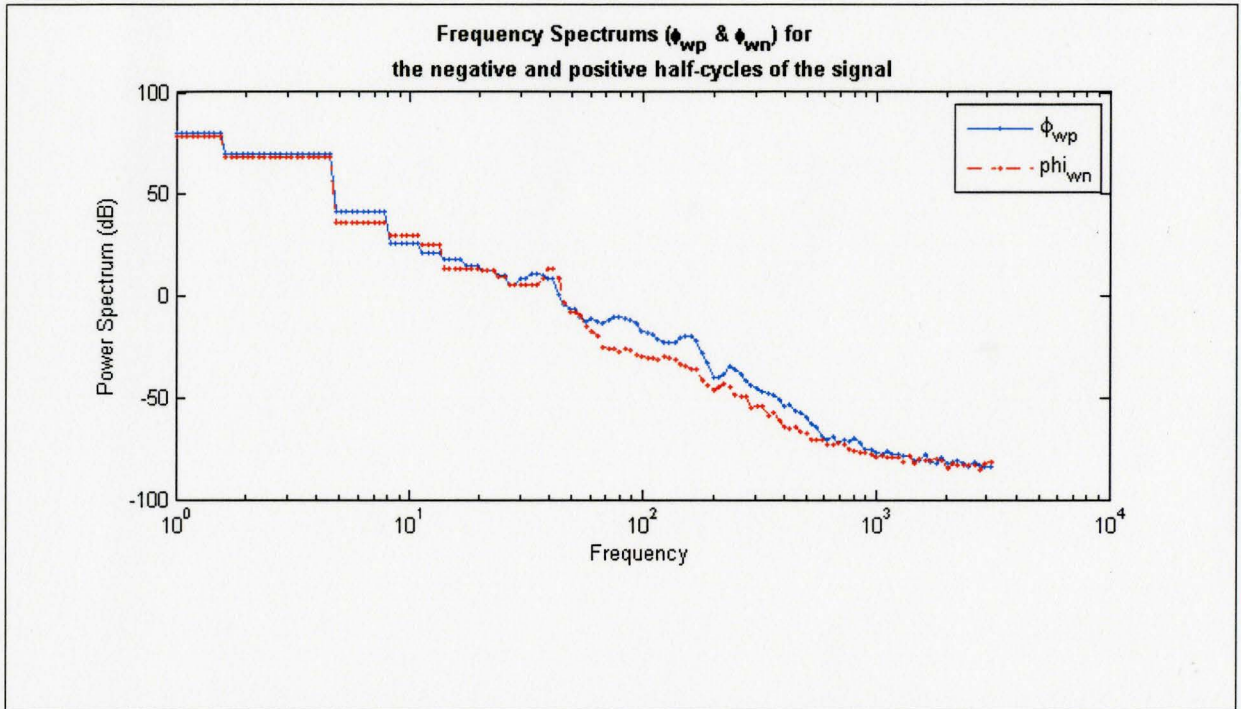


Figure 32: Frequency spectrums for positive and negative half cycles

Comparing the results showed that inverse of power spectra in the X matrix provides better information than X matrix itself. Therefore throughout the rest of this section power spectrum inverse is used for analysis as the X matrix. The positive and negative spectrum coefficients of the signals form the “X” variable matrix for PCA and PLS analysis. For PLS analysis, markers obtained from analysis of MRI data for each patient constitutes the “Y” matrix (Section 4.1).

5.2.2 PCA on FFT

For standing position data, the “X” matrix contains 1500 variables; 300 variables for each sensor (accelerometer) and 150 variables for each half cycle of each accelerometer power spectrum (Table 2). These variables are the coefficients of the power spectrum inverse.

	<i>Pat</i> ₊	<i>Pat</i> ₋	<i>FLat</i> ₊	<i>FLat</i> ₋	<i>FMed</i> ₊	<i>FMed</i> ₋	<i>TLat</i> ₊	<i>TLat</i> ₋	<i>TMed</i> ₊	<i>TMed</i> ₋
<i>patient 1</i>	...									
<i>patient 2</i>				...						
⋮							...			
<i>patient N</i>										...

Table 2: “X matrix of the spectrum magnitudes for PCA and PLS analysis; Pat: Patella, FLat: Lateral Femur, FMed: Medial Femur, TLat: Lateral Tibia, TMed: Medial Tibia

After performing an initial PCA on the Data and removing outliers (4 observations), PCA analysis on the X data gave a model with 39 components ($R^2 = 0.963$, $Q^2 = 0.833$). The first 5 components of the model captured 66% of the variation ($Q^2 = 57\%$). Figure 33 shows the model overview plot of the Data.

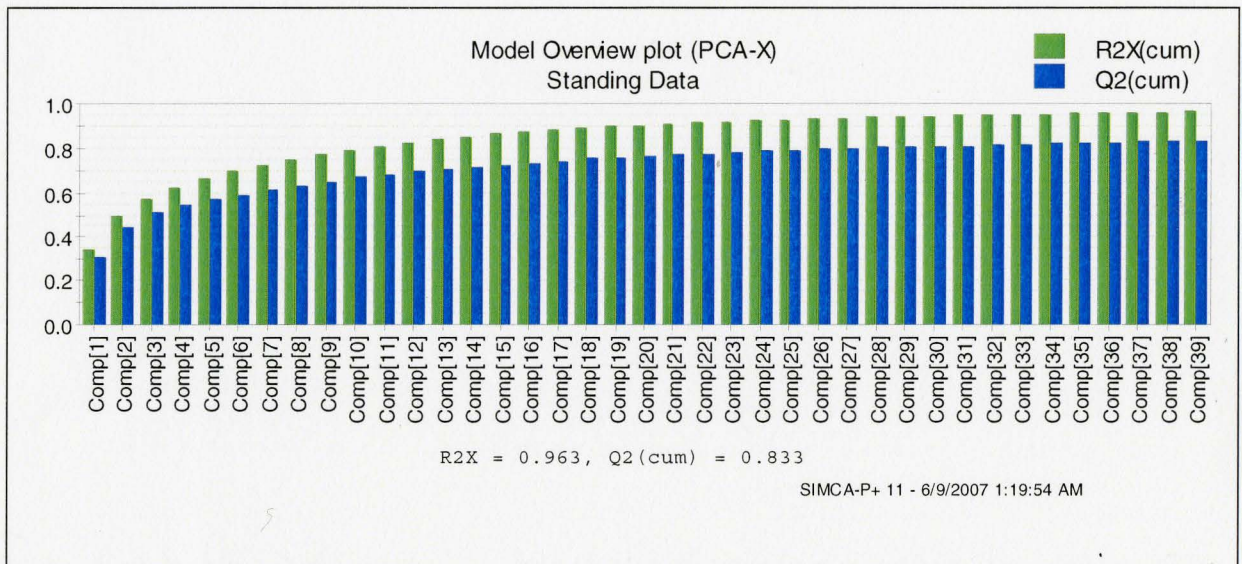


Figure 33: model overview plot of the Standing Data (Power Spectrum)

The component contribution plots (Figure 34 to Figure 36) show that component 1 is mainly capturing the difference in average amplitude of the spectra over all frequencies

and the second and third components are capturing the variations in very low and mid frequency range.

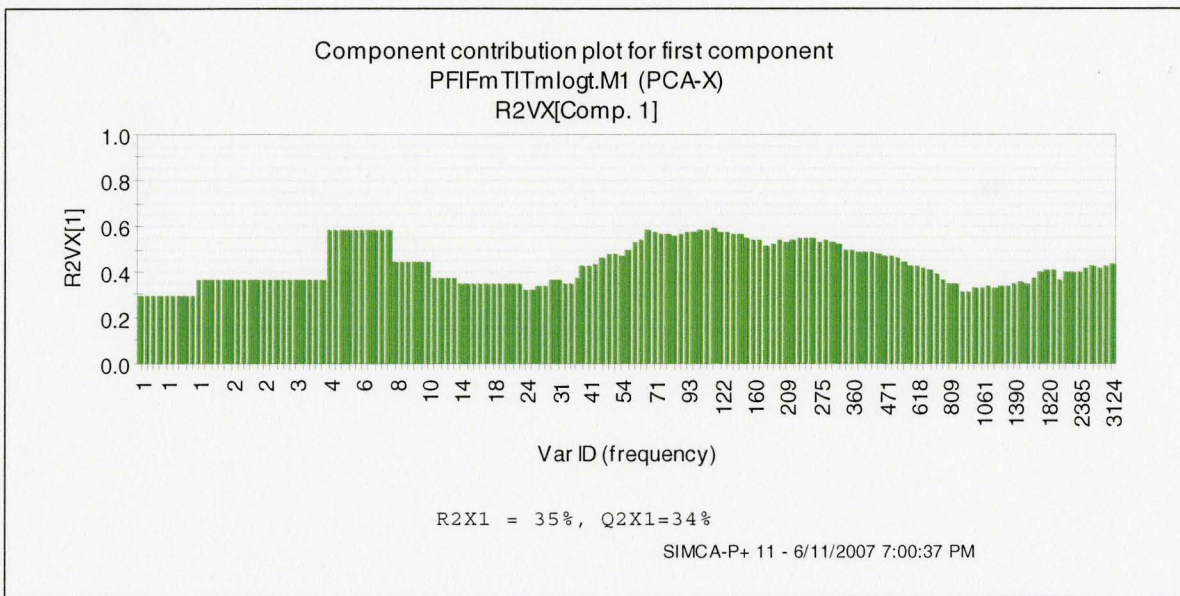


Figure 34: Component contribution plot for the first component (PCA on Frequency)

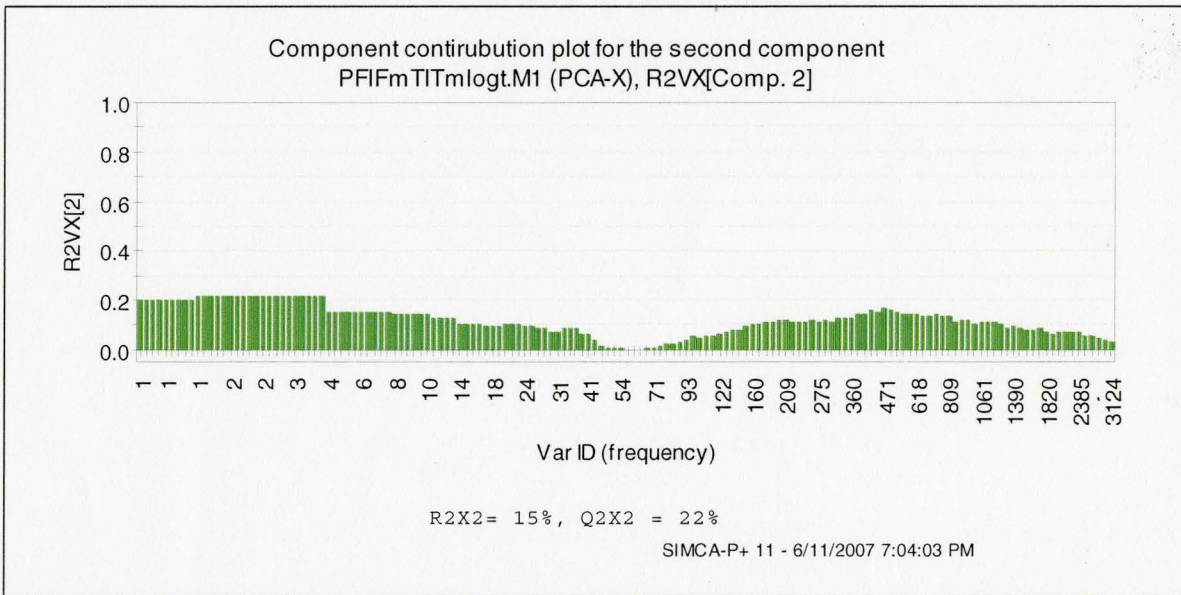


Figure 35: Component Contribution plot for the second component (PCA on Frequency)

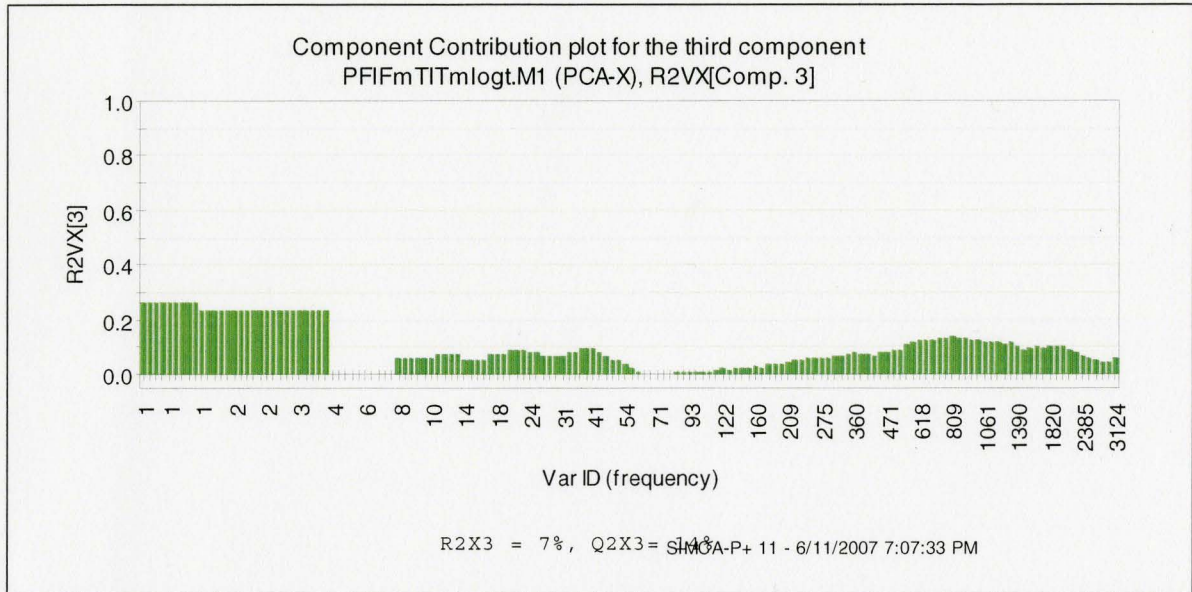


Figure 36: Component contribution plot for the third component (PCA on Frequency)

Figure 37 shows the $t1/t2$ and $t3/t2$ scatter plots of the model, colored according to the average severity of cartilage damage in the knee (0=healthy, 3=severe damage). It is evident that there is a trend from healthy to damaged cartilage. A contribution plot between healthy and damaged cartilage knees (Figure 38) shows that the power spectra of healthy knees has less energy (magnitude) in the high frequency region of the spectra (compared to damaged knees). It should be noted that since these contribution plots have been obtained by performing PCA on the inverse of the power spectra, therefore the contribution plot is showing the inverse of the changes and not the true changes in the power spectrum of the two groups.

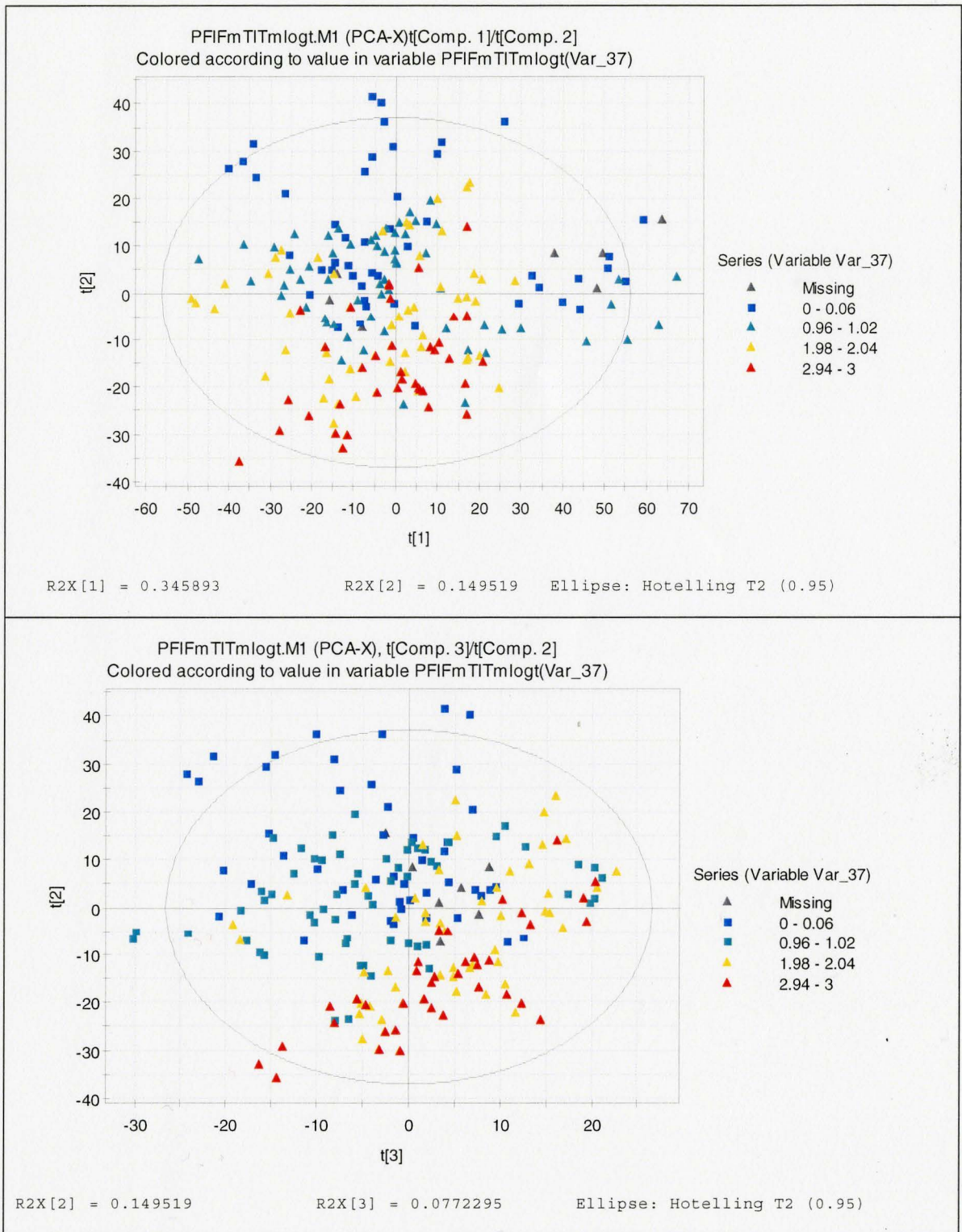


Figure 37: t1/t2 and t3/t2 Scatter plots of the PCA model for frequency data

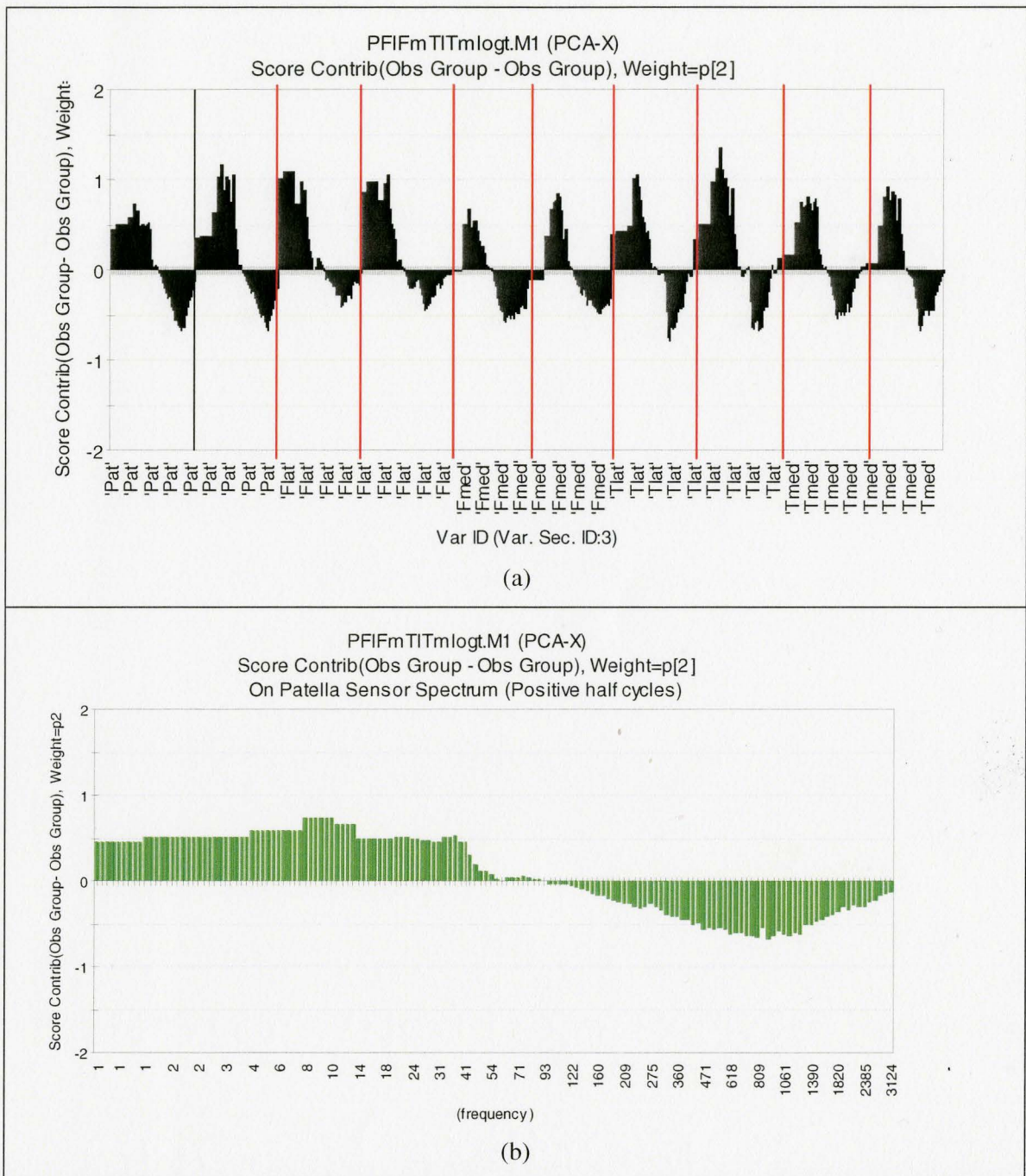


Figure 38: component contribution plot (Comp 2) between healthy (0-1) and unhealthy (2-3) cartilage knees (X: Inverse of power spectra). (a: for all sensors, b: only patella sensor, positive half cycle

The formation of osteophyte is strongly correlated with cartilage health. This can be shown by coloring Figure 37b according to average osteophyte growth level (0 to 2) (Figure 39). As mentioned in previous chapters, osteophyte formation is known to be some kind of defense mechanism for the knee to stabilize itself when cartilage surface is damaged or deformed (see section 3.1.1).

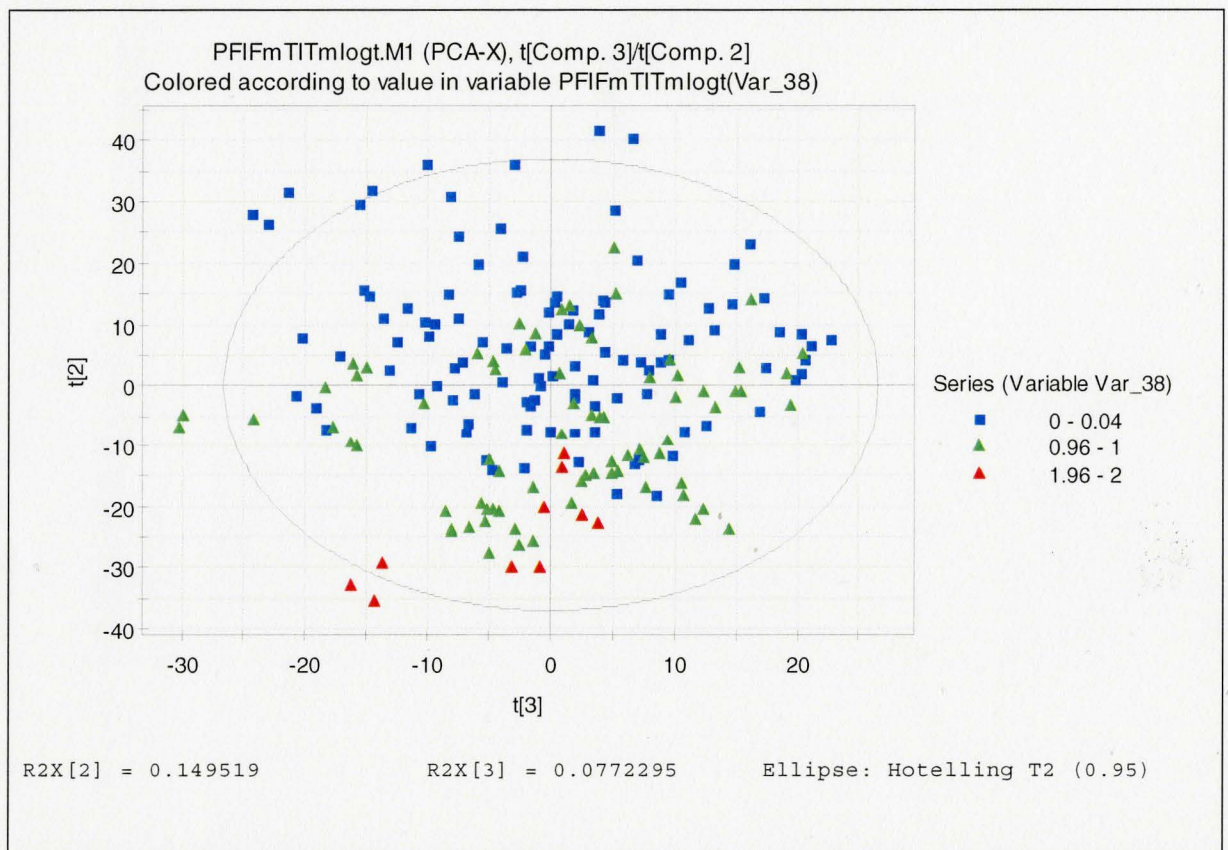


Figure 39: t2/t3 Scatter plot colored according to average severity of osteophyte formation in the knees.

There are several methods that can be used to classify cartilage damage severity from the calculated scores (t). One method is to use “Soft Independent Modeling of Class

Analogy” or SIMCA. In SIMCA one model is built for each class of observations. Any new observation is fed to all class models and the distance from model (DModX) or the probability of belonging to each class (PModX) is calculated for all classes. Then using Cooman graphs or probability scatter plots the proper class is assigned to that observation (for more information see SIMCA-P manual). However since there is a strong interconnection between observations of different classes in our dataset, the above method, does not really provide a strong classifier. Another method would be to separate different classes using Kernel algorithms such Support Vector Machines (SVM). This method will further be investigated as the future work for this project.

5.2.3 PLS on FFT

A PLS analysis on the data, with the Y data being the average severity of damage to the cartilage gives a model with two components ($R^2Y = 0.55$, $Q^2 = 0.33$). In PLS analysis, sometimes when there is a large number of X variables it is possible to improve the quality of fit by removing or pruning variables that are less significant in building the model. Such data usually consists of variables that are not correlated with “Y” space or contain great level of noise. For this purpose one can draw the Variable Importance Plot (VIP) and remove the variables that are least significant to the overall model (Figure 40). Data pruning is done in several recursive stages. By doing so, it was possible to improve quality of fit by 4% and prediction rate by 18 %. The new R^2 and Q^2 increased to 59% and 51% respectively. Total number of variables remaining in the model after pruning

was 502 (from 1500 variables in the original model) Figure 41 shows the t_1/t_2 scatter plot of the PLS model. The colors are chosen according to the average severity level of cartilage degeneration (cartilage health scores). Then again there is a trend from healthy to damaged cartilage, mainly in the t_1 direction. Figure 42 also shows the loading plot before and after pruning of the unimportant variables. It shows that the variables that are not very significant in building the model are the ones that have small w^* values (low correlation with Y data) compared to the remaining variables. Most of the variables that remained in the model after pruning belong to the 0 to 1000 Hz group. It can also be seen that t_1 is most explanative of Y and higher frequencies are positively correlated with larger Y's.

It appears there are two separate classes of healthy joints, in two different areas of the component score plot (t_1, t_2), one on the top left and the other on the bottom left corner of the plot. Further analysis showed that the group of healthy people on the top left mainly consists of middle-aged patients in whom the articulating surface might have changed properties. The bottom left corner mainly consists of healthy and young patients. Further investigation on the contribution plots (on PCA of the spectra) showed that the difference is due to the power level of the spectra in higher frequency regions. However since there might be various reasons for such separation it is not possible to find a physical cause for this clustering.

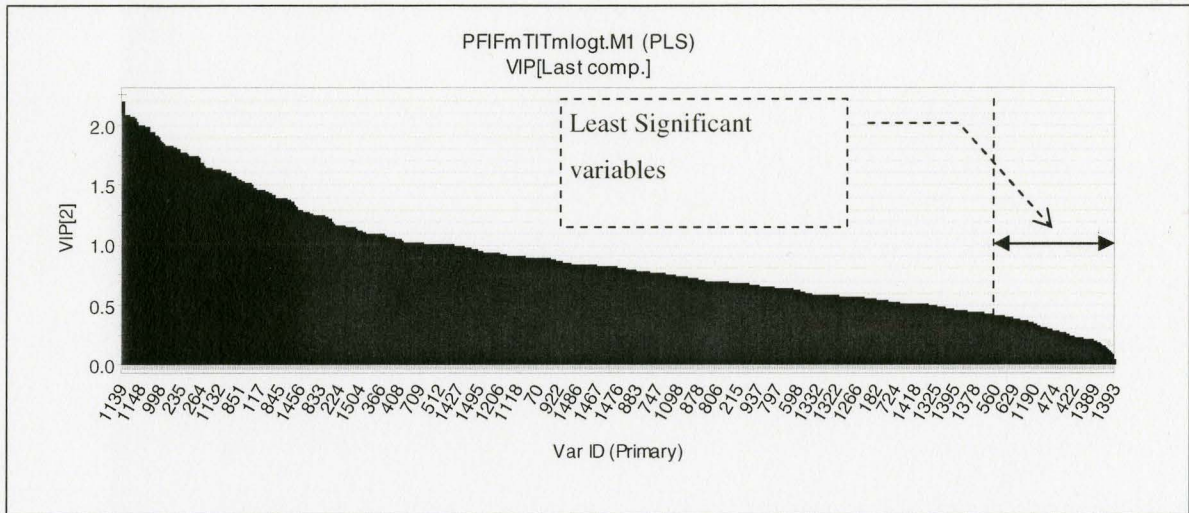


Figure 40: Variable Importance Plot (VIP), PLS model (Frequency Data)

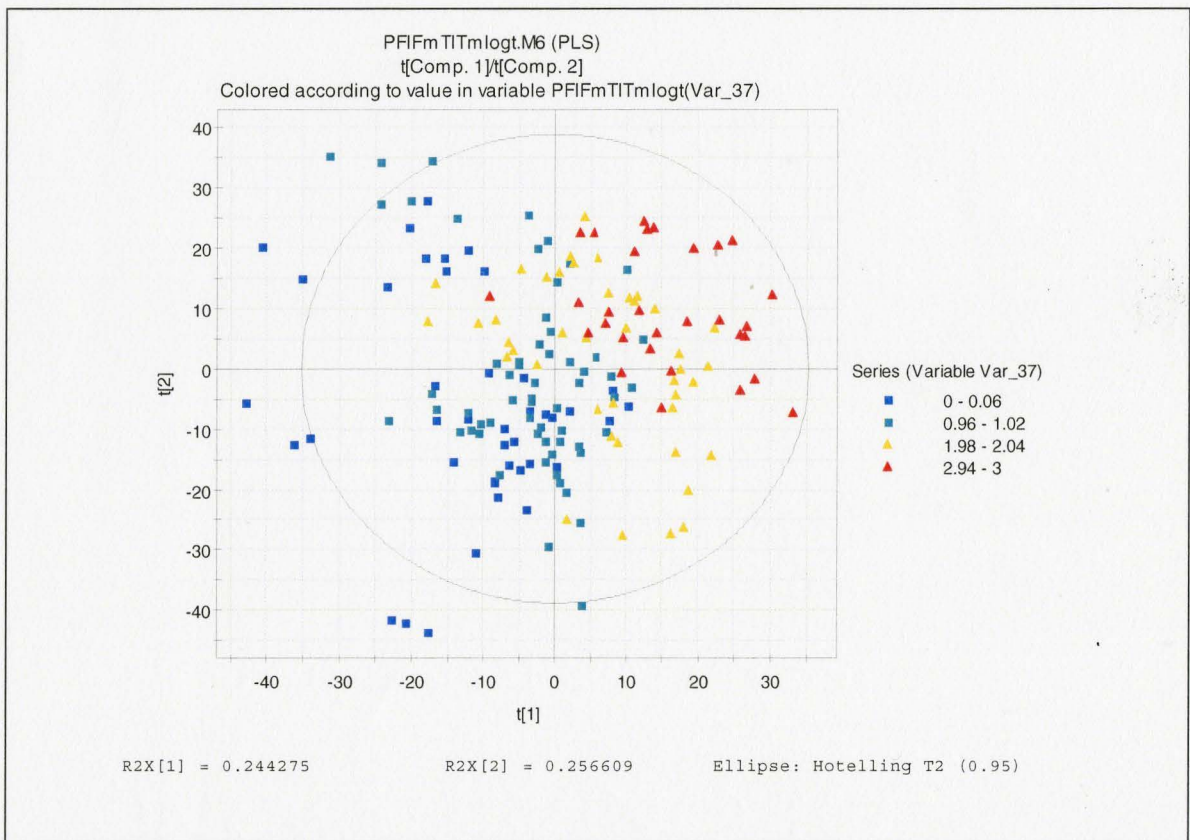


Figure 41: t_1/t_2 scatter plot of the PLS components (Frequency Analysis Data), colored according to average severity of the cartilage damage.

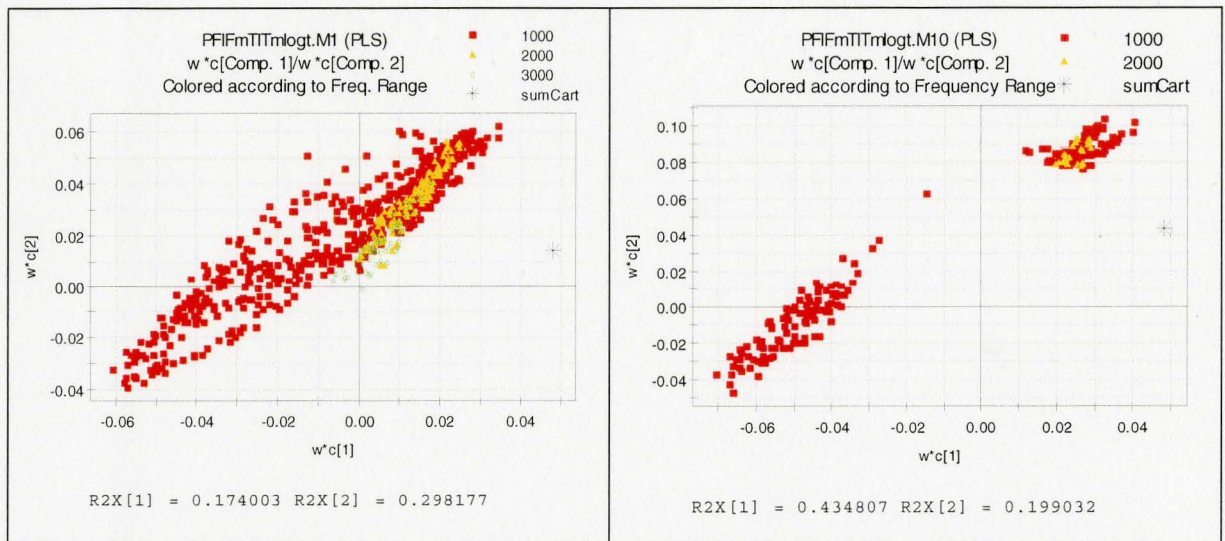


Figure 42: Left) Loading Plot before pruning the variables, Right) Loading Plot after pruning the variables (Y: Average Cartilage score (SumCart)). PLS analysis on the frequency data.

Figure 43 shows the observed versus predicted values of Y (average level of cartilage degeneration). It seems the overall level of prediction is good, however the variation from one level to another is large and does not provide adequate level of prediction between levels. The observations marked by green triangles belong to the test set and were not used in building the model. The data available for the X matrix includes 5 sets of variables from 5 sensors around the knee. Table 3 shows the quality of fit when different combinations of sensor variables were used together in the PLS model before pruning the data. Best results were obtained when all variables were used in building the model.

Sensor(s)	# of Comp.	R^2_x (%)	R^2_y (%)	Q^2_y (%)
Tibia Sensors	2	18	44	27
Femur Sensors	2	50	47	22
Patella Sensors	2	70	40	20
Tibia & Femurs Sensors	2	47	51	27
Tibia & Patella Sensors	2	49	54	32
Femur and Patella Sensors	2	51	53	31
All Sensors	2	47	55	33

Table 3: Quality of fit for different combination of sensors (PLS model, Y= Ave. Cartilage degeneration level, no variable pruning). PLS on Frequency data.

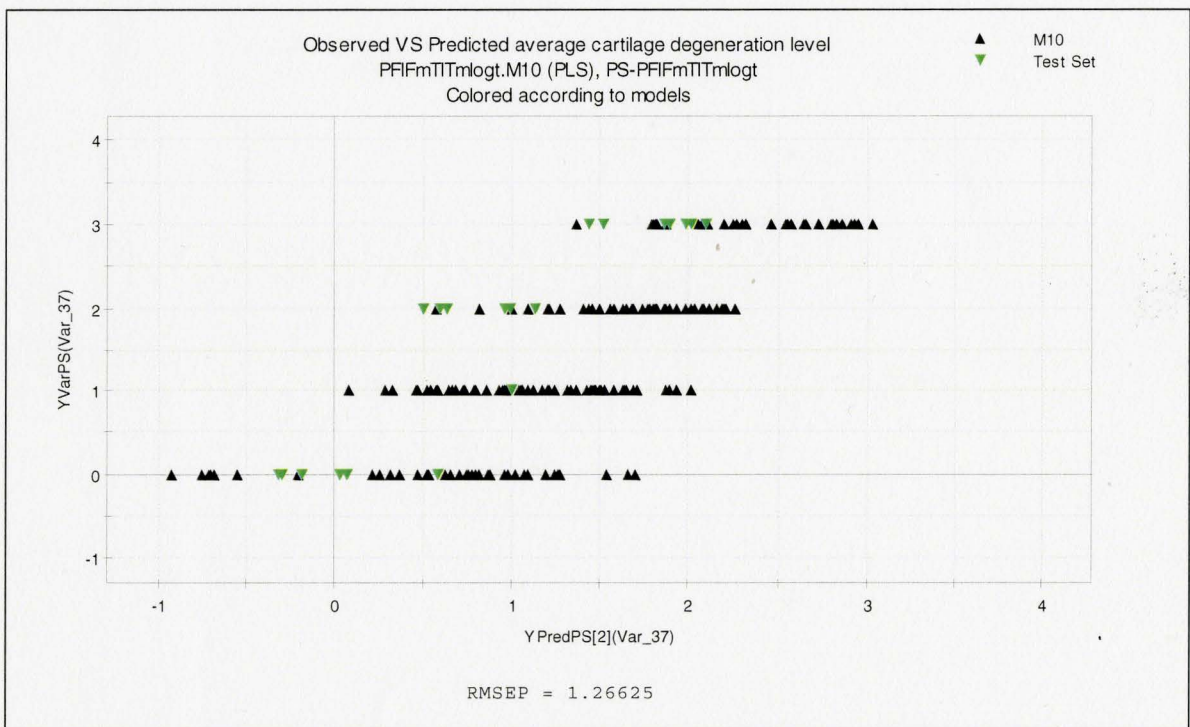


Figure 43: Observed VS predicted Y (Ave. Level of cartilage degeneration) for PLS model (X = Frequency Data, Y = Ave. Cart. Degeneration)

When the same recursive variable pruning procedure was applied to osteophyte formation level there was a 9% improvement in quality of fit and 15% improvement in Q^2 ($R^2_y = 54\%$ and $Q^2_y = 46\%$). Figure 44 and Figure 45 show the t1/t2 scatter plot and the Observed versus Predicted values of Y (osteophyte formation level).

The results of the analysis show that for both cartilage degeneration and osteophyte formation levels, the low frequency region (0 to 1 KHz) is the range that conveys information. This of course makes sense because skin tissue attenuates the high frequency region and in the case of osteophyte formation, the deformation of the articulating surface is what is being recorded by the accelerometers. This hypothesis (very low frequency region conveying the information) also suggests that performing the tests in a manner that bounds the patients to perform the FE cycles within a specified speed range (number of cycles per minute) would improve the results.

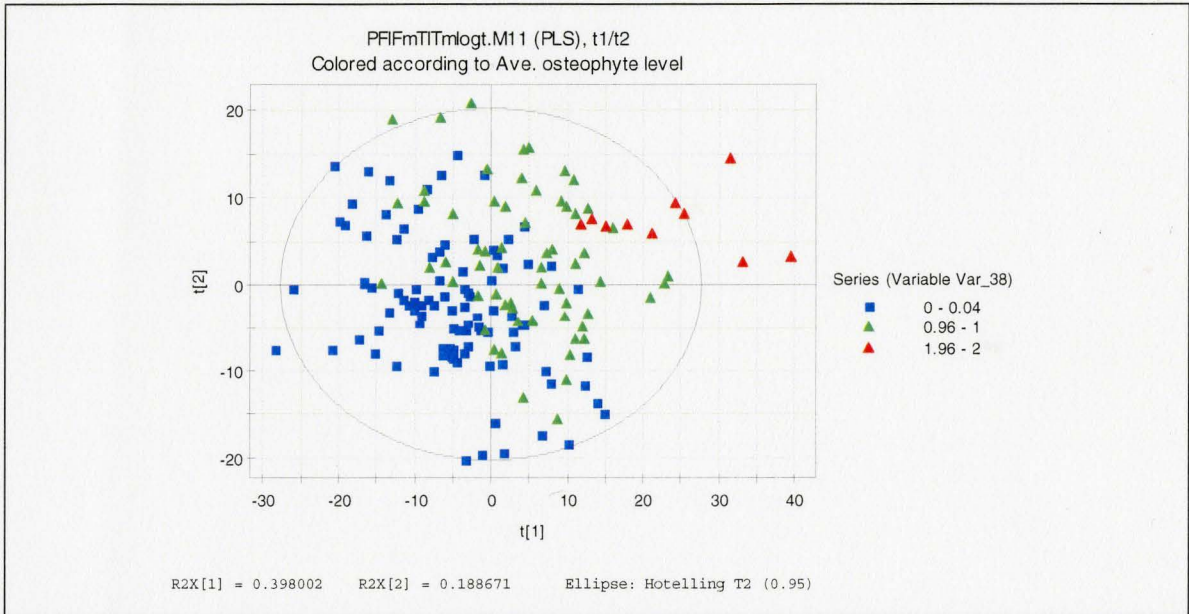


Figure 44: t1/t2 scatter plot of the PLS model (Y= average osteophyte formation level). PLS on the frequency data

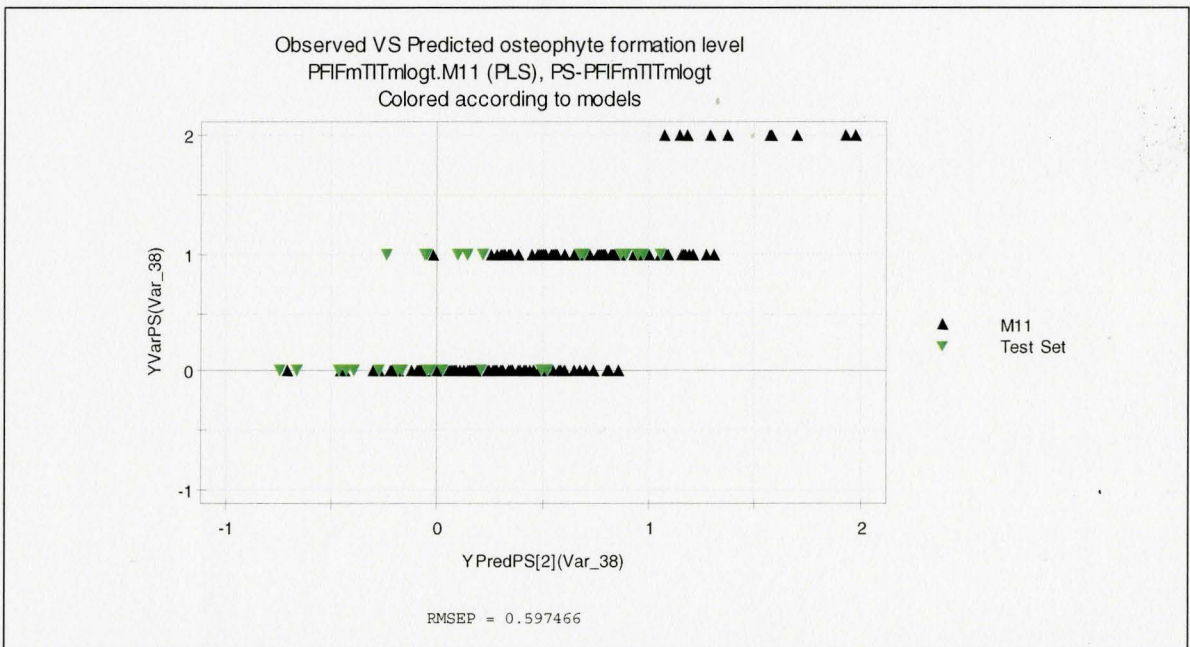
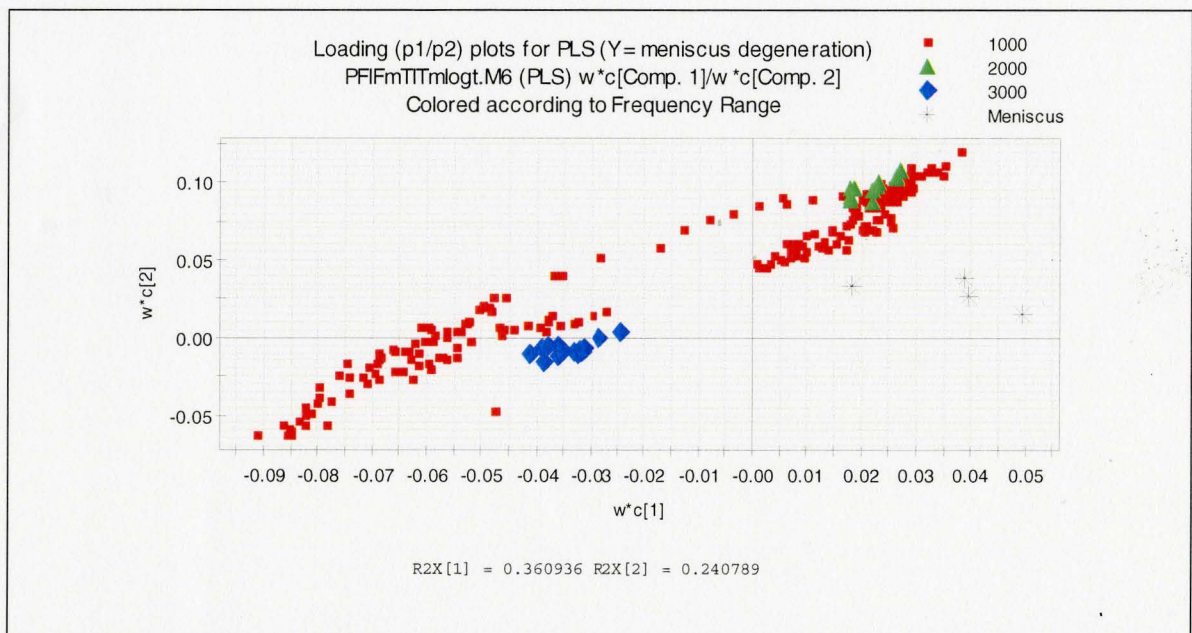


Figure 45: Observed VS Predicted average osteophyte formation level. PLS on the frequency data

Variable pruning is also an effective method for finding the influential variables in the model. When the meniscus damage level variables were used as the Y variables, pruning of variables showed that in addition to low frequency regions, parts of the mid and high frequency region are also important in building the model (Figure 46). The model used here was the log-wise model in which frequency components were chosen in a log-wise manner. This variable selection reduces the weights of high frequency while it puts more emphasis on lower frequency region. Pruning analysis suggests that log-wise selection of frequency components may not be a good method when it comes to building models for meniscus tear.



**Figure 46: Loading plots (p1/p2) for meniscus degeneration level after variable pruning.
 PLS on the frequency data**

According to above statement, a data set that has more components of higher frequency range may give better results to modeling meniscus problems. A part of our future work,

in continuation of this thesis is to assess the correlation between meniscus tear and frequency of recorded sound. This finding may help to build better models of the system in the future.

There is a strong correlation between formation of osteophytes and cartilage health. PLS analysis was therefore performed between X data and Y variables related to cartilage health (MRI scores of cartilage at different compartments) and the Y variables related to osteophyte formation as well as using the combination of the two Y groups. The results are shown in Table 4. Data pruning was again used to improve the prediction rate of the model.

Before variable pruning				After variable pruning						
	Comp #	R2X (%)	R2Y (%)	Q2Y (%)	Comp #	#X Var	R2X (%)	R2Y (%)	Q2Y (%)	X/Y Overview Plot
Cartilage	2	52	33	21	2	371	64	34	26	<p>X/Y Overview Plot for Cartilage Scores</p> <p>R2Y[1] = 0.3, R2Y[2] = 0.05 Q2Y[1] = 0.24 Q2Y[2] = 0.03</p>
Osteophyte	5	69	44	02	2	378	58	32	20	<p>X/Y Overview Plot for Osteophyte Vars.</p> <p>R2Y[1] = 0.24, R2Y[2] = 0.08 Q2Y[1] = 0.16 Q2Y[2] = 0.05</p>
Cartilage + Osteophyte	4	66	39	14	2	475	56	32	21	<p>X/Y Overview plot for cartilage and osteophyte variables</p> <p>R2Y[1] = 0.25, R2Y[2] = 0.07 Q2Y[1] = 0.17, Q2Y[2] = 0.05</p>

Table 4: quality of fit before and after data pruning for different combination of individual groups of Y variables (Cartilage and Osteophyte)

PCA and PLS analysis on the data obtained from patients in the sitting position did not have noticeable correlation with the MRI scores. This is in agreement with the hypothesis that the recorded signals that correlate with MRI scores are mainly crepitus vibrations and the low frequency data that results as an imprint of the surface of cartilage and bone

abnormalities. These signature vibrations are generated under loaded condition, which supports findings of O'Rourke et al [13]. In the sitting position there is no load on the cartilage surface and therefore the signals recorded will not contain much useful information.

5.2.4 Summary and conclusion

In this section PCA and PLS analysis techniques were used on power spectra of the vibrations recorded from each patient's knees. Beforehand, the signals were preprocessed by detrending and then removing click sounds (using wavelet transforms). The signals were then analyzed using PCA and PLS to see if there is any correlation between the MRI scores and the power spectrum of the signals. The results for PCA analysis show that there is a trend from healthy to un-healthy joints, More specifically there is a strong correlation between this "health trend" and formation of osteophytes and cartilage damage level. The rest of the MRI scores such as bone marrow edema and subchondral cyst did not reveal any correlation to the vibration data. It also seems that there is a correlation between meniscus tear and the vibration data. However many patients with Osteoarthritis also have meniscus damage and therefore with the current set of observations it is not possible to comment on this issue. This issue needs further investigation with a more controlled set of observations. Data pruning plays an important role in enhancement of prediction here. There are many variables in the X space that are not correlated with Y variables, and their presence in the model can reduce predictability

of Y space. In some cases, data pruning increased prediction of Y space by up to 18 percent. Because of the interconnectivity of features in the Y space and poor localization abilities of this technique it is not really possible to detect the specific location of a defect. However there is a good prediction of the overall level of joint health, specifically in case of cartilage damage and the presence osteophytes. In the case of PLS analysis, regressing X variables against average cartilage degeneration level, and after pruning, resulted in a model with Q^2 less than 50%. Although this level of prediction may not be sufficient in diagnostics, the score plots of the PLS model can still provide useful information about the joint's health trend. These score plots can be used the same way as the PCA score plots are used. Although PLS score plots have a more structured appearance than PCA score plots, they are actually more sensitive to variations and using them must be with caution. Choosing between PCA or PLS score plots is one the issues that needs to be further more investigated.

5.3 Analysis of wavelet transforms

5.3.1 Wavelet transforms

Wavelet transform is very similar to short-time Fourier transform (STFT) in nature. In STFT a moving window of fixed width is multiplied by the signal and then the Fourier transform of the windowed signal is calculated (Figure 47). The size of this window determines the compromise between time and frequency domain resolution.

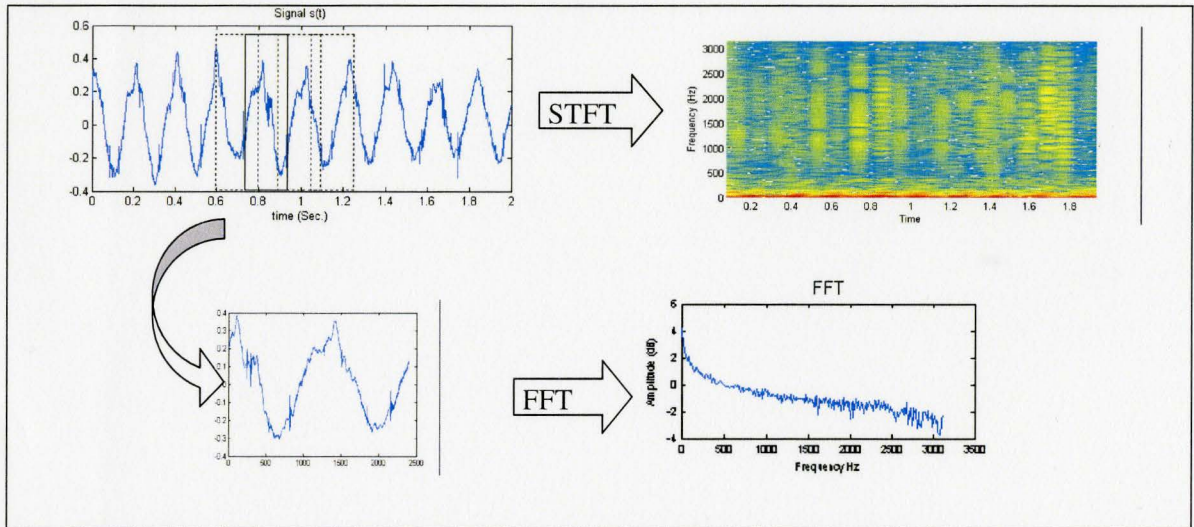


Figure 47: Short Time Fourier Transform (STFT)

In wavelet transform a waveform of limited duration is convolved with the signal at different scales. This waveform is called the mother wavelet (Figure 48)

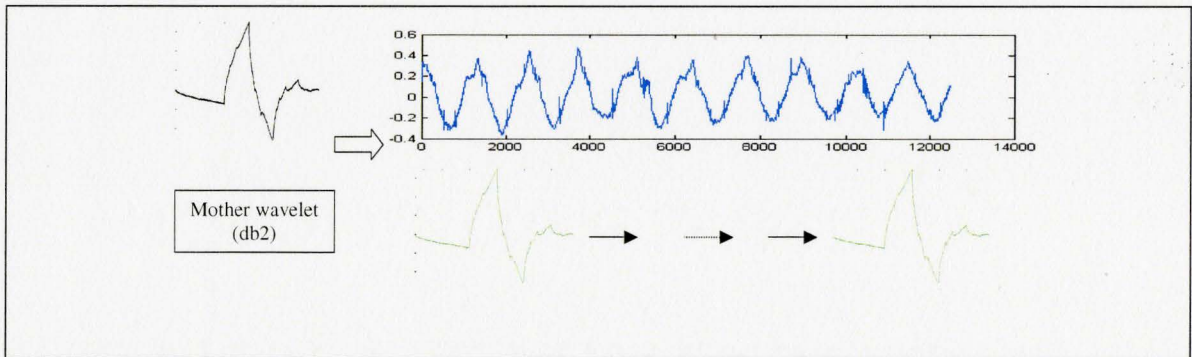


Figure 48: A mother wavelet and convolution with s(t)

The continuous Fourier transform frequency coefficients are obtained by:

$$F(\omega) = \int_{-\infty}^{+\infty} f(t)e^{-j\omega t} dt \tag{5.28}$$

Where ω is the angular frequency. A short time Fourier transform is defined by:

$$F_s(\omega, t) = \int_{-\infty}^{+\infty} f(u)g(t-u)e^{-j\omega u} du \quad (5.29)$$

$F_s(\omega, t)$ is the Fourier transform coefficient. In continuous wavelet transform, coefficients are defined by:

$$C(\text{Scale}, \text{Position}) = \int_{-\infty}^{+\infty} f(t)\psi(\text{Scale}, \text{Position})dt \quad (5.30)$$

Here, C is the wavelet coefficient at different scales and positions and ψ is the mother wavelet.

Scales and translation:

As mentioned above, wavelets operate on scales and position. The scale of a wavelet determines wavelet's level of stretch. Figure 49 shows a wavelet stretched at different scales.

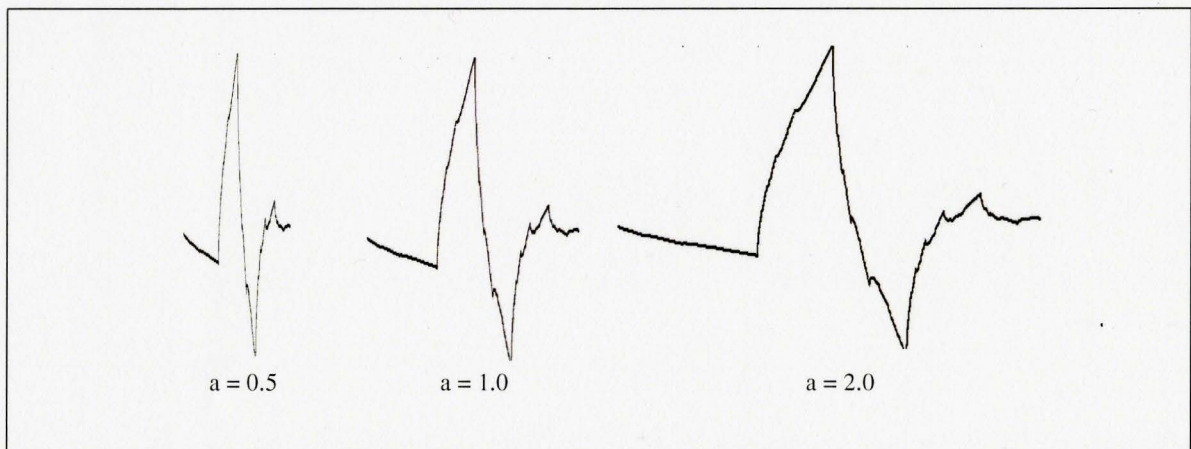


Figure 49: db2 wavelet (Ψ) at different scales (a)

The smaller the scale factor, the more compressed a wavelet is. Translation or shifting of a wavelet is shown by $\Psi(x/a-b)$. Depending on the way “a” and “b” are selected the transformation is called continuous or discrete. In continuous wavelet transform (CWT) we have:

$$C(a,b) = \int_{-\infty}^{+\infty} s(t) \frac{1}{\sqrt{a}} \psi\left(\frac{t-b}{a}\right) dt \quad (5.31)$$

$$a \in \mathbb{R}^+ - \{0\}, b \in \mathbb{R}$$

The CWT however, sacrifices the computation time over accuracy. If the scales and translation are chosen as:

$$C(a,b) = \int_{-\infty}^{+\infty} s(t) \frac{1}{\sqrt{a}} \psi\left(\frac{t-b}{a}\right) dt \quad (5.32)$$

$$a \in 2^j, b \in k2^j, (j,k) \in \mathbb{Z}^2$$

then this type of transformation is called discrete wavelet transform (DWT).

The inverse of wavelet transform is defined by (continuous synthesis):

$$s(t) = \frac{1}{K_\psi} \int_{\mathbb{R}^+} \int_{\mathbb{R}} C(a,b) \frac{1}{\sqrt{a}} \psi\left(\frac{t-b}{a}\right) \frac{da.db}{a^2} \quad (5.33)$$

where K_ψ is a constant that depends on Ψ . In case of discrete synthesis the above equation changes to:

$$s(t) = \sum_{j \in \mathbb{Z}} \sum_{k \in \mathbb{Z}} C(j,k) \psi_{j,k}(t) \quad (5.34)$$

In discrete wavelet transform, the signal is decomposed into two components at each stage; a low frequency, high scale component called the “approximate” of the signal and a high frequency, low scale component called the “detail” of the signal. This is similar to filtering the signal using low-pass and high-pass filters (Figure 50)

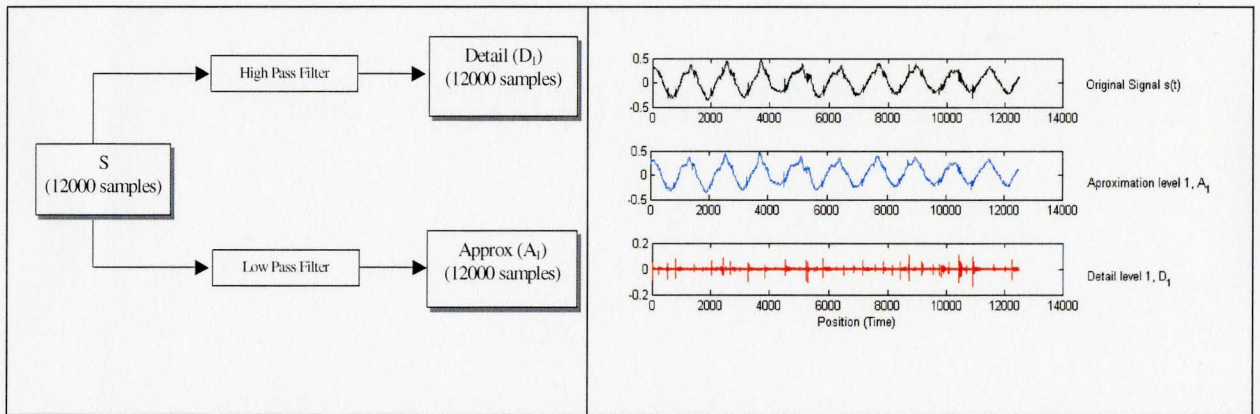


Figure 50: Decomposition of the signal “s” into its detail and approximate ($s = D_1 + A_1$)

If “j” is kept fixed and $C(j,k)$ is summed over “k” then we get:

$$D_j(t) = \sum_{k \in \mathbb{Z}} C(j,k) \psi_{j,k}(t) \quad (5.35)$$

D_j is detail of the signal at level “j”. The original signal will be the sum of all D_j :

$$s = \sum_{j \in \mathbb{Z}} D_j \quad (5.36)$$

Let us assume “J” is chosen as a reference for “j”. Now the approximate of the signal at level J can be written as:

$$A_J = \sum_{j > J} D_j \quad (5.37)$$

And of course:

$$s = A_J + \sum_{j \leq J} D_j \quad (5.38)$$

It is interesting to note that $D_j \perp D_i$ for $j \neq i$. ϕ is a function associated with Ψ . This function is used to define the approximation of the signal. When the signal is decomposed into the approximate and the detail coefficients, the number of obtained sample points doubles. For example if the signal has 1000 points, the resulting approximate and detail of the signal will each have 1000 points. It turns out that 1 out of every two consecutive coefficient points is enough to maintain all the information in the original signal. Thus at each decomposition level, only half the coefficients (for example odd numbered coefficients) are kept. This procedure is called downsampling. The downsampled coefficients at level “n” are called cA_n and cD_n . Figure 51 illustrates how a signal is decomposed at several stages using wavelet transform. For more information on wavelets and their applications refer to “Wavelet Toolbox User Guide, by Mathworks Inc.

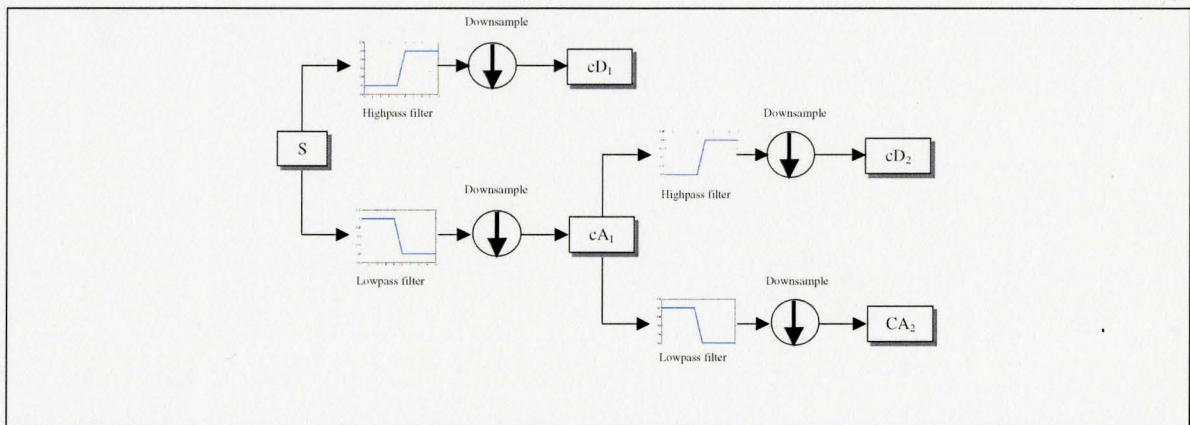


Figure 51: DWT in two stages

Wavelet Packet Analysis (WPA) is similar to DWT except that at each level, in addition to the approximates of the signal, the details also get decomposed into new approximation and details as well. Figure 52 illustrates this idea.

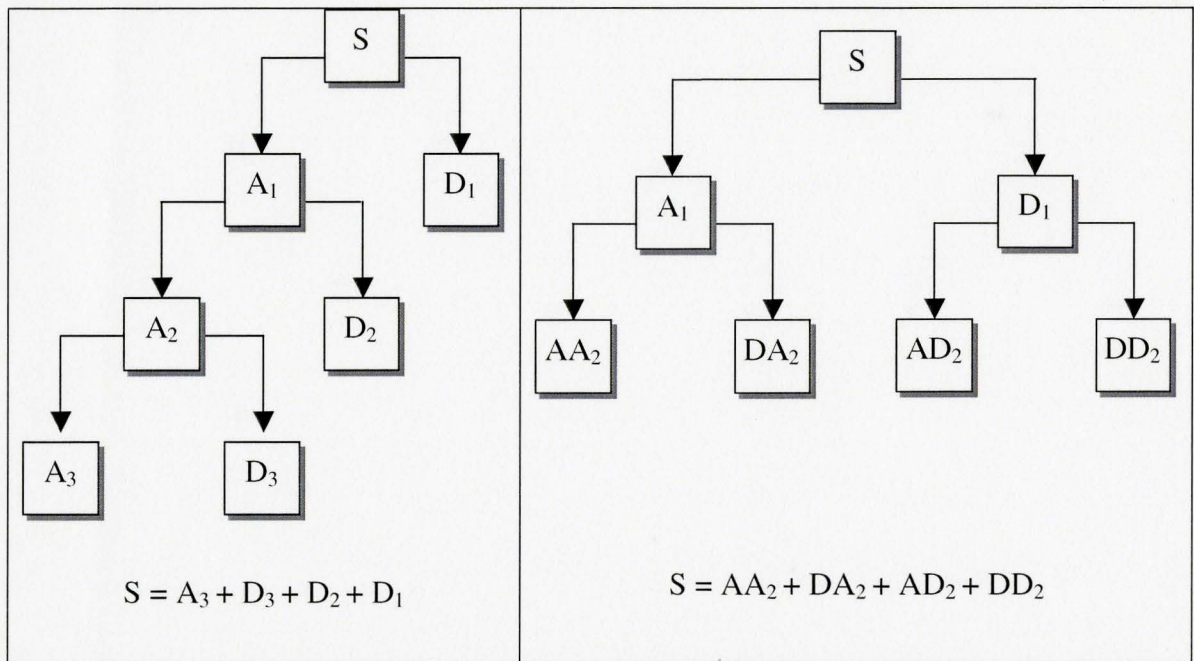


Figure 52: DWT (Left) versus Packet Wavelet analysis (Right)

Wavelets come in different shapes. In general a function that is continuous, has null moments²⁷ and decreases quickly towards zero can be a candidate to become a wavelet. However wavelets that have practical use, usually have more profound properties such as orthogonality, existence of ϕ , having several vanishing moments and $\int \psi(x) dx = 0$. It is possible to define pseudo frequency for a wavelet scale. F_a or the scale frequency of a wavelet is defined as:

$$F_a = \frac{\Delta \cdot F_c}{a} \tag{5.39}$$

where F_c is the center frequency of the wavelet (F_c is the frequency maximizing FFT of a wavelet modulus). F_a is the pseudo frequency of the wavelet at scale “a” and Δ is the sampling period ($1/F_s$). Figure 53 shows how center frequency of a wavelet relates to its shape and period.

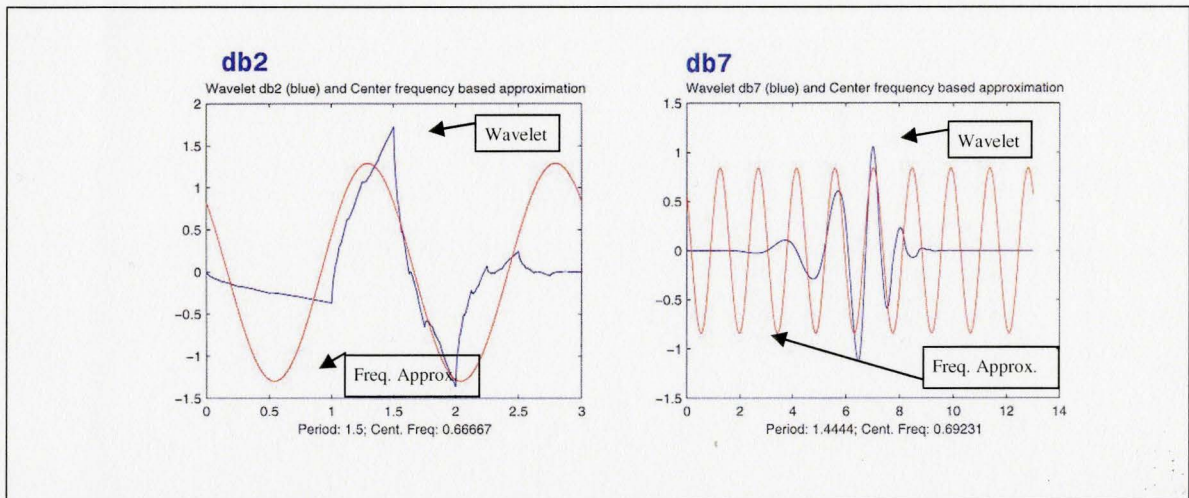


Figure 53: center frequency (F_c) of a wavelet (adopted from wavelet toolbox tutorial, mathworks inc)

There are several types of wavelet families and different criteria that define the properties and qualities of the wavelets and their families, such as speed of convergence to zero in both time and frequency domain, symmetry, number of vanishing moments, regularity and existence of scaling function ϕ . Figure 54 shows some of the wavelets that are available for analysis. The simplest type of wavelets is the Haar wavelet (Figure 54). This

²⁷ A function's $k+1$ moments are equal to zeros when: $\int_R t^j \psi(t) dt = 0$ for $j=0, \dots, k$

wavelet was the first wavelet ever created. Another set of wavelets that were named after their creator are the Daubechies family of wavelets. Dabechies wavelets are written as “dbN” where N is the order of the wavelet. Finding the proper wavelet for a specific application is more of a trial and error operation. Knowing properties of the wavelets and the characteristics we need to find in the signal may help to make a proper selection. In this project several different types of wavelets were tried and it appeared that the db1 (Haar) wavelet gives the best results.

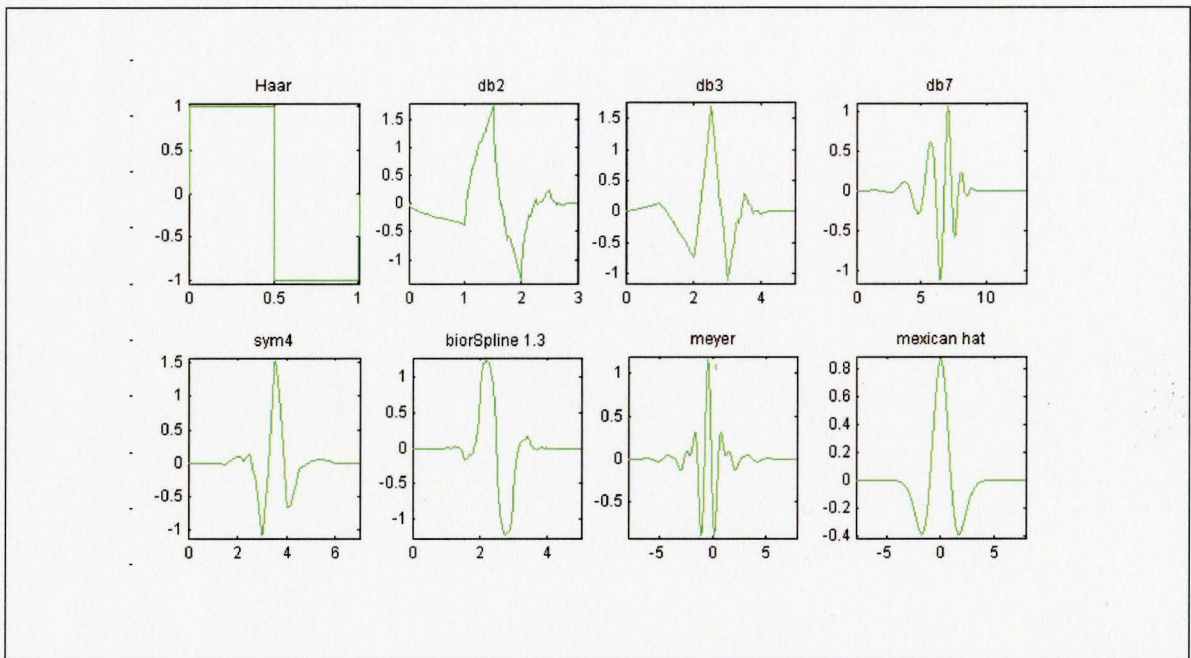


Figure 54: different wavelet shapes

Before using the wavelet transforms in PCA or PLS analysis they need to be prepared for the analysis. Perhaps the most popular method is to calculate the average power of coefficients [equation (5.40)] at each decomposition level (i).

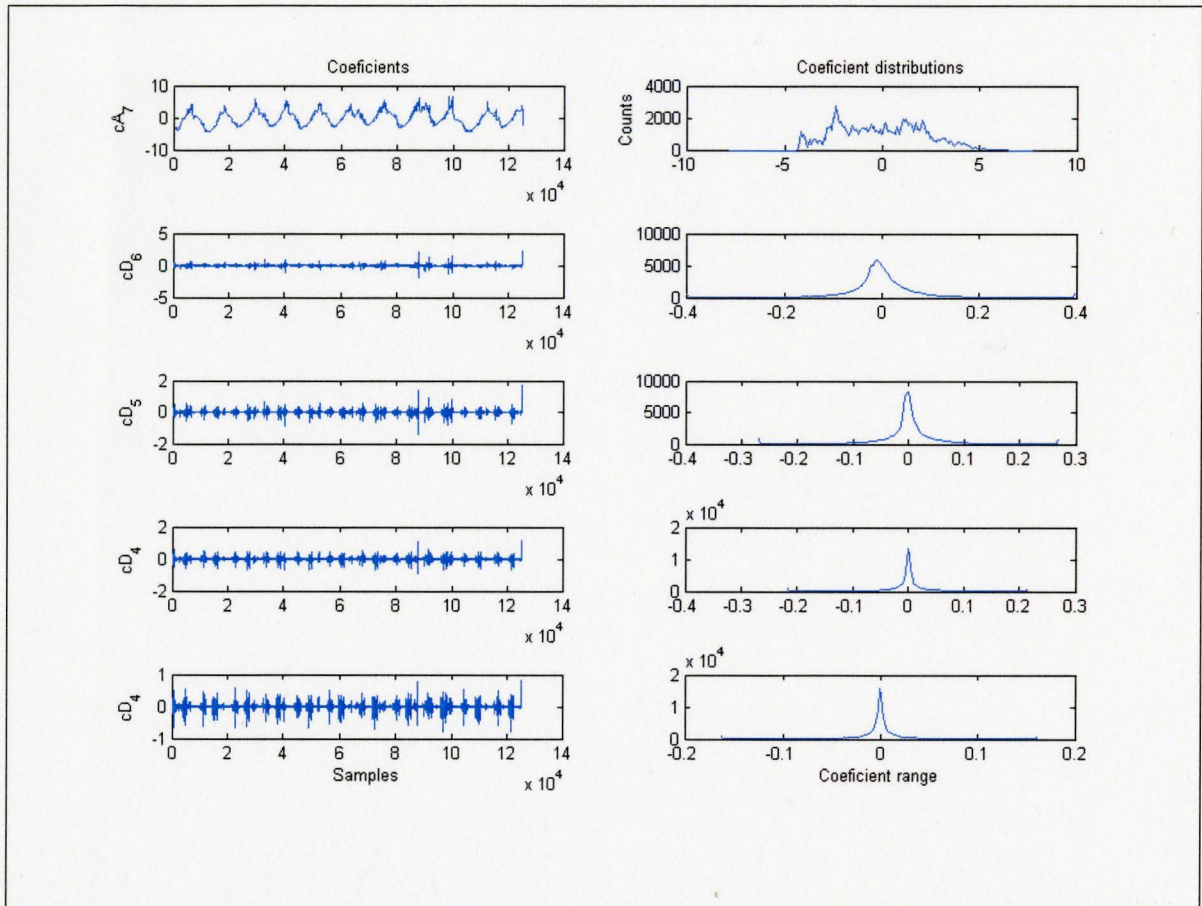


Figure 55: distributions of wavelet coefficients at different levels for the coefficients of a stationary wavelet transform

5.3.2 PCA on histograms of wavelet coefficients

For each sensor (accelerometer) the recorded vibration signals were decomposed into their wavelet coefficients (10 detail levels and one approximate; db1 wavelet) and then the histograms of the coefficients at each level were calculated. Choosing 200 bins for each histogram (a range of -3.5 to 3.5 standard deviations) yielded 2200 variables for each accelerometer. When the centre frequencies of wavelets at each level were

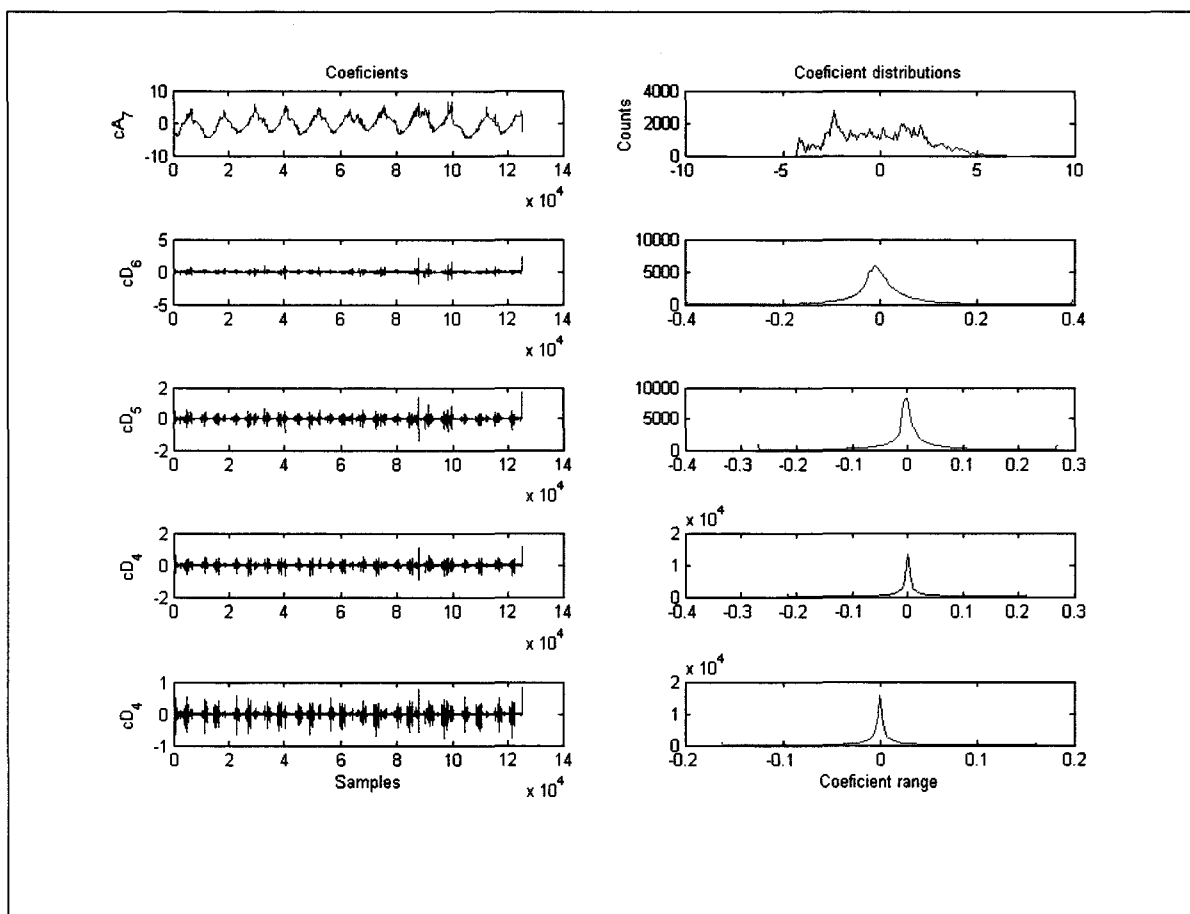


Figure 55: distributions of wavelet coefficients at different levels for the coefficients of a stationary wavelet transform

5.3.2 PCA on histograms of wavelet coefficients

For each sensor (accelerometer) the recorded vibration signals were decomposed into their wavelet coefficients (10 detail levels and one approximate; db1 wavelet) and then the histograms of the coefficients at each level were calculated. Choosing 200 bins for each histogram (a range of -3.5 to 3.5 standard deviations) yielded 2200 variables for each accelerometer. When the centre frequencies of wavelets at each level were

calculated it was realized that the center frequency for level one detail coefficients is 3.1 KHz. Since previous frequency analysis showed that this range of frequency does not contain useful information about cartilage damage or osteophyte formation, cD_1 was omitted from the “X” variable data set. Hence the final X data set will contain 10000 variables; 2000 variables for each accelerometer. Table 5 shows the scale frequency for levels 1 to 10 of db1 wavelet.

Detail	cD_{10}	cD_9	cD_8	cD_7	cD_6	cD_5	cD_4	cD_3	cD_2	cD_1
Scale Frequency (Hz)	6	12	24	48	97	195	389	778	1550	3100

Table 5: Scale frequency for levels 1 to 10 of db1 wavelet

In the first step an initial PCA analysis was performed on the “X” dataset and the model was checked for any strong outliers. After removing the outliers (4 observations) and performing PCA again a model with $R^2_x = 39\%$ and $Q^2_x = 27\%$ (11 components) was obtained. Figure 56 shows the model overview plot of the “X” dataset.

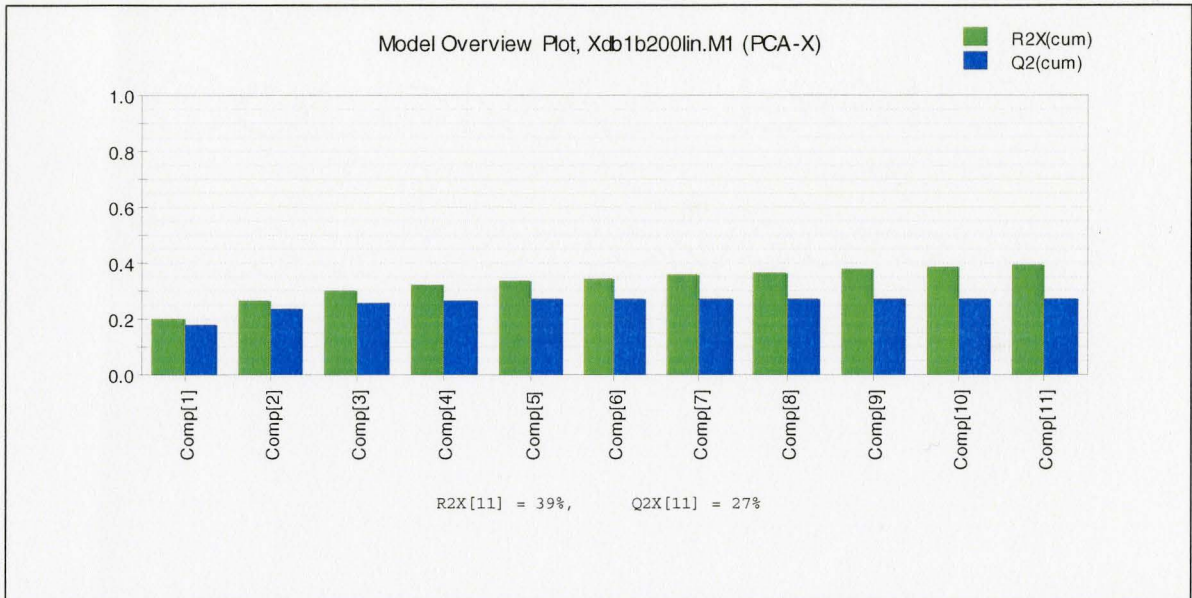


Figure 56: model overview plot (PCA on wavelet histograms)

Component contribution plots (Figure 57 and Figure 58) show that component 1 is mainly capturing the variations in the lower details (higher frequencies) and the second component is capturing variations related to all levels but more specifically mid-level details.

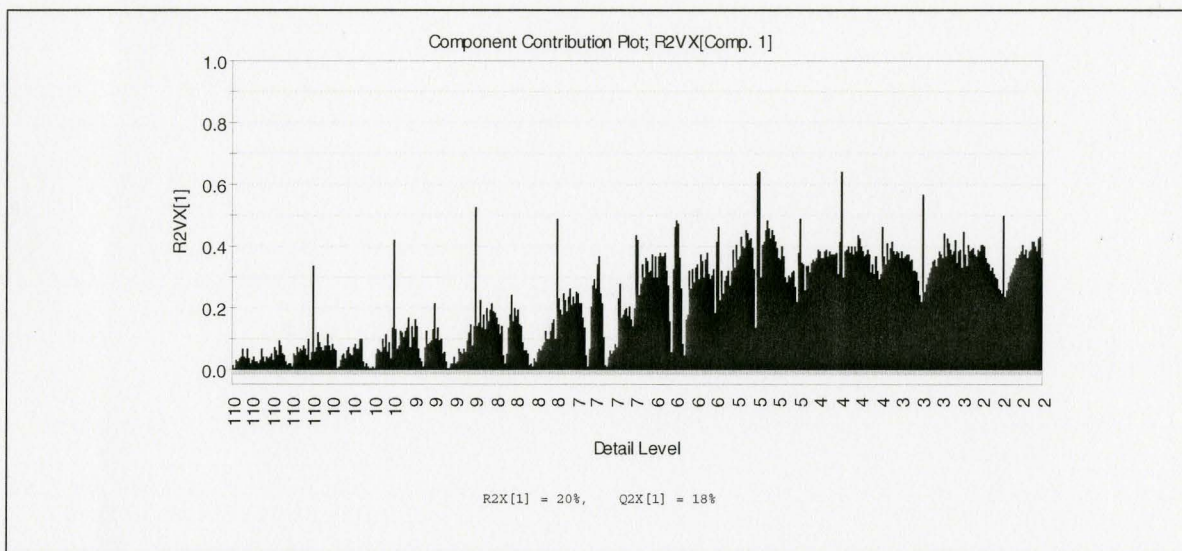


Figure 57: Component Contribution plot for coefficient histograms at all details (only patella sensor variables shown); Comp. #1 (PCA on wavelet histograms), Level 110 = approximate at level 10 (the numbers on the abscissa show the approximate range of variables for each detail)

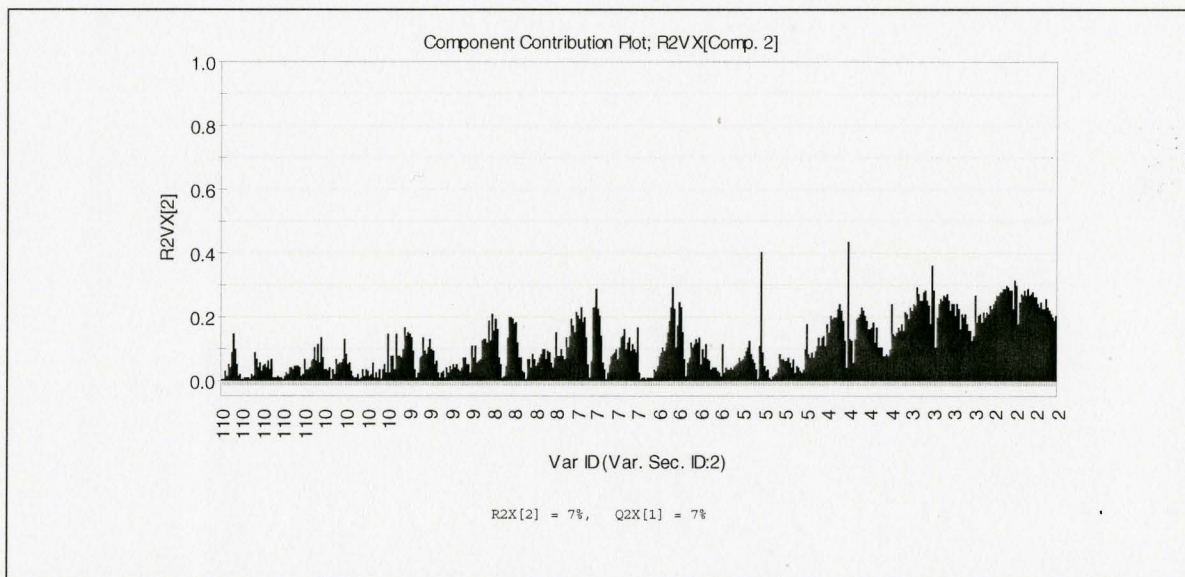


Figure 58: Component Contribution plot for coefficient histograms, at all details; Comp. #2 (PCA on wavelet histograms, only patella sensor variables shown), Level 110 = approximate at level 10 (the numbers on the abscissa show the approximate range of variables for each detail)

Another component that seems to have useful information for the score plots is component 4. The component contribution plot for this component is shown in Figure 59.

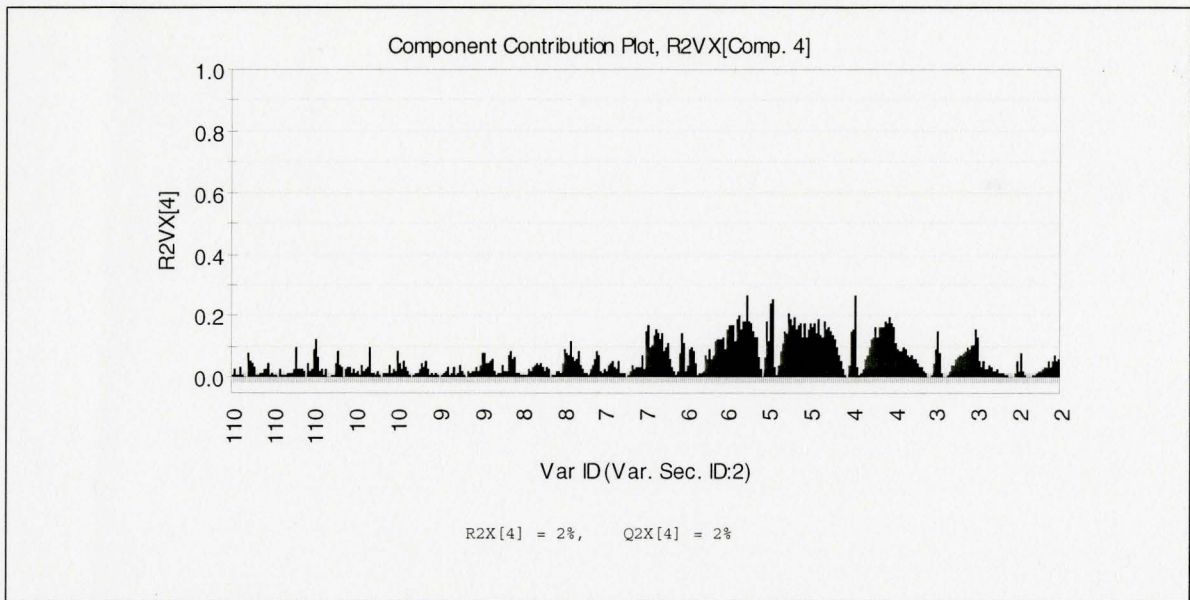


Figure 59: Component Contribution plot for coefficient histograms, at all details; Comp. #4 (PCA on wavelet histograms, only patella sensor variables shown), Level 110 = approximate at level 10 (the numbers on the abscissa show the approximate range of variables for each detail)

Figure 59 shows that this component is capturing some of the variation in detail levels 3 to 7. Figure 60 (a & b) show the score plots of the PCA model colored according to cartilage damage severity. Figure 60b shows that there is a trend from the healthy knees to the knees with cartilage damage. The contribution plot (Figure 61) between healthy and damaged knees (unhealthy compared to healthy knees) shows that compared to the healthy knees (cartilage health), wavelet coefficients of unhealthy knees, at higher scales (lower frequencies), are more concentrated around zero and at lower scales (higher frequencies) they have a wider dispersion.

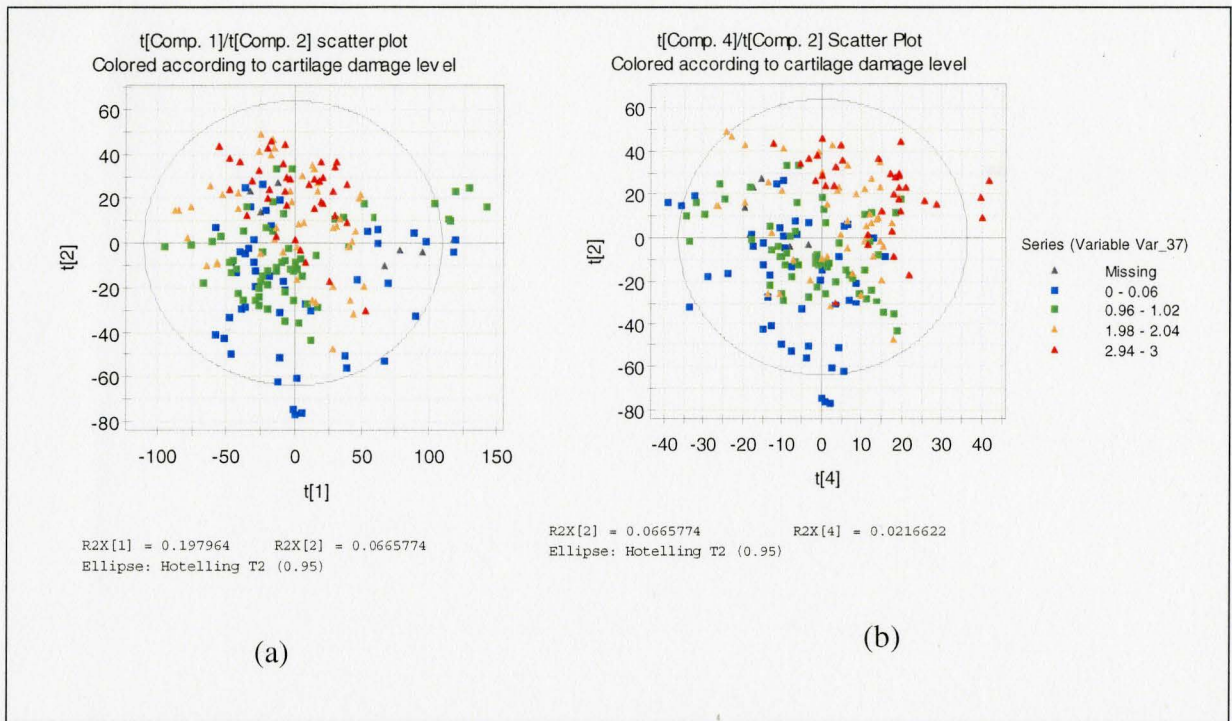


Figure 60: t1/t2 and t4/t2 score plots of the PCA model for wavelet dataset

A wider dispersion corresponds to more energy content in that frequency region. Therefore it can be concluded that healthy knees have more energy in the lower frequency region and less energy in the higher frequency region of the spectra. These findings are in agreement with the results obtained in previous section; Frequency analysis.

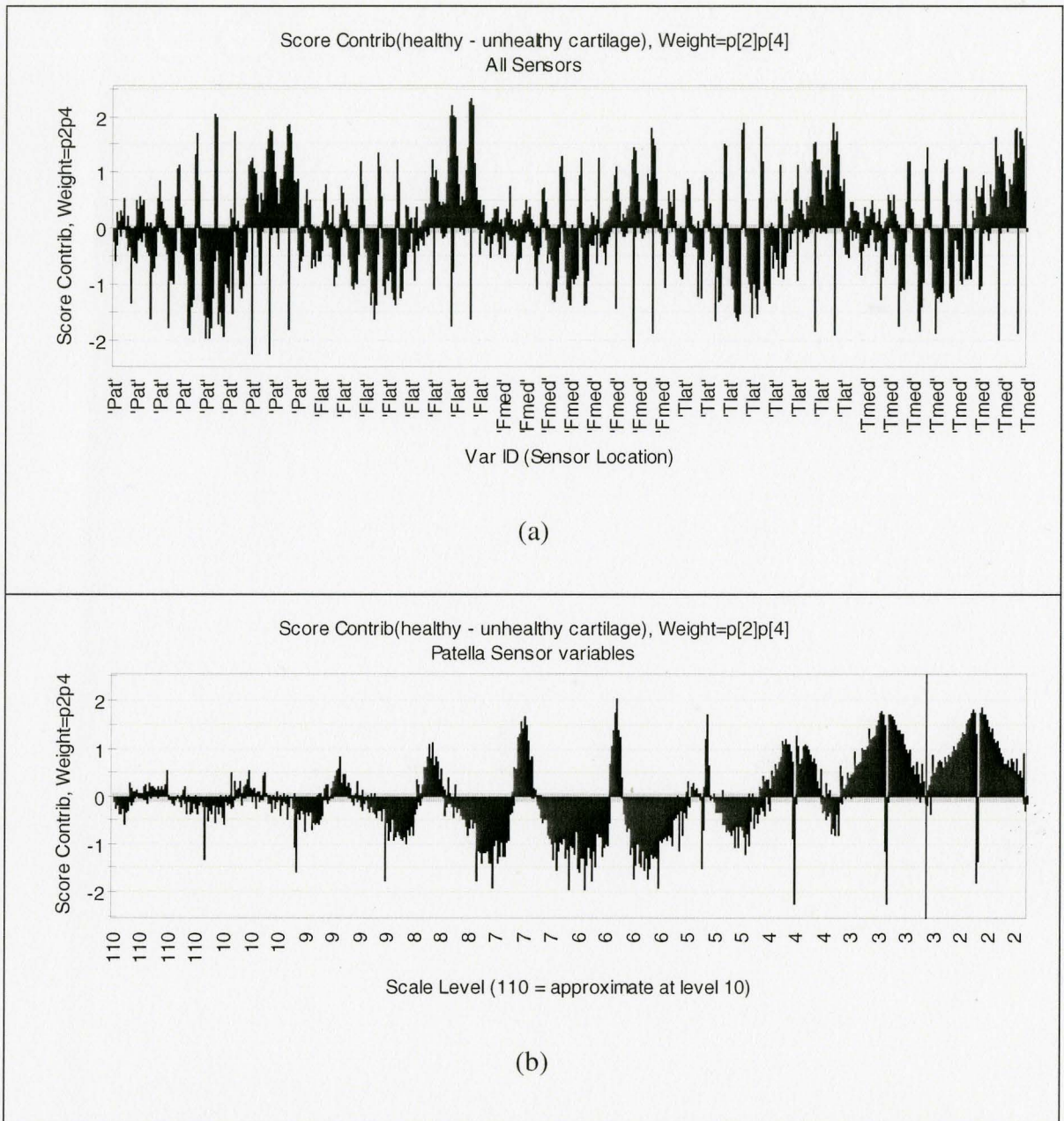


Figure 61: Contribution plot between healthy (0-1) and unhealthy (2-3) cartilage knees (wavelet scales 2 to 10); a) for all sensors, b) only shown for the patella sensor.

Figure 62 shows a blow-up of the histograms, shown in Figure 61, for some of the low and one of the high frequency regions of the wavelet histograms (low frequency region is assumed to be approximately less than 250 Hz or coefficient levels above 4). It shows how unhealthy knees (cartilage scores 2-3) have larger wavelet coefficients at higher and mid frequencies and vice versa.

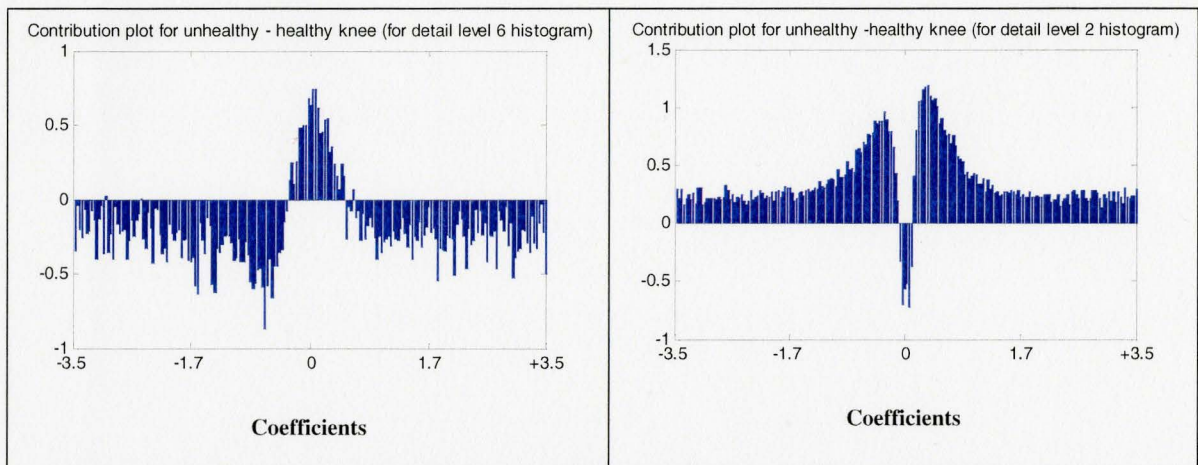


Figure 62: Contribution plot for the difference of unhealthy from healthy knee; Left: low frequency (Det. 6), Right: High Frequency (Det. 2)

Figure 63 shows the t2/t4 score plot colored according to average osteophyte score. As mentioned before, osteophyte formation is strongly correlated with cartilage loss; the correlation between average cartilage damage and average osteophyte formation in our population was 80%.

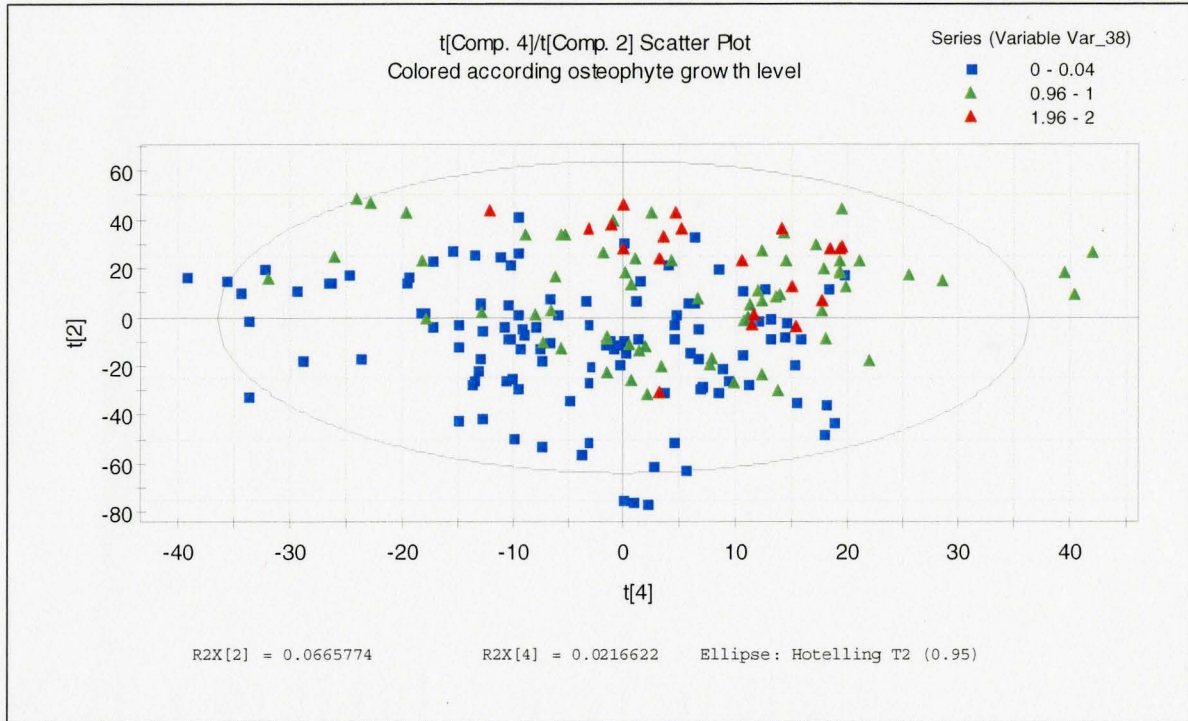


Figure 63: t_2/t_4 score plot of the PCA model for the wavelet dataset colored according to average osteophyte score

5.3.3 PLS on the wavelets

After performing an initial PCA analysis and removing strong outliers (4 observations), a PLS model was obtained by analyzing the cartilage scores (Y space) and wavelet data (X space). The first 14 components captured 97% of the variability in Y space (R^2_y) with predictability (Q^2_y) of 39%. The model was then improved by removing the less significant variables. The improved model has 14 components, $R^2_x = 51\%$, $R^2_y = 96\%$ and $Q^2_y = 63\%$ (total 5500 variables in the X space). Figure 64 shows the overview plot

of this model. Model overview plot suggests that t_1 and t_3 contain the most useful information about the model.

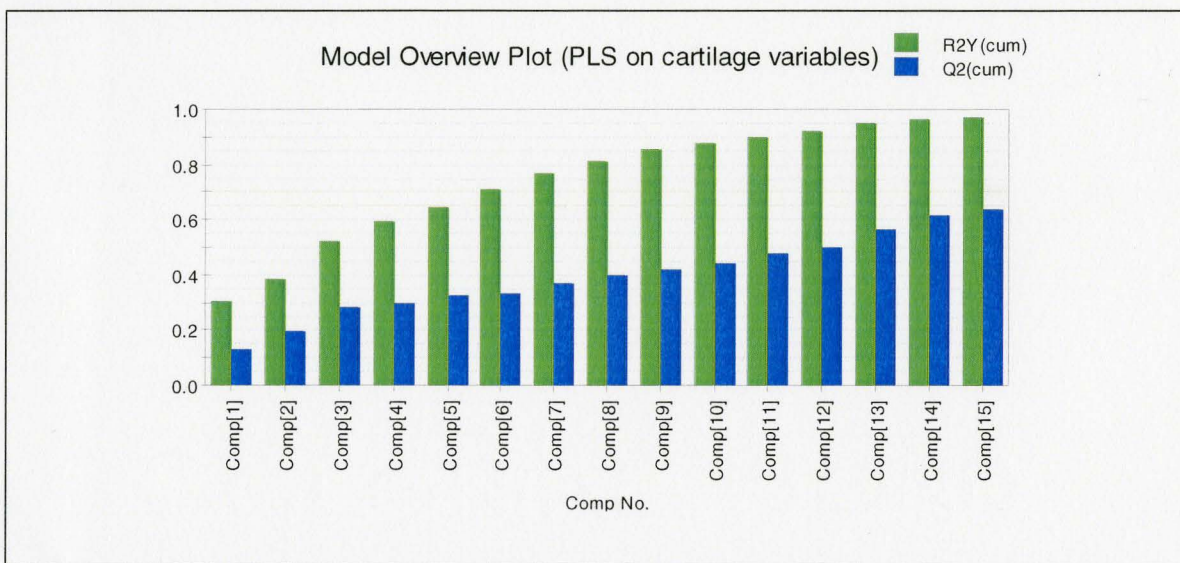


Figure 64: Model Overview Plot of the PLS model on the cartilage variables (after pruning extra variables)

Figure 65 shows the t_1/t_3 score plot of the model. The color of the plot has been chosen according to the average severity of cartilage damage (average cartilage score). It seems that, overall, the model is capable of predicting average severity of cartilage damage. When individual Y-Predicted ($Y =$ cartilage score) plots for each compartment (Figure 66 to Figure 68) were observed, it was realized that modeling individual cartilage scores of the knee did not provide adequate predictability. It seems the model is more capable of predicting an overall degree or an average degree of cartilage damage.

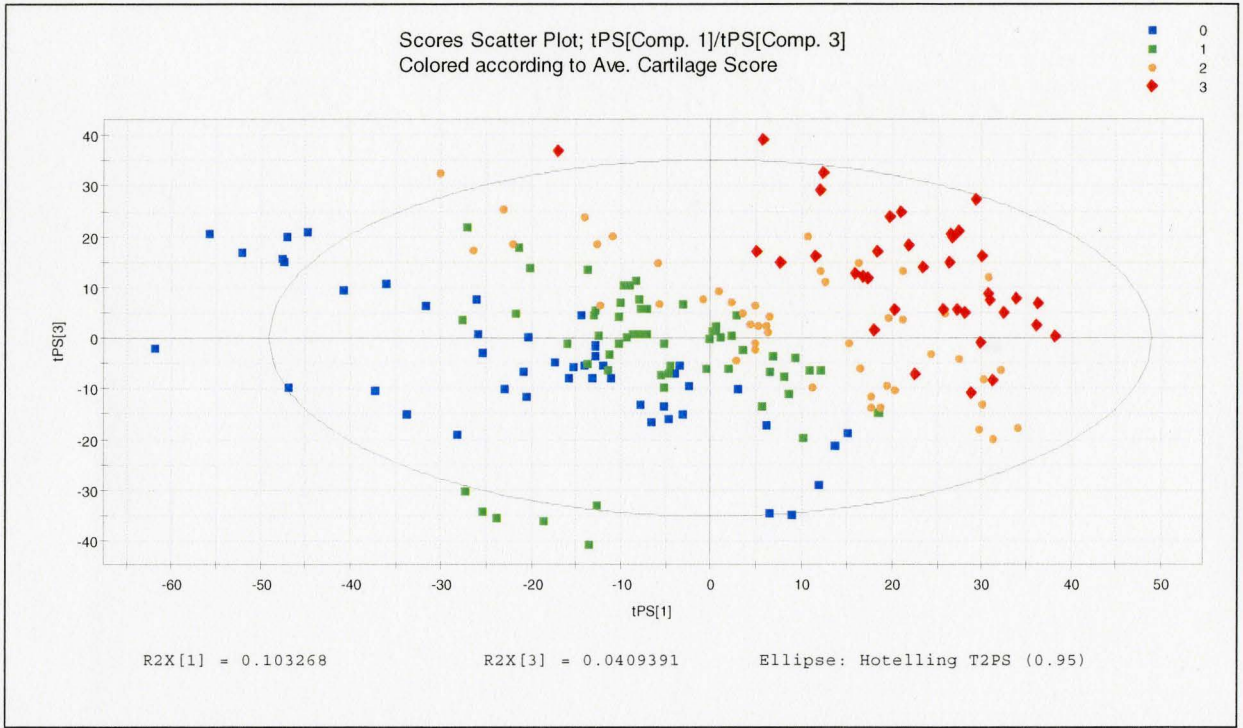


Figure 65: t_1/t_3 Score Scatter plot, colored according to average cartilage score

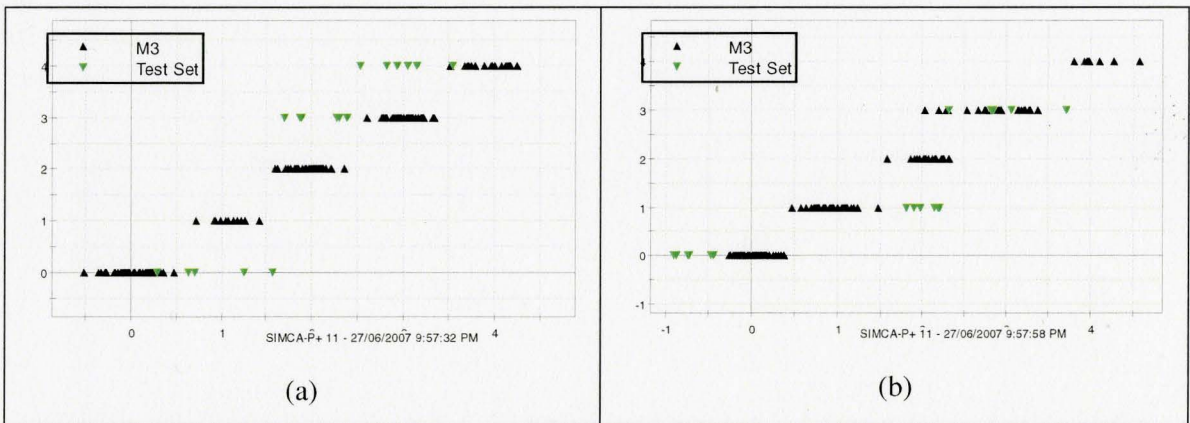


Figure 66: Y, Observed VS Predicted for cartilage score at a: Medial Femur (FMed), b: Lateral Femur (FLat)

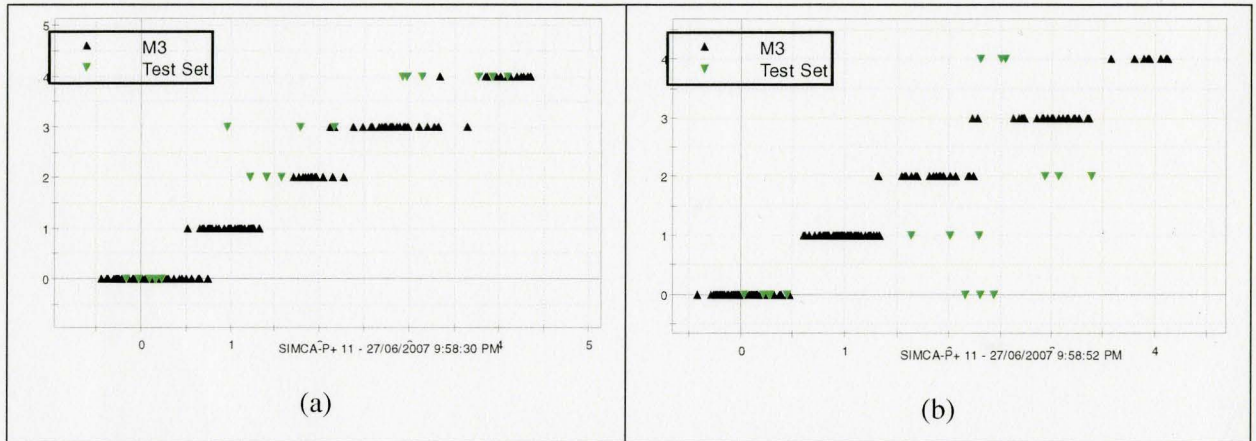


Figure 67: Y, Observed VS Predicted for cartilage scores at a: Medial Tibia (Tmed), b: Lateral Tibia (Tlat)

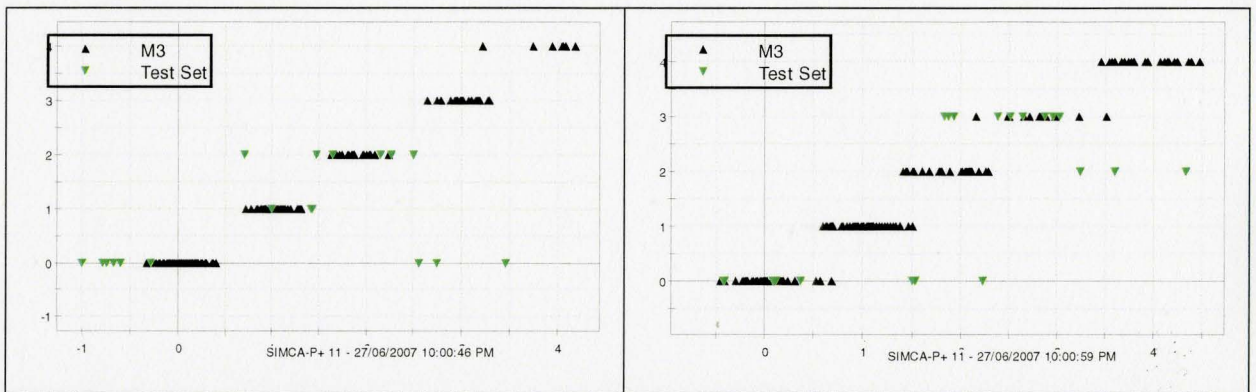


Figure 68: Y, Observed VS Predicted for cartilage scores at a: Trochlea (FT), b: Patella

Another model was obtained by regressing the “X” variables against individual scores for osteophyte formation. The model was again improved by pruning the less significant variables. The final model has 15 components with $R^2_x = 50\%$, $R^2_y = 96\%$ and $Q^2_y = 59\%$. Figure 69 shows the overview plot of the model. It shows that the first three components are capturing most of the variations in the Y space.

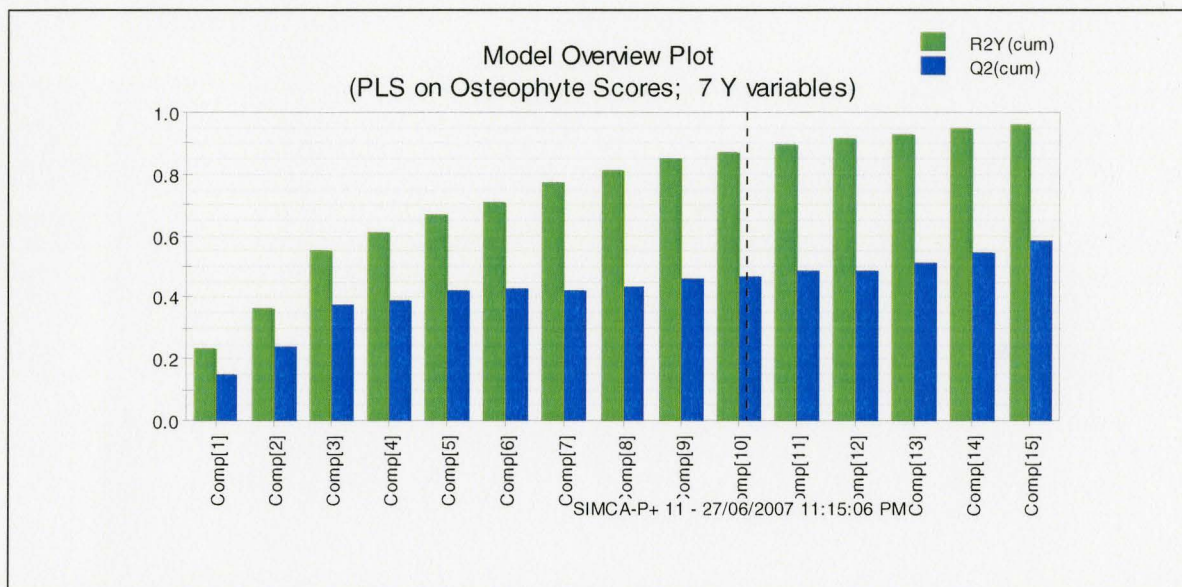


Figure 69: Model overview plot for PLS model on individual osteophyte scores (after Pruning)

Figure 70 shows the t_1/t_2 and t_1/t_3 score plots of the model, colored according to average osteophyte score. It is evident that healthy knees (score = 0) are separated from knees with large formations of osteophyte (score 2). The scores that are enclosed in squares belong to the test set.

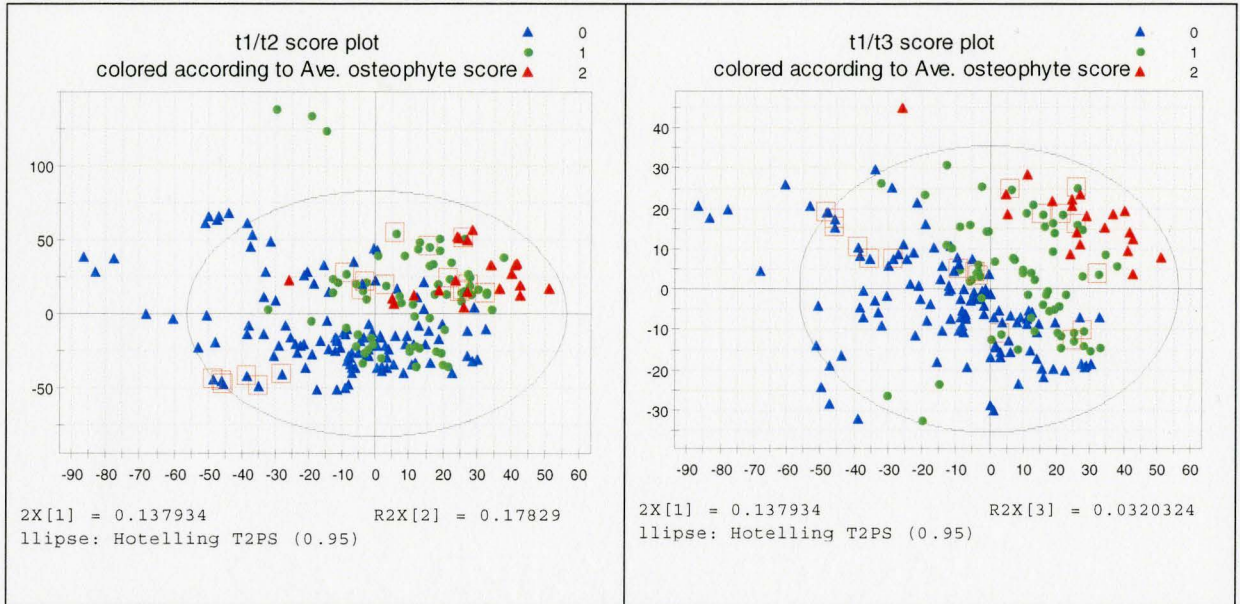


Figure 70: t_1/t_2 (left) and t_1/t_3 (right) score plots of the PLS model colored according to average osteophyte score

The score plots show that although formation of osteophytes can be predicted (more accurately than the cartilage scores), again localization of the osteophytes is not accurate and the model is more successful in predicting the average scores of different knee compartments. For this reason a PLS model based on the average scores of the cartilage and osteophyte (average of various compartments of the knee) was developed (# of Comp = 5, $R^2_x = 41\%$, $R^2_y = 89\%$, $Q^2_y = 70\%$). Figure 71 shows the model overview plot

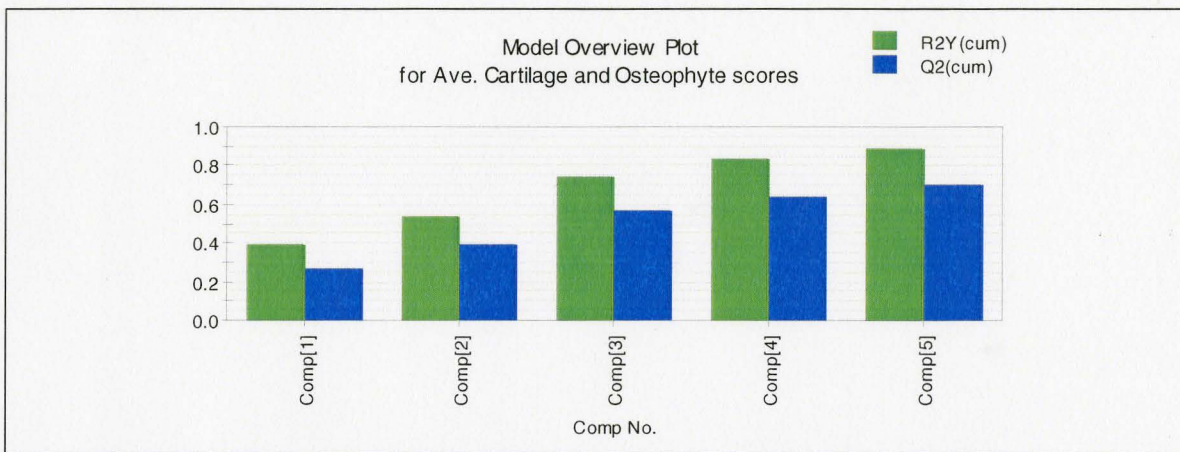


Figure 71: Model Overview Plot for average cartilage and osteophyte scores

Figure 72 shows the X/Y overview plot of the model

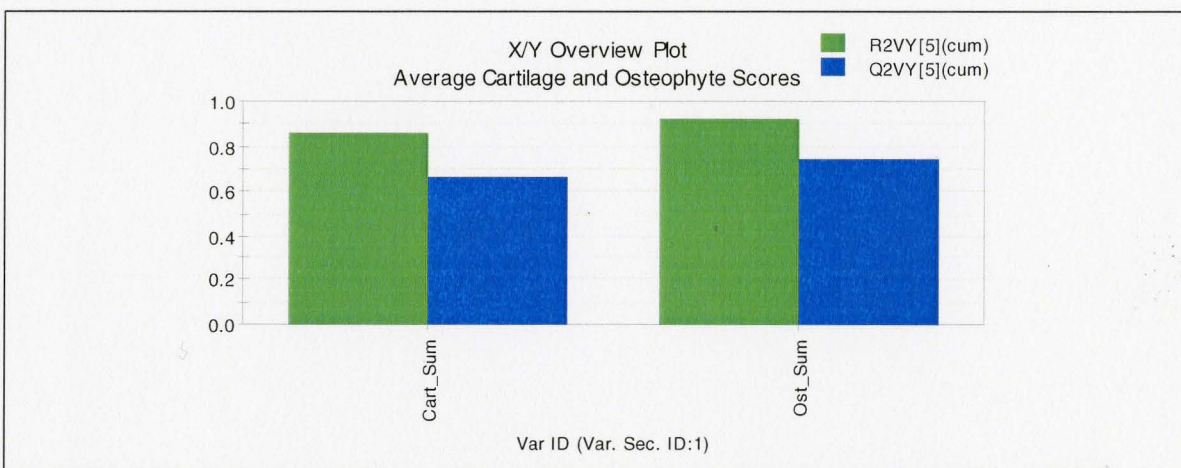


Figure 72: X/Y Overview plot of the PLS model for average cartilage and osteophyte scores

Figure 73 shows the observed versus predicted value for the average cartilage and osteophyte scores. Observations in green belong to the test set.

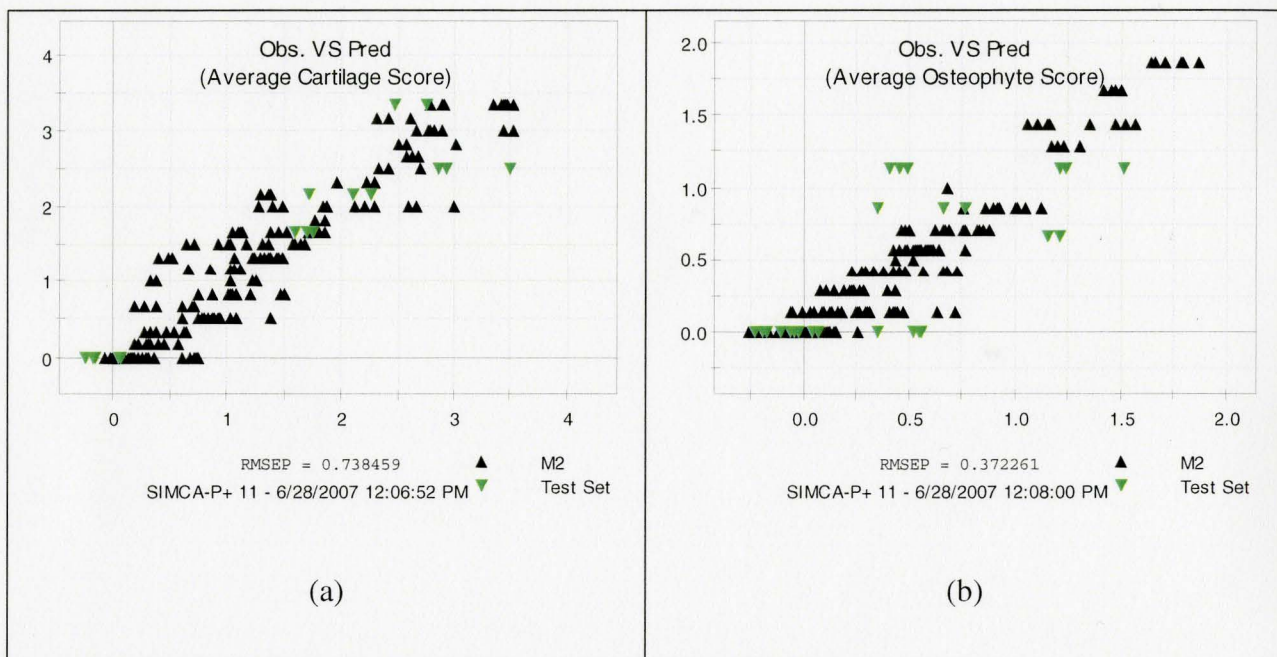


Figure 73: Observed versus Predicted value for a: Average Cartilage Score, b: Average Osteophyte Score

A few notes on the errors

Scoring the MRI sheets is a sensitive and delicate job. The level of accuracy can change from person to person and therefore the scoring system by itself can introduce errors to the model. In order to have an estimate of the level of each model's predictability, we needed to have a measure of human error and a measure of the round off error due to scoring procedure. To measure the repeatability, several observations (MRI Images) were scored twice at different times. The variations of the scores were calculated by the following formula

$$SS_{PE} = \sum_{i=1}^m \sum_{u=1}^{n_i} (y_{iu} - \bar{y}_i)^2 \quad (5.41)$$

And the percentage of error due to pure error was calculated as:

$$\%SS_{PE} = \frac{SS_{PE}}{SS_y} \quad (5.42)$$

The results for osteophyte and cartilage scores are shown in Table 6. Although the observations were only repeated twice (for 28 observations), it still gives an idea of the scale of Pure Error in obtaining the cartilage and osteophyte scores from the MRI images. One source of error introduced into the Y space data is error due to round-off error. Since the scores are assigned as integer values (0 to 4 for cartilage and 0 to 2 for osteophyte), the discontinuity of the scores also introduces some error. If round-off error has a uniform distribution then:

$$f(x) = \frac{1}{b-a} \quad a \leq x \leq b \quad (5.43)$$

The variance of the above distribution can be calculated from:

$$\sigma^2 = \frac{(b-a)^2}{12} \quad (5.44)$$

For “a-b = 1” (integer round off), percentage of variance due to round off can be calculated from:

$$\%SS_{RE} = \frac{\sum \frac{1}{12}}{SS_y} \quad (5.45)$$

Table 6 shows the percentage of error due to pure and round-off errors. It should be noted that round-off error is in fact part of pure error. It is evident that the percentage of human error is relatively high and part of this large pure error is because of the large round off error. However it should be noted that distribution of pure error here is not normal and this can in turn increase the error percentages calculated here.

Compartment	Cartilage						Osteophyte						
	Med Fem	Lat Fem	Med Tib	Lat Tib	Troch.	Pat	Med Fem	Lat Fem	Med Tib	Lat Tib	Troch.	Pat	Tib Spine
Pure Error	0.36	0.45	0.28	0.44	0.53	0.33	0.39	0.6	0.59	0.3	0.65	0.18	0.35
Round off Error	0.04	0.04	0.04	0.05	0.04	0.05	0.15	0.17	0.22	0.2	0.25	0.16	0.19

Table 6: Percentage of error due to Pure Error and the component of it due to round-off.

5.3.4 Summary and conclusion

In this section PCA and PLS methods were used to extract features from the wavelet transforms of the vibration signals. Before the PCA or PLS analysis, the data had to be prepared. The method of choice here was to use the distributions of the wavelet coefficients. One of the benefits of using such distributions is that they have the ability to isolate the knee clicks; knee click usually contain much higher than average magnitudes and by using distribution plots for each coefficient level, the coefficients contributing to the clicks will be accumulated in the farthest bins of the histograms and therefore can be isolated. These knee clicks can seriously alter the results of the analysis, especially if Fourier transform is to be used. PCA analysis of the wavelet histograms showed that the

score plots of the model are able to show the difference between healthy and unhealthy knees for both the cartilage and osteophyte scores. It was realized that these two types of joint disorder are highly correlated with each other and the analysis shows there is an 80% correlation between the averages of their scores. It was also found that this method does not provide adequate classification on the individual cartilage and osteophyte scores at different compartments of the knee but provides good results for the averages of them. The reason is that the development of these symptoms does not usually happen in one compartment of the knee and is rather spread through out the joint. Another reason is that vibration signals at such low frequencies do not really convey much information about location of the disorders. However as far as it is concerned with diagnostics of these disorders, what is important is the detection or estimation of the overall health of the joint. These PLS and PCA models can be used for estimation of the overall health status. In addition to this application, this method can be used as a tool to measure the friction in the joint, for monitoring purposes, which has application in pharma-tech industries the method can be used for observation of the effects of drugs or synovial injections on the overall friction level of the joint [14].

Chapter 6

Summary and Conclusion

The aim of this research was to develop a technology to assess tissue health in patients suffering from osteoarthritis. Previous work done by Yacoub [14] and Rangayan [17, 19 and 49] showed that there is a good correlation between the stage of the OA and vibration signals generated during the flexion/extension cycle. Our goal was to further analyze this hypothesis in more depth and to build an apparatus that would be practically and robustly used by the examiner to detect and monitor the health status of the knee.

Based on a good understanding of the motions involved in the flexing of the human knee, an apparatus was built to house the sensors to measure the vibrations emitting from the knee during flexion/extension cycle. Five accelerometers located at medial & lateral sides of tibia, medial & lateral sides of femur and on the patella record the vibrations generated by the knee during a flexion/extension cycle. Due to the sensitivity of the accelerometers, this apparatus (brace) was designed to be as noiseless as possible, it attempted to minimize the movement of the sensors on the skin and tried to maintain the position of the sensors on the bone during the knee motion. The brace was also flexible enough that it did not restrict the motion of the knee and also had to be easy to put on. Most of the mentioned properties were successfully built into the design. However, because of the different anatomical shapes and sizes in people, it was not possible to make it completely autonomous and at some points required external force by the examiner to provide a

secure grip for the patellar sensor. Except for this minor problem, the rest of the requirements were met and we were able to successfully examine the patients with it.

Volunteers were recruited for the study. Most of the volunteers were patients suffering various degrees of OA, referred by the physicians. We also included volunteers with healthy knees in the study as well. Overall 50 volunteers took part in the study with a range from healthy to severe OA. In collaboration with another research project, each patient underwent a complete MRI scan of each knee. The MRI images were later analyzed by a radiologist and scores were given to different symptoms of the osteoarthritis found at different compartments of the knee. After the MRI scan, vibration signals of both knees each patient were recorded under the loaded and unloaded conditions for a duration of 20 seconds of continuous extension/flexion of the knee. the sampling rate for data acquisition was 6250 Hz.

The recorded vibrations were converted from time domain to frequency domain using Fourier and wavelet transforms. PCA and PLS analysis were then performed on the processed data (power spectrum density of the Fourier transforms and wavelet coefficient histograms). For the PLS analysis, the Y space data consisted of the MRI scores given to each compartment of the knee and the average over all compartments (for each of the symptoms).

Our analysis shows that there is a strong correlation between cartilage health (cartilage scores), formation of osteophytes (osteophyte score) and the vibration signals recorded from patients' knees. For both cases of PCA and PLS analysis, we obtained better results

when wavelet transformation was used to transform the data from time domain to frequency domain. Our analysis shows that there is an obvious trend from healthy to unhealthy knees in terms of cartilage and osteophyte formation scores in the score plots (average values over all compartments of the knee). Because of the strong correlation between cartilage health and osteophyte formation (more than 80% in our population) it is not possible to distinguish the effects of each symptom in the analysis. We were also not able to isolate or localize the symptoms in each compartment of the knee. The reason is two fold; first OA usually develops in all compartments of the knee and second the frequency of the signals recorded is very low and does not have enough resolution to distinguish symptoms at different compartments of the knee. In the score plots, we also found a separation of knees with degeneration and/or torn menisci (medial anterior horn). However, again, because of the strong correlation between cartilage and meniscus health it is not possible to reliably point out to it. We did not find any other strong correlation between the vibration signals and the other symptoms of osteoarthritis observed from the MRI images (such as bone marrow edema or subchondral cyst).

Overall, we conclude that there is strong correlation between vibration signals and some of the symptoms of osteoarthritis such as formation of osteophytes and cartilage health. This technique can be used in estimation of the overall health status of the joint.

6.1 Future work

In order to validate this technology, it is essential to increase the number of observations (patients) and include observations from more categories and groups of people. It is suggested that the focus be put on three groups of people:

- Patients with Osteoarthritis (all ranges from healthy to severe OA); which will be used to improve detection of OA in the general population.
- Repeated measurements on patients with synovial injections: this group of people will be used to check the ability of this technology for monitoring of the injection performance before and after the injection of intra-articular therapeutic agents such as hyaluronic acid..
- Young patients with meniscus tear: although the method was able to detect meniscus tear problems, because of the strong correlation between meniscus tear and cartilage damages it was not really possible to see the performance of this technology in this regard. By focusing on young patients who have no symptoms of OA, an independent assessment of meniscus effects can be performed.

Another issue that needs to be followed up is the ability of the technology (software) to make decisions on the overall state of the patients; although score plots provide useful information about the state of health, this information needs to be interpreted in the form of classifications of patients into various classes, or in the form of predictions of the

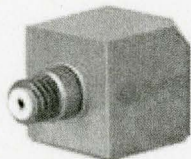
degree of OA, etc. Methods such as support vector machines or decision-making algorithms such as fuzzy logic can be useful here and their implication should be further studied. Yacoub (2006) has performed an initial study on classification methods applied to this problem.

In addition to passive vibrations recorded from patients, active vibrations (impulse response of the joint) were also recorded which will later be analyzed.

Appendix A

Product Data

Product data for PCB accelerometers (model no. 333B52)



Model 333B52

Product Type: Accelerometer, Vibration Sensor

Modal array, ceramic shear ICP® accel., 1000 mV/g, 0.5 to 3k Hz, 10-32 side conn., adhesive mount

[View Spec Sheet \(PDF\)](#)

View [photo](#) and [drawing](#) .



PERFORMANCE	ENGLISH	SI
Sensitivity(± 10 %)	1000 mV/g	102 mV/(m/s ²)
Measurement Range	± 5 g pk	± 49 m/s ² pk
Frequency Range(± 5 %)	0.5 to 3000 Hz	0.5 to 3000 Hz
Resonant Frequency	≥ 20 kHz	≥ 20 kHz
Phase Response(± 5 °)(at 70°F [21°C])	2.5 to 3000 Hz	2.5 to 3000 Hz
Broadband Resolution(1 to 10,000 Hz)	0.00005 g rms	0.0005 m/s ² rms [1]
Non-Linearity	≤ 1 %	≤ 1 % [2]
Transverse Sensitivity	≤ 5 %	≤ 5 % [3]
ENVIRONMENTAL		
Overload Limit	± 4000 g pk	± 39,000 m/s ² pk
Temperature Range	0 to +150 °F	-18 to +66 °C
Temperature Response	See Graph	See Graph [1]
Base Strain Sensitivity	0.01 g/με	0.1 (m/s ²)/με [1]
ELECTRICAL		
Excitation Voltage	18 to 30 VDC	18 to 30 VDC
Constant Current Excitation	2 to 20 mA	2 to 20 mA
Output Impedance	≤ 500 ohm	≤ 500 ohm
Output Bias Voltage	7 to 12 VDC	7 to 12 VDC

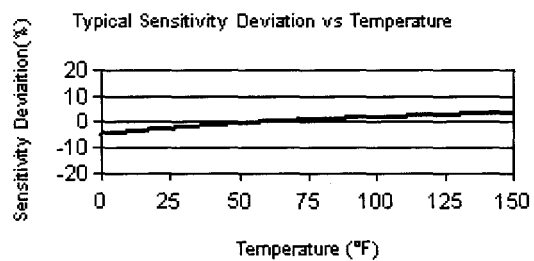
Discharge Time Constant	0.7 to 2.0 sec	0.7 to 2.0 sec
Spectral Noise(10 Hz)	3.8 µg/√Hz	37 (µm/s ²)/√Hz [1]
(100 Hz)	1.1 µg/√Hz	11 (µm/s ²)/√Hz [1]
(1 kHz)	0.4 µg/√Hz	3.9 (µm/s ²)/√Hz [1]
PHYSICAL		
Sensing Element	Ceramic	Ceramic
Sensing Geometry	Shear	Shear
Housing Material	Titanium	Titanium
Sealing	Hermetic	Hermetic
Size (Length x Width)	0.68 in x 0.45 in	17.3 mm x 11.4 mm
Weight	0.26 oz	7.5 gm [1]
Electrical Connector	10-32 Coaxial Jack	10-32 Coaxial Jack
Electrical Connection Position	Side	Side
Mounting	Adhesive	Adhesive
SUPPLIED ACCESSORIES:		
Model 080A109 Petro Wax (1)		
Model 080A90 Quick Bonding Gel (1)		
Model ACS-1 NIST traceable frequency response (10 Hz to upper 5% point). (1)		
OPTIONAL VERSIONS		
T- TEDS Capable of Digital Memory and Communication Compliant with IEEE P1451.4		
Output Bias Voltage	7.5 to 13 VDC	
TLA- TEDS LMS International - Free Format		
Output Bias Voltage	7.5 to 13 VDC	
TLB- TEDS LMS International - Automotive Format		
Output Bias Voltage	7.5 to 13 VDC	
TLC- TEDS LMS International - Aeronautical Format		
Output Bias Voltage	7.5 to 13 VDC	

All specifications are at room temperature unless otherwise specified.

NOTES:

- [1] Typical.
- [2] Zero-based, least-squares, straight line method.
- [3] Transverse sensitivity is typically ≤ 3%.
- [4] See PCB Declaration of Conformance PS023 for details.

CE [4]



Product data for impact hammer used in this project



Model 086D80

Product Type: Impact Hammer, Impulse Hammer

Miniature Instrumented Impulse Hammer w/force tips, 0 to 50 lbf (includes Model 084A17 & 018G10 cable)

[View Spec Sheet \(PDF\)](#)

View [photo](#) and [drawing](#) .



PERFORMANCE	ENGLISH	SI
Sensitivity(± 15 %)	100 mV/lbf	22.5 mV/N
Measurement Range	± 50 lbf pk	± 220 N pk
Frequency Range(-10 dB)(Hard Tip)	20 kHz	20 kHz [1][2][3]
Resonant Frequency	≥ 100 kHz	≥ 100 kHz
Non-Linearity	≤ 1 %	≤ 1 % [1]
ELECTRICAL		
Excitation Voltage	18 to 30 VDC	18 to 30 VDC
Constant Current Excitation	2 to 20 mA	2 to 20 mA
Output Impedance	<100 ohm	<100 ohm
Output Bias Voltage	8 to 12 VDC	8 to 12 VDC
Discharge Time Constant	≥ 100 sec	≥ 100 sec [1]
PHYSICAL		
Sensing Element	Quartz	Quartz
Sealing	Epoxy	Epoxy
Hammer Mass	0.10 oz	2.9 gm [4]
Head Diameter	0.25 in	6.3 cm
Tip Diameter	0.10 in	2.5 cm
Hammer Length	4.00 in	101.6 cm
Electrical Connection Position	Bottom of Handle	Bottom of Handle
Extender Mass Weight	0.044 oz	1.25 gm
Electrical Connector	5-44 Coaxial	5-44 Coaxial [5]
Cable Type	035 Twisted Pair	035 Twisted Pair [4]
Cable Length	10 ft	3.05 m [4]

SUPPLIED ACCESSORIES:
Model 001A20 Case (1)
Model 018G10 Miniature coaxial cable, vinyl insulation jacket, 10-ft, 5-44 to 10-32 coaxial plug (1)
Model 080A109 Petro Wax (1)
Model 084A13 Extender mass (1)
Model 084A14 Plastic handle assembly (2)
Model 084A17 Aluminum handle with 5-44 connector (1)
Model 084A28 Vinyl impact cap, red (3)
Model HCS-2 Calibration of Series 086B to 086D instrumented hammers only (1)

All specifications are at room temperature unless otherwise specified.

NOTES:

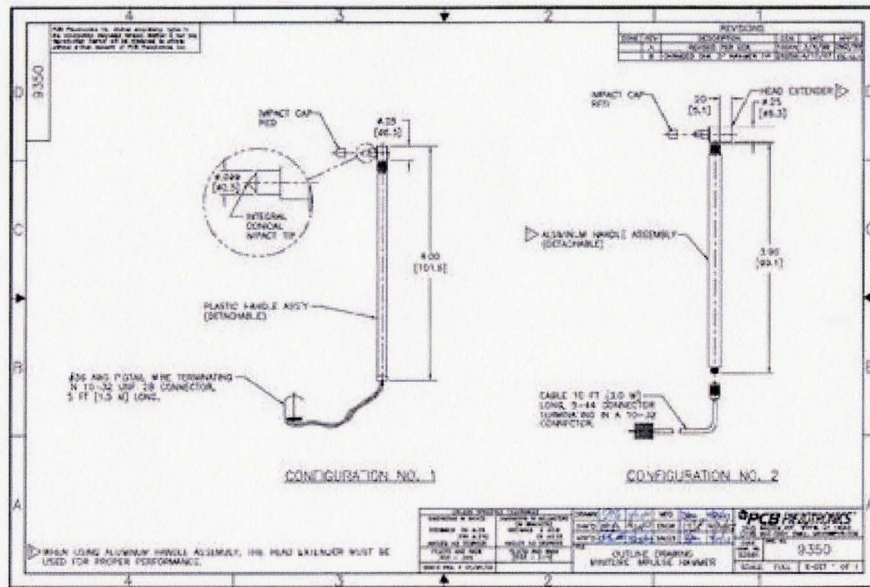
[1] Typical.

[2] Varies depending on test structure. These values are from hitting a stiff steel mass. Hammer did not have extender mass attached.

[3] When using the aluminum handle, the extender mass must be used.

[4] With plastic handle attached.

[5] With aluminum handle attached.



Appendix B

Detecting the FE axis of the knee

Hollister et al [28] revealed that knee joint, in fact does have a fixed axis of rotation. Using mechanical axis finder they managed to find the axis of rotation for 7 fresh specimens. According to their paper, the flexion/extension (FE) axis runs through the collateral ligament origins and superior to the intersection of the cruciate ligaments. They also managed to confirm the results using MRI scanning. They indicate that the FE axis passes through the origins of the medial collateral and lateral collateral ligaments in all dissected knees. The left/right (LR) axis passed through the intersection of the anterior cruciate ligament (ACL) on tibia and directed in the proximity of the intersection of PCL at the femoral notch. The length of patellar groove runs perpendicular to this axis (FE). One of the interesting findings of Hollister et al is that when the FE axis is viewed end on, the posterior femoral condyles are superimposed and appeared circular. They concluded that FE axis is fixed in the distal femur and is directed posteroinferiorly from medial to lateral. The offset from condylar surface averages 3° in the coronal and transverse planes. The surface of the femur that articulates with tibia is conical; the lateral condyle has a smaller radius than the medial condyle. Lateral joint surface is closer to FE axis. They also mention that the surface of condyles is rounded to allow movement about the LR axis. Their study concludes that motion of human knee occurs about two fixed non-orthogonal axes. The study suggests that knee motion is pure rotation about these axes. The FE axis is not in the coronal plane, nor is LR in sagittal plane. Most of motion

takes place in the sagittal plane but there is still rotation and varus/valgus motion outside of this plane.

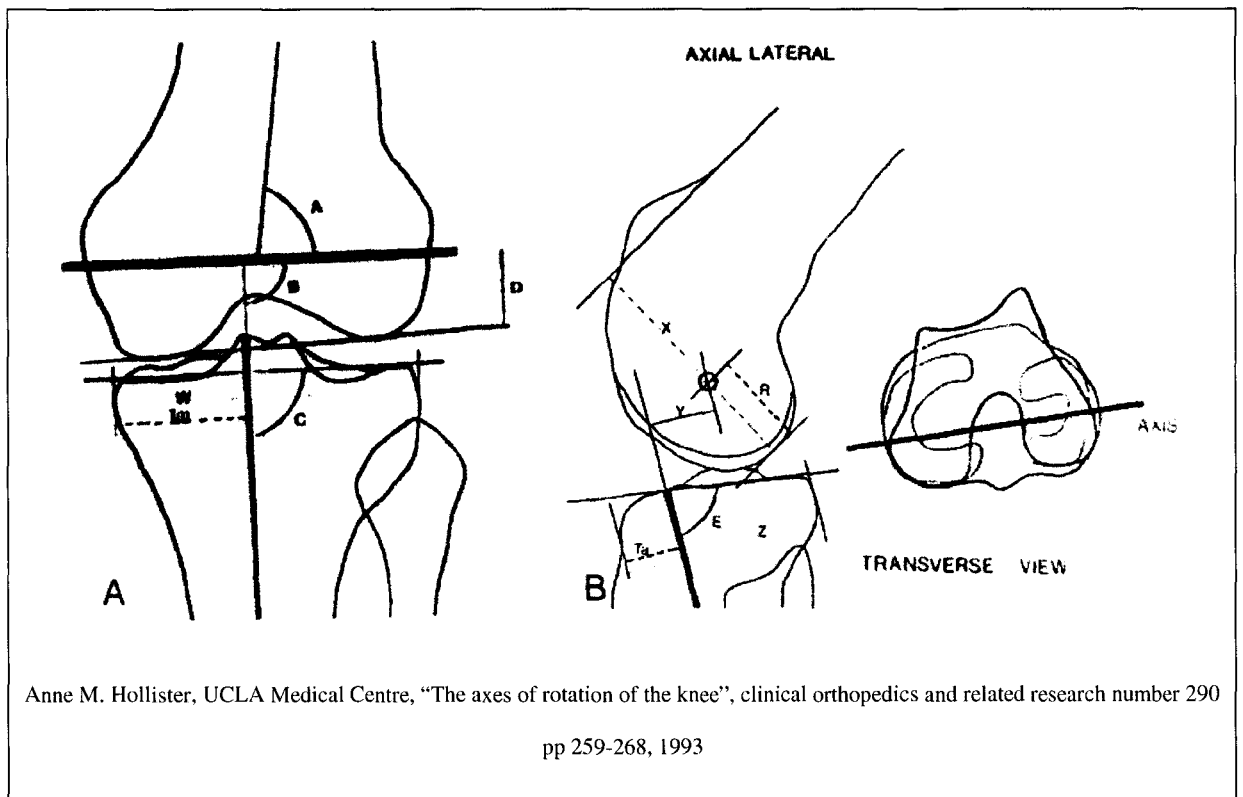


Figure 74: 3A AND 3B. (A) Diagrammatic representation of axes in AP view with axis parallel to the plate. A is the angle the FE axis makes with the shaft of the femur; B is the angle between the FE and L.R axes in the AP plane. C is the angle between the LR axis and the tibial plateau. The distances D, W, and Tm are the distances between the FE axis and the joint surface, the AP width of the tibia, and the medial tibia and the LR axis respectively. (B) Diagrammatic representation of axes in axial lateral view with x-ray beam parallel to the FE axis. E is the angle between the LR axis and the tibial plateau in the axial lateral plane; X is the distance between the anterior femoral shaft and the posterior-medial femoral condyle. R is the distance between the FE axis and the posterior-medial femoral condyle. Y is the perpendicular distance between the two axes. Z is the AP dimension of the tibia and Ta is the distance of the L.R axis from the anterior tibia.

<i>Knee</i>	<i>A°</i>	<i>B°</i>	<i>C°</i>	<i>D°</i>	<i>E°</i>	<i>Tibial Axis</i>			<i>Femoral Axis</i>
						<i>Tm/W</i>	<i>Ta/Z</i>	<i>Y/W</i>	<i>R/X</i>
1	80	89	89	3.0	82				
2	83	88	90	5.0	88				
3	87	87	88	5.0	88				
4	83	89	87	5.0	80				
5	85	87	88	5.0	84				
6	85	90	93	3.0	88				
Mean	84	88	89	4.3	85				
±SD	2.4	1.2	2.1	1.0	3.5				

Measurements of the angles of the axes with the bones in the AP and axial lateral views.

<i>Knee</i>	<i>Tibial Axis</i>			<i>Femoral Axis</i>
	<i>Tm/W</i>	<i>Ta/Z</i>	<i>Y/W</i>	<i>R/X</i>
1	43.3	35.7	35.7	29.2
2	46.5	41.9	11.3	36.1
3	53.3	19.6	35.2	41.4
4	42.8	23.5	49.0	40.9
5	49.3	25.0	30.8	31.6
6	50.0	45.1	27.5	32.3
Mean	47.5	31.8	31.6	35.3
±SD	4.1	10.6	12.3	5.1

Table 7: A) Location of axes of rotation, B) Location of the axes described as a percent of femoral and tibial dimensions. Tm/W, percentage ration locating tibia axis on AP view; Ta/Z percentage ratio locating tibial axis on axial lateral view; Y/W percentage ratio depicting interaxial distance relative to tibial plateau width; R/X percentage ratio locating femoral axis on axial lateral view.

Bibliography

1. Kuettner KE, Goldberg V. Osteoarthritic disorders. *Am Acad Orthop Surg*. 1995;xxi-v.
2. Guccione A, Felson D, Anderson J. The effects of specific medical conditions on functional limitations of elders in the framingham study. *Am J Public Health*. 1994;84:351-357.
3. Lawrence R, Helmick C, Arnett F. Estimates of the prevalence of arthritis and selected musculoskeletal disorders in the united states. *Arthritis Rheum*. 1998;41:778-799.
4. Global economic and health care burden of musculoskeletal disease [homepage on the Internet]. World Health Organization. 2001. Available from: www.boneandjointdecade.org.
5. van Saase JL, van Romunde LK, Cats A, Vandenbroucke JP, Valkenburg HA. Epidemiology of osteoarthritis: Zoetermeer survey. comparison of radiological osteoarthritis in a dutch population with that in 10 other populations. *Ann Rheum Dis*. 1989 Apr;48(4):271-80.
6. Lawrence, J S Bremner, J M Bier,F. Osteo-arthrosis. prevalence in the population and relationship between symptoms and x-ray changes. *Annals of the rheumatic diseases*. 1966;25(1):1.
7. Anderson JJ, Felson DT. Factors associated with osteoarthritis of the knee in the first national health and nutrition examination survey (HANES I). evidence for an association with overweight, race, and physical demands of work. *Am J Epidemiol*. 1988 Jul;128(1):179-89.

8. Buckland-Wright C. Protocols for precise radio-anatomical positioning of the tibiofemoral and patellofemoral compartments of the knee. *Osteoarthritis Cartilage*. 1995 Sep;3 Suppl A:71-80.
9. Vignon E, Piperno M, Le Graverand MP, Mazzuca SA, Brandt KD, Mathieu P, et al. Measurement of radiographic joint space width in the tibiofemoral compartment of the osteoarthritic knee: Comparison of standing anteroposterior and lyon schuss views. *Arthritis Rheum*. 2003 Feb;48(2):378-84.
10. Buckland-Wright JC, Wolfe F, Ward RJ, Flowers N, Hayne C. Substantial superiority of semiflexed (MTP) views in knee osteoarthritis: A comparative radiographic study, without fluoroscopy, of standing extended, semiflexed (MTP), and schuss views. *J Rheumatol*. 1999 Dec;26(12):2664-74.
11. Nevitt MC, Sharma L. OMERACT workshop radiography session I. *Osteoarthritis Cartilage*. 2006;14 Suppl A:A4-9.
12. Brandt KD, Mazzuca SA, Conrozier T, Dacre JE, Peterfy CG, Provvedini D, et al. Which is the best radiographic protocol for a clinical trial of a structure modifying drug in patients with knee osteoarthritis? *J Rheumatol*. 2002 Jun;29(6):1308-20.
13. Ike R, O'Rourke KS. Compartment-directed physical examination of the knee can predict articular cartilage abnormalities disclosed by needle arthroscopy. *Arthritis Rheum*. 1995 Jul;38(7):917-25.

14. Yacoub F. Diagnosis of knee joint using vibration analysis [dissertation]. McMaster University; 2007.
15. Steindler A. Auscultation of joints. *J Bone joint surg Am.* 1937;19:121-136.
16. McCoy GF, McCrea JD, Beverland DE, Kernohan WG, Mollan RA. Vibration arthrography as a diagnostic aid in diseases of the knee. A preliminary report. *J Bone Joint Surg Br.* 1987 Mar;69(2):288-93.
17. Rangayyan RM, Frank CB, Bell GD, Smith R. In: Analysis of knee joint sound signals. 1988; ; 1988.
18. Krishnan S, Rangayyan RM, Bell GD, Frank CB. Auditory display of knee-joint vibration signals. *J Acoust Soc Am.* 2001 Dec;110(6):3292-304.
19. Rangayyan RM, Krishnan S, Bell GD, Frank CB, Ladly KO. Parametric representation and screening of knee joint vibroarthrographic signals. *IEEE Trans Biomed Eng.* 1997 Nov;44(11):1068-74.
20. Krishnan S, Rangayyan RM, Bell GD, Frank CB. Adaptive time-frequency analysis of knee joint vibroarthrographic signals for noninvasive screening of articular cartilage pathology. *IEEE Trans Biomed Eng.* 2000 Jun;47(6):773-83.
21. Krishnan S, Rangayyan RM. Automatic de-noising of knee-joint vibration signals using adaptive time-frequency representations. *Med Biol Eng Comput.* 2000 Jan;38(1):2-8.

22. Krishnan S, Rangayyan RM, Bell GD, Frank CB, Ladly KO. Adaptive filtering, modelling and classification of knee joint vibroarthrographic signals for non-invasive diagnosis of articular cartilage pathology. *Med Biol Eng Comput.* 1997 Nov;35(6):677-84.
23. Marieb EN. *Essentials of human anatomy and physiology.* 8th ed. Pearson Benjamin Cummings; 2006.
24. E-orthopod, enabling your orthopaedic practice [homepage on the Internet]. USA: medical multimedia group LLC. Available from: www.eorthopod.com/public.
25. Knee ligament anatomy [homepage on the Internet]. Portland: Orthopaedic Associates of Portland. 2007. Available from: www.orthoassociates.com/knee_lig.htm.
26. Nordin M, P.T., Frankel VH. *Basic biomechanics of the musculoskeletal system.* 3rd ed. Lippincott Williams Wilkins; 2001. pp 141-142
27. Selvik G. A stereophotogrammetric system for the study of human movements. *Scand J Rehabil Med Suppl.* 1978;6:16-20.
28. Hollister AM, Jatana S, Singh AK, Sullivan WW, Lupichuk AG. The axes of rotation of the knee. *Clin Orthop Relat Res.* 1993 May;(290)(290):259-68.
29. Sati M, de Guise JA, Larouche S, Drouin G. Quantitative assessment of skin-bone movement at the knee. *The Knee.* 1996 August, 1996;3(3):121-38.

30. Davis MA, Ettinger WH, Neuhaus JM, Cho SA, Hauck WW. The association of knee injury and obesity with unilateral and bilateral osteoarthritis of the knee. *Am J Epidemiol.* 1989 Aug;130(2):278-88.
31. McAlindon T, Zhang Y, Hannan M, Naimark A, Weissman B, Castelli W, et al. Are risk factors for patellofemoral and tibiofemoral knee osteoarthritis different? *J Rheumatol.* 1996 Feb;23(2):332-7.
32. Cicuttini FM, Spector T, Baker J. Risk factors for osteoarthritis in the tibiofemoral and patellofemoral joints of the knee. *J Rheumatol.* 1997 Jun;24(6):1164-7.
33. Hart DJ, Doyle DV, Spector TD. Incidence and risk factors for radiographic knee osteoarthritis in middle-aged women: The chingford study. *Arthritis Rheum.* 1999 Jan;42(1):17-24.
34. Ding C, Cicuttini F, Scott F, Glisson M, Jones G. Sex differences in knee cartilage volume in adults: Role of body and bone size, age and physical activity. *Rheumatology (Oxford).* 2003 Nov;42(11):1317-23.
35. Faber SC, Eckstein F, Lukasz S, Muhlbauer R, Hohe J, Englmeier KH, et al. Gender differences in knee joint cartilage thickness, volume and articular surface areas: Assessment with quantitative three-dimensional MR imaging. *Skeletal Radiol.* 2001 Mar;30(3):144-50.

36. Kujala UM, Kettunen J, Paananen H, Aalto T, Battie MC, Impivaara O, et al. Knee osteoarthritis in former runners, soccer players, weight lifters, and shooters. *Arthritis Rheum.* 1995 Apr;38(4):539-46.
37. Berthiaume MJ, Raynauld JP, Martel-Pelletier J, Labonte F, Beaudoin G, Bloch DA, et al. Meniscal tear and extrusion are strongly associated with progression of symptomatic knee osteoarthritis as assessed by quantitative magnetic resonance imaging. *Ann Rheum Dis.* 2005 Apr;64(4):556-63.
38. TRUETA J, HARRISON MH. The normal vascular anatomy of the femoral head in adult man. *J Bone Joint Surg Br.* 1953 Aug;35-B(3):442-61.
39. HARRISON MH, SCHAJOWICZ F, TRUETA J. Osteoarthritis of the hip: A study of the nature and evolution of the disease. *J Bone Joint Surg Br.* 1953 Nov;35-B(4):598-626.
40. Pottenger LA, Phillips FM, Draganich LF. The effect of marginal osteophytes on reduction of varus-valgus instability in osteoarthritic knees. *Arthritis Rheum.* 1990 Jun;33(6):853-8.
41. Hannan MT, Felson DT, Pincus T. Analysis of the discordance between radiographic changes and knee pain in osteoarthritis of the knee. *J Rheumatol.* 2000 Jun;27(6):1513-7.
42. Kijowski R, Stanton P, Fine J, De Smet A. Subchondral bone marrow edema in patients with degeneration of the articular cartilage of the knee joint. *Radiology.* 2006 Mar;238(3):943-9.

43. Croft P, Jordan K, Jinks C. "Pain elsewhere" and the impact of knee pain in older people. *Arthritis Rheum.* 2005 Aug;52(8):2350-4.
44. Cerejo R, Dunlop DD, Cahue S, Channin D, Song J, Sharma L. The influence of alignment on risk of knee osteoarthritis progression according to baseline stage of disease. *Arthritis Rheum.* 2002 Oct;46(10):2632-6.
45. Haq I, Murphy E, Dacre J. Osteoarthritis. *Postgrad Med J.* 2003 Jul;79(933):377-83.
46. Krishnan S, Rangayyan RM, Bell GD, Frank CB. Auditory display of knee-joint vibration signals. *J Acoust Soc Am.* 2001 Dec;110(6):3292-304.
47. Najarian K, Splinter R. *Biomedical signal and image processing.* Taylor and Francis; 2006.
48. Press WH. *Numerical recipes in FORTRAN : The art of scientific computing.* 2nd ed. Cambridge ; New York: Cambridge University Press; 1992. pp 494-500
49. Moussavi ZM, Rangayyan RM, Bell GD, Frank CB, Ladly KO, Zhang YT. Screening of vibroarthrographic signals via adaptive segmentation and linear prediction modeling. *IEEE Trans Biomed Eng.* 1996 Jan;43(1):15-23.
50. Nordin M, P.T., Frankel VH. *Basic biomechanics of the musculoskeletal system.* 3rd ed. Lippincott Williams Wilkins; 2001.

51. Moskowitz R. W. Altman R. D., Hochberg M. C. Buckwalter J. A. Goldberg V. M. Osteoarthritis, Diagnosis and medical/ Surgical management. 4th ed. Lippincott, Williams Wilkins 2007